Infrared Radiofluorescence Dating: New Insights into the (Upper) Dating Limit, Grain Size and Feldspar Chemistry

Dissertation

der Mathematisch-Naturwissenschaftlichen Fakultät

der Eberhard Karls Universität Tübingen

zur Erlangung des Grades eines

Doktors der Naturwissenschaften

(Dr. rer. nat.)

vorgelegt von

Ms. Gwynlyn Reinette Buchanan

aus Zaf/Südafrika

Tübingen

2024

Gedruckt mit Genehmigung der Mathematisch-Naturwissenschaftlichen Fakultät der Eberhard Karls Universität Tübingen.

Tag der mündlichen Qualifikation:	18.07.2024
Dekan:	Prof. Dr. Thilo Stehle
1. Berichterstatter/-in:	Prof. Dr. Sumiko Tsukamoto
2. Berichterstatter/-in:	Prof. Dr. Kathryn Fitzsimmons

Acknowledgements

I dedicate this dissertation to you, reader, the wonderful soul who has come to this dissertation in search of answers, questions or a direction in which to guide your own infrared radiofluorescence research. Welcome, put the kettle on and settle down with me. I hope this work goes some small way to contributing to your own.

This research would not have been possible without the support, patience and gentle constructive criticism of my supervisor Prof. Dr. Sumiko Tsukamoto, thank you for taking me under your wing and not letting me fall through the cracks. I am extremely grateful to the Leibniz Institute for Applied Geophysics and Prof. Dr. Manfred Frechen for the opportunity and funding to do the research. Special thanks go to Sonja Riemenschneider and Sabina Mogwitz in the luminescence lab for their training and constant support in sample preparation, to Dr. Junjie Zhang for his advice and support and to all my other friends of the red-light Frank Oppermann, Karsten Vollmer, Petra Posimowski and Dr. Astrid Techmer for all the coffee room and lunch table conversations, encouragement and putting up with my attempts at German. To my fellow PhD candidates Neda Rahimzadeh, Marcus Richter, Valentina Argante, Erick Prince thank you for the encouragement, countless ideas, helpful explanations and for putting up with my endless chatting, without our shared experience I could not have persevered to this point. Thanks also should go to my co-workers in Tübingen who have supported me through the final phase.

Lastly but most importantly to my parents Gina and Grant, who have interrogated me mercilessly and are still unclear as to what my research entails but encourage and support me regardless. To my friends who have safeguarded my sanity with laughter and tears, and sometimes a tough love approach (shout out to Dana: who asked me every time we spoke if I was done yet, for over a year.). I miss you all every day and I love you all more than words can say.

"It always seems impossible until it's done"

-Nelson Mandela

Contents

List of Tables and Figures

Abbreviations

Abbreviation	Definition
DASH	Detection and Stimulation Head
D_e	Equivalent Dose
DRC	Dose Response Curve
IRCL	Infrared Cathodoluminescence
IRPL	Infrared Photo Luminescence
IR-RF	Infrared Radiofluorescence
IRSL	Infrared Stimulated Luminescence
RT	Room Temperature
UV LED	Ultra violet light emitting diode
OSL	Optically Stimulated Luminescence
MET-$pIRIR_x$	Multiple Elevated Temperature, post-Infrared, Infrared stimulated measurements in which (x is the temperature of stimulation)
$pIRIR_x$	post-Infrared, Infrared Stimulated Luminescence (x is the temperature of the second measurement)
RF_x	Infrared Radiofluorescence (x is the temperature of measurement)
VSL	Violet Stimulated Luminescence

Abstract

Accurate luminescence dating of feldspar has long been hampered by the effect of athermal signal loss (anomalous fading) when using luminescence dating techniques that make use of recombination centres. Infrared radiofluorescence (IR-RF) dating is a luminescence dating technique that makes use of the principal trap and is therefore theorised to not suffer from fading to a significant extent. Extensive laboratory investigations have been done to better constrain and exploit the IR-RF signal and mechanisms but remarkably few have applied the technique to large sequences of natural sediments with known age control. In this dissertation the utility and effectiveness of IR-RF dating was investigated and tested on coarse-, mid- and polymineral fine-grains of feldspar with a view to evaluating the upper dating limit of IR-RF as well as compared IR-RF with the recently developed novel infrared photoluminescence (IRPL) dating technique. Initially 10 coarse-grained K-feldspar samples (~25 to ~900 ka) from the Luochuan loess-paleosol sequence were measured and compared with age control and it was found that a bleaching time of 1500 s (between the natural and regenerated measurements) underestimated across all but the youngest sample while a longer bleach of 20 000 s resulted in good agreement with the age control up to 300 ka (5 samples) and underestimated for the older samples. Construction of the natural and laboratory dose response curves across the sequence revealed significantly different curve shapes for the shorter bleaching time and consistent curve shapes for the longer bleaching time, highlighting the importance of the longer bleach time. The potential of the IR-RF signal for dating was then tested on 6 polymineral fine-grained samples, and it was observed that the IR-RF signal did not describe the characteristic decreasing stretched exponential curve shape, these results were compared with Na- and K-feldspar mid-grain fractions of the same samples. The essentially flat curves were attributed to the dominance of Na- feldspar and quartz in the polymineral fine grains. Despite the flat IR-RF signals and poor dose recoveries, the age results for the polymineral fine-grains were consistent with age control up to 300 ka, the Na-feldspar mid-grains up to 350 ka and the K-feldspar mid-grains up to 200 ka. A comparison of two IR-RF signals (at room temperature, RF_{RT}; and at 70 °C, RF_{70}) and two IRPL signals (stimulated at 880 nm, $IRPL_{880}$; and at 955 nm, $IRPL_{955}$) on 4 coarse-grained coastal sediments (~ 133 to 223 ka) from Sardinia showed good agreement with age control for all signals within 2σ. The IR-RF signal is an effective dating tool up to 300 ka for coarse- and polymineral fine-grains and it's performance is comparable with IRPL dating.

Zusammenfassung

Die genaue Lumineszenz-Datierung von Feldspat wurde lange Zeit durch den athermischen Signalverlust (anomales Fading) bei der Verwendung von Lumineszenz-Datierungstechniken, die Rekombinationszentren nutzen, beeinträchtigt. Die Infrarot-Radiofluoreszenz-Datierung (IR-RF) ist eine Lumineszenz-Datierungstechnik, die sich die Elektronenfallen zunutze macht und daher theoretisch nicht in nennenswertem Umfang unter Fading leidet. In der Vergangenheit wurden umfangreiche Laboruntersuchungen durchgeführt, um das IR-RF-Signal und die Mechanismen besser einzugrenzen und zu nutzen, aber bemerkenswert wenige Studien haben die Technik auf große Sequenzen natürlicher Sedimente mit bekannter Alterskontrolle angewendet. In dieser Dissertation wurde die Nützlichkeit und Effektivität der IR-RF-Datierung an grob-, mittel- und polymineralischen Feldspatkörnern untersucht und getestet, um die obere Datierungsgrenze der IR-RF zu ermitteln und die IR-RF mit der kürzlich entwickelten neuen Infrarot-Photolumineszenz (IRPL) Datierungstechnik zu vergleichen. Zunächst wurden 10 grobkörnige K-Feldspat-Proben (~25 bis ~900 ka) aus der Luochuan-Löß-Paläosol-Sequenz gemessen und mit der vorhandenen Alterskontrolle verglichen. Es zeigte sich, dass eine Bleichzeit von 1500 s (zwischen den natürlichen und den regenerierten Messungen) bei allen Proben außer der jüngsten zu einer Unterschätzung führte, während eine längere Bleichzeit von 20 000 s eine gute Übereinstimmung mit der Alterskontrolle bis 300 ka (5 Proben) ergab und bei den älteren Proben unterschätzt wurde. Die Konstruktion der Dosis-Wirkungs-Kurven aus der Natur und dem Labor über die gesamte Sequenz hinweg ergab signifikant unterschiedliche Kurvenformen für die kürzere Bleichzeit und einheitliche Kurvenformen für die längere Bleichzeit, was die Bedeutung der längeren Bleichzeit hervorhebt. Das Potenzial des IR-RF-Signals für die Datierung wurde dann an 6 polymineralischen feinkörnigen Proben getestet, und es wurde festgestellt, dass das IR-RF-Signal nicht die charakteristische abnehmende gestreckte exponentielle Kurvenform beschrieb; diese Ergebnisse wurden mit Na- und K-Feldspat-Mittelkornfraktionen derselben Proben verglichen. Die im Wesentlichen flachen Kurven wurden auf die Dominanz von Na-Feldspat und Quarz in den polymineralischen Feinkörnern zurückgeführt. Trotz der flachen IR-RF-Signale und der schlechten Dosisausbeute stimmten die Altersergebnisse für die feinen Polymineralkörner mit der Alterskontrolle bis 300 ka, für die mittleren Na-Feldspat-Körner bis 350 ka und für die mittleren K-Feldspat-Körner bis 200 ka überein. Ein Vergleich von zwei IR-RF-Signalen (bei Raumtemperatur, RF_{RT}; und bei 70 °C, RF_{70}) und zwei IRPL-Signalen (stimuliert bei 880 nm, $IRPL_{880}$; und bei 955 nm, $IRPL_{955}$) an 4 grobkörnigen Küstensedimenten (~ 133 bis 223 ka) aus Sardinien zeigte eine gute Übereinstimmung mit der Alterskontrolle für alle Signale innerhalb von 2σ. Das IR-RF-Signal ist ein wirksames Datierungsinstrument bis zu 300 ka für grob- und polymineralische Feinkörnchen und seine Leistung ist mit der IRPL-Datierung vergleichbar.

Chapter 1: Introduction

1.1 Background in luminescence dating

Luminescence dating is a powerful geochronological dating method that is used extensively to date sediments from the Quaternary, which is critically important to our understanding of both archeology and the recent history of the geological, hydrogeological and climatic processes on Earth. Luminescence dating is an absolute dating technique that makes use of the ubiquitous minerals of quartz and feldspar as dosimeters to date the most recent burial event that the mineral has experienced. Luminescence dating exploits the mechanism in which mineral dosimeters accumulate electrons in the principal trap over time with exposure to radiation from radioactive elements, including uranium (U), thorium (Th) and potassium (K), and cosmic radiation while buried; as well as the release mechanism of the depletion of electrons during exposure to sunlight or elevated temperatures (Fig. 1.1.).

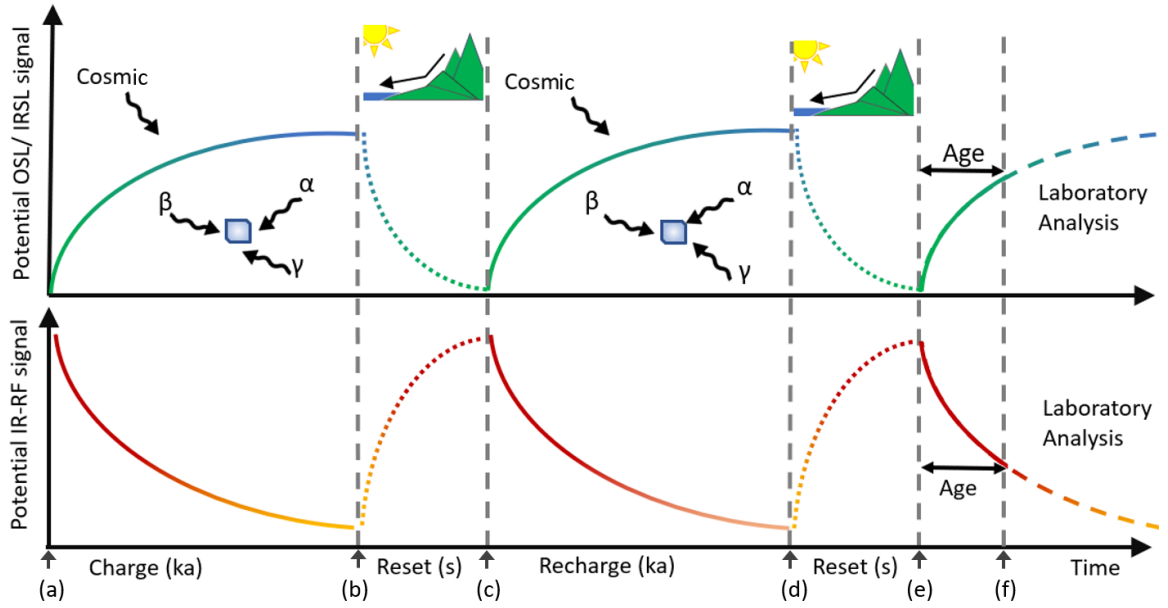

Fig.1.1: Illustration of the mechanisms exploited by luminescence dating (modified after Mellet, C.L., 2013). (a) The mineral is formed/buried and exposed to α, β and γ radiation from radioactive elements as well as cosmic radiation (the potential luminescence signal increases over time); (b) the mineral is eroded, transported and exposed to sunlight (the luminescence signal is partially or fully reset to zero); (c) and (d) are a repeated cycle of reburial (accumulation of luminescence signal) and sunlight exposure (luminescence signal resetting) respectively; (e) the mineral is once more reburied (accumulation of luminescence signal) and (f) the sample is collected, analysed in the lab and the time since reburial (e) is determined.

Thermoluminescence (TL) was first used to determine the timing of the last firing of clay and pottery artifacts (e.g., Aiken et al., 1964) in archeological studies. Later TL was initially applied to sediments using a suitable, repeatable technique by Wintle and Huntley (1980, 1982) and Wintle (1980), in which the application of heat to a dosimeter elicited a proportional luminescence response. Optically stimulated luminescence (OSL) of quartz was later introduced by Huntley et al. (1985) as a way to focus on light sensitive traps that are more easily reset by sunlight, by stimulating the sample using light with a narrow and specific wavelength range. Hütt et al. (1988) was the first to apply infrared stimulation to feldspar leading to the development of the infrared stimulated luminescence (IRSL) signal for dating. After decades of research a large number of methods, analyses and different stimulation wavelength ranges have been developed and tested on both quartz and feldspar. Conventionally, quartz signals are stimulated and detected in the blue range (OSL) while feldspar signals are stimulated using the infrared range and detected in the blue range (IRSL).

While quartz is often favoured in luminescence dating as it is generally considered to have a stable, fast and easy-to-bleach signal; it saturates earlier than feldspar, resulting a comparatively low dating limit (~150 ka) depending upon the regional dose rate (Wallinga, 2002). Quartz, on occasion, has also exhibited other challenging properties such as dim luminescence signals (Preusser et al., 2006) or the absence of the Fast component (Steffen et al., 2009). Where a higher dating limit is required or where quartz is not favoured due to challenging properties, feldspar is preferred. Feldspar has a great deal of potential to date older materials in the Quaternary, but suffers from the disadvantage of athermal signal instability (anomalous fading), which results in age underestimations (Wintle, 1973). In the past, anomalous fading has been theorised to be due to the quantum tunneling of electrons out of the principal trap, and was generally associated with shallow unstable traps. However, new observations by Kumar et al. (2023) have revealed that fading is primarily a result of changes in recombination efficiency due to the loss of available traps at recombination centres and that the effect of a direct loss of electrons in the principal trap was minor. A plethora of work has been done to solve the fading problem, namely: 1) arduous post-measurement mathematical fading corrections (Kars et al., 2008; Huntley and Lamothe., 2011), 2) elevated temperature measurements after an initial infrared stimulation (pIRIR), e.g.: $pIRIR_{225}$ (Thomsen et al., 2008) and $pIRIR_{290}$ (Thiel et al., 2011), 3) multi-elevated temperature (MET) pIRIR (Li and Li, 2010), and 4) using alternative signals that make use of luminescence

mechanisms of the principal trap such as infrared radiofluorescence (IR-RF) (Trautmann et al., 1999) and infrared photoluminescence (IRPL) (Prasad et al., 2017; Kumar et al., 2018). The observations of Kumar et al. (2023) showing that the effect of anomalous fading on the principal trap is minor could elevate the importance and encourage more mainstream use of IR-RF and IRPL dating in the future.

The IR-RF, initially characterized by Trautman et al. (1999), is the infrared emission resulting from stimulation of the principal trap through exposure to continuous ionizing radiation. The IR-RF signal, centered at 865 nm (1.43 eV), is directly proportional to the number of electrons entering empty principal traps during irradiation (Trautman et al., 1999; Erfurt and Krbetschek., 2003), while IRSL and elevated temperature IRSL signals are more complex and are a result of recombination of electrons in secondary traps after ejection from the principle trap. The IR-RF signal has great potential for dating with several advantages over conventional IRSL, namely: 1) high resolution dose response curves which are expected to extend the age range; 2) the measurement time is generally shorter than that of conventional single aliquot protocols; 3) there is the possibility that the IR-RF signal does not fade as the principal trap is being utilized.

Testing the upper limits of a dating technique is an important exercise in understanding its applicability and potential. Erfurt and Krbetschek (2003) showed that depending upon the regional dose rate an upper equivalent dose limit of between 1200-1500 Gy could be attainable. Work done at elevated temperature (RF_{70}) has elicited promising equivalent dose (D_e) results of up to 2000 Gy (Frouin et al., 2017). Focusing on dose recovery experiments, Murari et al. (2018) found that laboratory generated D_es of ~3500 Gy are possible. In contrast, in an inter-laboratory comparison of a sample with a geological dose of > 2.5 MGy Murari et al. (2021) deduced an average D_e of 1265 ± 329 Gy using measurements from eight participating laboratories; a D_e that Sontag-Gonzalez and Fuchs (2022) were able to retrieve in their investigation of the influence of neighboring IR-RF emissions. Additionally, a recent study on one sample by Kreuzer et al. (2022) revealed an upper limit of 1200 Gy, and they show that signals at higher dose ranges are prone to larger underestimations with an increase in dose. As a result, they encourage caution with D_e results over 1200 Gy and consider these to be minimum ages to account for likely underestimations (Kreuzer et al., 2022).

While laboratory experimentation is vital to improving and understanding the mechanisms, methodologies and limits employed in luminescence dating, testing these improved methodologies on natural samples and sequences is critically important and gives us invaluable information about the field applicability of these methods. In this dissertation I aim to evaluate the applicability of IR-RF dating on natural sediments by answering the following research questions:

1) How does the IR-RF signal perform when dating coarse grained sediments in nature? What is the upper dating limit of IR-RF in nature?

2) Are polymineral fine-grains a suitable dosimeter with regards to the IR-RF signal in nature, or does the polymineral nature of the material result in different signals and exclude it?

3) How does the IR-RF signal compare with the recently developed IRPL signal when dating sediments?

1.2 Infrared Radiofluorescence

1.2.1 Origin of the IR-RF signal and relevant models

A physical model describing the mechanism for the IR-RF signal was first proposed by Trautmann et al. (1999), in which they theorize that the IR-RF signal results from the transition of an electron through the excited state from the conduction band to the ground state of the principal trap. Fig.2 is a summary of luminescence dating models from Murari et al. (2021), illustrating the widely accepted IR-RF model and comparing it with other luminescence dating models. Exposure to continuous ionizing radiation from radiogenic elements (U, Th, K) and cosmogenic radiation results in the availability and flow of electrons from the valence band to the conduction band [a]. There are three paths the electrons can take, they can recombine either radiatively [b] or non-radiatively [excluded for clarity], or they can be trapped in the principal trap (ground state) [c]. The passing of electrons through the excited state to the ground state results in the release of photons and the filling of principal traps, termed the IR-RF signal. Initially this signal is at its brightest, with continued exposure to ionizing radiation the number of available traps decreases and the IR-RF signal decreases resulting in an IR-RF signal that is a decreasing exponential curve. With prolonged exposure to ionizing radiation as the principal traps are filled an increasing number of electrons are theorized to recombine radiatively [b] which results in UV and visible light emissions at high doses, this was observed by Trautmann et al. (1999).

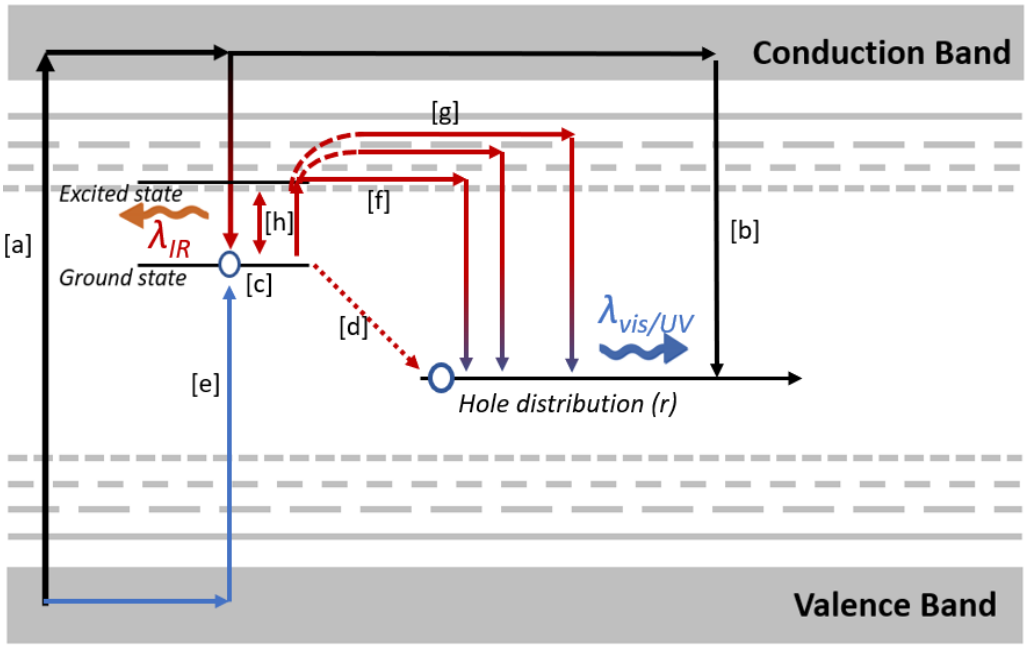

Fig. 1.2: Summary illustration of the different luminescence dating transition models involved in IR-RF, IRSL, pIRIR and IRPL measurements based on Trautmann et al (1999), Jain and Ankaergaard (2011) and Kumar et al. (2020), and modified after Murari et al. (2021). Arrows indicate electron transitions: black lines indicate natural pathways; red arrows indicate the involvement of IR light as either as an output or as an input of energy. Transition from black to red shows the IR-RF signal, red to blue the IRSL signal induced by IR stimulation. [a] Constant flow of electrons travel from the valence to the conduction band as a result of exposure to ongoing ionizing radiation. Electrons combine radiatively [b] or populate the principal trap [c] (other possible pathways excluded for clarity, include the immediate drop back to the valence band and the recombination of electrons non-radiatively). Electrons entering the principal trap produce IR-RF when passing through the excited state. A proportion of electrons can tunnel directly from the principal trap to proximal holes [d]. During IRSL measurements electrons in the principal trap when stimulated with infrared light will reach the excited state, migrate locally and recombine with proximal holes [f]. Higher temperature measurements (e.g. $pIRIR_{290}$) provide phonon-assistance and result in the electrons diffusing through the band tail states and recombine with distal holes [g], which are observed to be more stable. In the case of IRPL measurements, electrons are stimulated by infrared light within the principal trap and release a photon but do not escape the trap [h].

The identification and physical nature of the defects related to the luminescence emissions in K-feldspar is a subject that is still undergoing research. Thus far, studies have largely used indirect measurements and correlation studies to assign traps and recombination centres (e.g., Erfurt, 2003b). The principal K-feldspar emissions and their likely associated origins were discussed by Krbetschek et al. (1997); however, due to the complexity of feldspar solid solution

and the many opportunities for the inclusion of substitute ions, isolating and verifying the origins of specific emissions is exceedingly difficult. Erfurt (2003a) and Erfurt and Krbetschek (2003a) proposed that the IR-RF emission could be a result of the excitation of Pb^{2+} to (Pb^{+}) * and relaxation to the Pb^{+} ground state (~1.43 eV) following observations that the IR-RF signal intensity increases with an increase of Pb content (30 ppm to 1400 ppm). In addition to Pb^{+}, Fe^{3+} ions have been theorised to be associated with the red to deep-red emission at approximately 1.7 eV (Prasad and Jain, 2018). Kumar et al. (2018) investigated whether the IR-RF signal correlated with that of their IRPL signals, and suggested that both signals likely originate in the same defects but that the IRPL stimulation probes specific defects (~1.3 eV) while the IR-RF signal may have contributions from other defects, e.g. the Fe^{3+}, leading to a more mixed response. Recent work reported that there was a correlation of K-content with the emission peak position using infrared cathodoluminescence (IRCL) experiments at 7 K (Kumar et al., 2020).

1.2.2 Signal characteristics

Extensive spectroscopic investigations of the IR-RF signal revealed that K-feldspar emits many peaks at different wavelengths, the most stable of which was at 865 nm with its intensity decreasing systematically with an increase in irradiation (Trautmann et al., 1998; 2000; Krbetschek and Trautmann, 2000). Two other peaks were observed at 710 nm and at 910 nm and had the potential to interfere with the main IR-RF peak (Trautmann, 1999; Schilles, 2002), of which the 710 nm peak was observed to be unstable and to increase with increasing dose (Trautmann, 1999). The need to remove the neighboring peaks provided the detection range needed to isolate the main IR-RF signal using the appropriate filter combinations.

Resetting or fully bleaching any luminescence signal is a critical step in the dating process. The early bleaching experiments conducted by Trautmann et al. (1999) were done in natural direct sunlight for 2 - 5 h, later investigation revealed that that shorter wavelengths (500 nm) were more efficient at bleaching the IR-RF signal (Trautmann, 2000). Buylaert et al. (2012) compared the built-in UV LEDs (700 mW/cm^2) in the Risø readers with an exposure time of 25 min (1500 s) with the Hönle SOL 2 solar simulator for 4 h, determining that 25 min with the UV LEDs was sufficient. While in contrast Varma et al. (2013) observed that the optimal bleaching time using the said UV LEDs was 800 s. Recently, Frouin et al. (2015) systematically and comprehensively

investigated the bleaching behavior of the IR-RF signal. They observed that the IR-RF signal can be completely bleached using wavelengths from 365 – 850 nm, and recommend a light spectrum comparable with the terrestrial solar spectrum with the following settings: 365 nm (10 mW/cm^2), 462 nm (63 mW/cm^2), 525 nm (54 mW/cm^2), 590 nm (37 mW/cm^2), 623 nm (115 mW/cm^2), and 850 nm (96 mW/cm^2) (Frouin et al., 2015). Bleaching induced phosphorescence has been observed at 865 nm directly after bleaching, it is particularly strong when using a solar simulator (Erfurt and Krbetschek, 2003b; Frouin et al., 2015; Schaarschmidt et al., 2019) and less significant to negligible when using the UV LEDs in the Risø readers (Buylaert et al., 2012; Varma et al., 2013) and a pause of 1hr to 15 min before irradiation was recommended respectively.

Several investigations have reported a mismatch in curve shape between consecutive IR-RF measurements separated by different bleaching settings and types (Schilles and Habermann, 2000) as well as between the natural and regenerated curves generated by the IR-RF measurement (Buylaert et al., 2012; Varma et al., 2013; Frouin et al., 2017, Murari et al., 2018). These mismatches were attributed to IR-RF sensitivity changes induced by bleaching (Schilles and Habermann, 2000; Buylaert et al., 2012; Varma et al., 2013; Frouin et al., 2017, Murari et al., 2018). Schilles and Habermann (2000) also observed differences in IR-RF intensity in their comparison of solar simulator bleaching (5.1-8.9 %) vs natural light bleaching (3.6-4.8 %). Erfurt and Krbetschek (2003) showed that the IR-RF sensitivity would affect dose estimation by 3 %. Different correction methods and factors were put forward to overcome the sensitivity changes based on the specific bleaching conditions used (Schilles and Habermann, 2000; Varma et al., 2013). Murari et al. (2018) investigated dose recovery tests in which they compared IR-RF dose estimations from regenerated measurements on the same sample as the natural signal (4 %) with dose estimations in which they used the signal from a modern sample as the "regenerated" signal (23 %). In order to account for the observed sensitivity changes Murari et al. (2018) suggested a modification of the horizontal slide method for dose estimation to account for the vertical component called the horizontal and vertical slide method.

1.2.3 Applications

After the introduction of the IRSAR protocol by Erfurt and Krbetschek (2003), IR-RF was mainly applied to coarse-grained K-feldspar. Limited work has been done in polymineral fine-grains (Schilles, 2002; Kreutzer et al., 2018b; Coussot et al., 2019) and preliminary work in single grain and spatially resolved studies (Schilles 2002; Trautmann et al., 2000b). IR-RF dating has been applied to a wide range of glacial-fluvial and fluvial settings in Germany, in particular it was favoured in the dating and constraining of the Saalian glacial and the Eemian interglacial cycles (Degering and Krbetschek (2007), Krbetschek et al. (2008) and Kreutzer et al. (2014); Lauer and Weiss (2018)). In general, these showed good agreement with IR-RF and other chronologies generated using a range of different trapped charge methods such as $pIRIR_{290}$, fading corrected $pIRIR_{225}$, and electron spin resonance (ESR) as well as U-series dating. In contrast, Buylaert et al. (2012) compared IR-RF dating of coastal marine and colluvial sediments independent age control (radiocarbon, OSL and $pIRIR_{290}$) with no correlation (overestimation of samples aged 20-45 ka and underestimation of samples aged ~128 ka). The application of IR-RF dating to well bleached aeolian sediments should be particularly suitable, however both Wünnemann et al. (2007) and Novothy et al. (2010) report significant over estimation of the IR-RF signal relative to fading corrected IRSL ages when measuring aeolian sediments from North west China and Hungary respectively. Frouin et al. (2017) used a modified IR-RF signal (RF_{70}: preheated and measured at 70 °C) on modern aeolian samples and showed reasonably good agreement with independent age control (polymineral fine-grain) though the scatter in D_e results was large. In a study of coastal dynamics Kreutzer et al. (2018) observed systematic overestimation of the IR-RF signal compared with quartz OSL ages, however also showed reasonable agreement of older (200-330 ka) samples with ESR. Scerri et al. (2018) reported IR-RF ages consistent with $pIRIR_{290}$ ages within 2 σ. IR-RF dating appears to agree with independent age control in some instances and not in others, suggesting that there are still methodological problems to over-come, e.g.: there is no commonly accepted standard bleaching protocol, no commonly accepted definition of the limit of the IR-RF signal (e.g., $2D_0$ of IRSL and OSL) and no agreed upon criteria for aliquot rejection other than dose recovery tests (e.g., recuperation and recycling ratios in IRSL).

References

Aitken, M.J., Tite, M.S., Reid, J., 1964. Thermoluminescence dating of ancient ceramics. Nat. 202, 1032-1033.

Buylaert, J.P., Jain, M., Murray, A.S., Thomsen, K.J., Lapp, T., 2012. IR-RF dating of sand-sized K-feldspar extracts: a test of accuracy. Radiat. Meas. 47, 759–765. https://doi.org/10.1016/j.radmeas.2012.06.021

Degering, D., Krbetschek, M.R., 2007. Dating of interglacial sediments by luminescence methods. In: The Climate of Past Interglacials. Developments in Quaternary Sciences. Elsevier, pp. 157–171. https://doi.org/10.1016/S1571-0866(07)80036-4

Erfurt, G., 2003a. Infrared luminescence of Pb+ centres in potassium-rich feldspars. Phys. Status Solidi 200.

Erfurt, G., 2003b. Radiolumineszenzspektroskopie und -dosimetrie an Feldspäten und synthetischen Luminophoren für die geochronometrische Anwendung PhD thesis Technische Universität Bergakademie Freiberg, Germany, p. 141.

Erfurt, G., Krbetschek, M.R., 2003a. Studies on the physics of the infrared radioluminescence of potassium feldspar and on the methodology of its application to sediment dating. Radiat. Meas. 37, 505–510. https://doi.org/10.1016/S1350-4487(03)00058-1

Erfurt, G., Krbetschek, M.R., 2003b. IRSAR - a single-aliquot regenerative-dose dating protocol applied to the infrared radiofluorescence (IR-RF) of coarse-grain K-feldspar. Ancient TL 21, 35–42.429–438. https://doi.org/10.1002/pssa.200306700

Frouin, M., Huot, S., Mercier, N., Lahaye, C., Lamothe, M., 2015. The issue of laboratory bleaching in the infrared-radiofluorescence dating method. Radiat. Meas. 81, 212–217. https://doi.org/10.1016/j.radmeas.2014.12.012

Frouin, M., Huot, S., Kreutzer, S., Lahaye, C., Lamothe, M., Philippe, A., Mercier, N., 2017. An improved radiofluorescence single-aliquot regenerative dose protocol for K-feldspars. Quat. Geochronol. 38, 13–24. https://doi.org/10.1016/j.quageo.2016.11.004

Huntley, D.J., Godfrey-Smith, D.I., Thewalt, M.L.W., 1985. Optical dating of sediments. Nat. 313, 105-107.

Huntley, D.J., Lamothe, M., 2001. Ubiquity of anomalous fading in K-feldspars and the measurement and correction for it in optical dating. Can. J. Earth. Sci. 38, 1093-1106. https://doi.org/10.1139/e01-013

Hütt, G., Jaek, I., Tchonka, J. 1988: Optical dating of K-feldspars optical response stimulation spectra. Quat. Sci. Rev. 7, 381-385.

Kars, R. H., Wallinga, J. & Cohen, K. M. 2008: A new approach towards anomalous fading correction for feldspar IRSL dating – tests on samples in field saturation. Radiation Measurements 43, 786–790. https://doi.org/10.1016/j.radmeas.2008.01.021

Krbetschek, M.R., Götze, J., Irmer, G., Rieser, U., Trautmann, T., 2002. The red luminescence emission of feldspar and its wavelength dependence on K, Na, Ca ± composition. Mineral. Petrol. 76, 167–177. https://doi.org/10.1007/s007100200039

Krbetschek, M.R., Erfurt, G., Degering, D., 2003. Radiofluorescence Dating: A Novel Method for Age Determination of Clastic Sediment Deposits from about 20 Ka to 300 Ka. Poster presentation; XVI Inqua Congress, Reno (USA).

Krbetschek, M.R., Degering, D., Alexowsky, W., 2008. Infrarot-Radiofluoreszenz-Alter (IR-RF) unter-saalezeitlicher Sedimente Mittel- und Ostdeutschlands. Z. Dtsch. Ges. Geowiss. 159, 133–140. https://doi.org/10.1127/1860-1804/2008/0159-0133

Kreutzer, S., Murari, M.K., Frouin, M., Fuchs, M., Mercier, N., 2017. Always remain suspicious: a case study on tracking down a technical artefact while measuring IR-RF. Ancient TL 35, 20–30.

Kreutzer, S., Duval, M., Bartz, M., Bertran, P., Bosq, M., Eynaud, F., Verdin, F., Mercier, N., 2018a. Deciphering long-term coastal dynamics using IR-RF and ESR dating: a case study from Médoc, south-west France. Quat. Geochronol. 48, 108–120. https://doi.org/10.1016/ j.quageo.2018.09.005

Kreutzer, S., Martin, L., Dubernet, S., Mercier, N., 2018b. The IR-RF alpha-Efficiency of K-feldspar. Radiat. Meas. 120, 148–156. https://doi.org/10.1016/j.radmeas.2018.04.019

Kreutzer, S., Mercier, N., Lamothe, M., 2022. Infrared-radiofluorescence: dose saturation and long-term signal stability of a K-feldspar sample. Radiat. Meas. 156, 106818.

Kumar, R., Kook, M., Murray, A.S., Jain, M., 2018. Towards direct measurement of electrons in metastable states in K-feldspar: do infrared-photoluminescence and radioluminescence probe the same trap? Radiat. Meas. 120, 1–17. https://doi.org/10.1016/j.radmeas.2018.06.018

Kumar, R., Martin, L.I.D.J., Poelman, D., Vandenberghe, D., De Grave, J., Kook, M., Jain, M., 2020. Site-selective mapping of metastable states using electron-beam induced luminescence microscopy. Sci. Rep. 10, 1270. https://doi.org/10.1038/s41598-020-72334-7

Kumar, R., Kook, M., Jain, M. 2022: Does hole instability cause anomalous fading of luminescence in feldspar? Jour of Lum. 252. https://doi.org/10.1016/j.lumin.2022.119403

Lauer, T., Weiss, M., 2018. Timing of the Saalian- and Elsterian glacial cycles and the implications for Middle – pleistocene hominin presence in central Europe. Sci. Rep. 8, 5111. https://doi.org/10.1038/s41598-018-23541-w

Lauer, T., Krbetschek, M.R., Frechen, M., Tsukamoto, S., Hoselmann, C., Weidenfeller, M., 2011. Infrared radiofluorescence (IR-RF) dating of middle pleistocene fluvial archives of the Heidelberg Basin (Southwest Germany). Geochron. 38, 23–33. https://doi.org/10.2478/s13386-011-0006-9

Li, B., Li, S.H., 2011. Luminescence dating of K-feldspar from sediments: A protocol without anomalous fading correction. Quat. Geochronol. 6, 468-479. https://doi.org/10.1016/j.quageo.2011.05.001

Mellett CL (2013) Luminescence dating. In: Clarke LE (ed) Geomorphological techniques (online edition). British Society for Geomorphology, London, pp 1–11. http://www.geomorphology.org.uk/assets/publications/subsections/pdfs/OnsitePublicationSubsection/90/4.2.6_luminescencedating.pdf

Murari, M.K., Kreutzer, S., Fuchs, M., 2018. Further investigations on IR-RF: dose recovery and correction. Radiat. Meas. 120, 110–119.

Murari, K.M., Kreutzer, S., King, G., Frouin, M., Tsukamoto, S., Schmidt, C., Lauer, T., Klasen, N., Richter, D., Friedrich, J., Mercier, N., Fuchs, M., 2021. Infrared radiofluorescence IR-RF dating: a review. Quat. Geochronol. 64, 101155.

Novothny, Á., Frechen, M., Horváth, E., Krbetschek, M.R., Tsukamoto, S., 2010. Infrared stimulated luminescence and radiofluorescence dating of aeolian sediments from Hungary. Quat. Geochronol. 5, 114–119. https://doi.org/10.1016/j.quageo.2009.05.002

Prasad, A.K., Jain, M., 2018. Dynamics of the deep red Fe 3+ photoluminescence emission in feldspar. J. Lumin. 196, 462–469. https://doi.org/10.1016/j.jlumin.2017.11.051

Prasad, A.K., Poolton, N.R.J., Kook, M., Jain, M., 2017. Optical dating in a new light: a direct, non-destructive probe of trapped electrons. Sci. Rep. 7, 461. https://doi.org/10.1038/s41598-017-10174-8

Preusser, F., Ramseyer, K., Schlüchter, C., 2006. Characterisation of low OSL intensity quartz 421 from the New Zealand Alps. Radiat. Meas. 41, 871–877. https://doi.org/10.1016/j.radmeas.2006.04.019

Scerri, E.M.L., Shipton, C., Clark-Balzan, L., Frouin, M., Schwenninger, J.-L., Groucutt, H.S., Breeze, P.S., Parton, A., Blinkhorn, J., Drake, N.A., Jennings, R., Cuthbertson, P., Omari, A.A., Alsharekh, A.M., Petraglia, M.D., 2018. The expansion of later Acheulean hominins into the Arabian Peninsula. Sci. Rep. 8, 17165. https://doi.org/10.1038/s41598-018-35242-5

Schilles, T., 2002. Die Infrarot-Radiolumineszenz von Feldspäten und ihr Einsatz in der Lumineszenzdatierung PhD thesis Ruprechts-Karls-Universität Heidelberg, Germany, p. 149

Schilles, T., Habermann, J., 2000. Radioluminescence dating: the IR emission of feldspar. Radiat. Meas. 32, 679–683. https://doi.org/10.1016/S1350-4487(00)00081-0

Schmidt, C., Kreutzer, S., DeWitt, R., Fuchs, M., 2015. Radiofluorescence of quartz: a review. Quat. Geochronol. 27, 66–77. https://doi.org/10.1016/j.quageo.2015.01.005

Sontag-González, M., Fuchs, M., 2022. Spectroscopic investigations of infrared-radiofluorescence (IR-RF) for equivalent dose estimation. Rad. Meas., 153. https://doi.org/10.1016/j.radmeas.2022.106733

Steffen, D., Preusser, F., Schlunegger, F., 2009. OSL quartz age underestimation due to 441 unstable signal components. Quat. Geochronol, 4, 353-362. https://doi.org/10.1016/j.radmeas.2018.08.019

Thiel, C., Buylaert, J.P., Murray, A., Terhorst, B., Hofer, I., Tsukamoto, S., Frechen, M., 2011. Luminescence dating of the Stratzing loess profile (Austria) - Testing the potential of an elevated temperature post-IR IRSL protocol. Quat. Int. 234, 23–31. https://doi.org/10.1016/j.quaint.2010.05.018

Thomsen, K.J., Murray, A.S., Jain, M., Bøtter-Jensen, L., 2008. Laboratory fading rates of various luminescence signals from feldspar-rich sediment extracts. Radiat. Meas. 43, 1474–1486. https://doi.org/10.1016/j.radmeas.2008.06.002

Trautmann, T., Krbetschek, M.R., Dietrich, A., Stolz, W., 1998. Investigations of feldspar radioluminescence: potential for a new dating technique. Radiat. Meas. 29, 421–425. https://doi.org/10.1016/S1350-4487(98)00012-2

Trautmann, T., Krbetschek, M.R., Dietrich, A. Stolz, W., 1999. Feldspar radioluminescence; a new dating method and its physical background. Jour. of Lumin. 85, 45-58. https://doi.org/10.1016/S0022-2313(99)00152-0

Trautmann, T., Krbetschek, M.R., Stolz, W., 2000b. A systematic study of the radioluminescence properties of single feldspar grains. Radiat. Meas. 32, 685–690. https://doi.org/10.1016/S1350-4487(00)00077-9

Varma, V., Biswas, R.H., Singhvi, A.K., 2013. Aspects of infrared radioluminescence dosimetry in K-feldspar. Geochron. 40, 266–273. https://doi.org/10.2478/s13386-013-0125-6

Wagner, G.A., Krbetschek, M.R., Degering, D., Bahain, J.J., Shao, Q., Falguères, C., Voinchet, P., Dolo, J.M., Garcia, T., Rightmire, G.P., 2010. Radiometric dating of the type-site for Homo heidelbergensis at Mauer, Germany. Proc. Natl. Acad. Sci. Unit. States Am. 107, 19726–19730. https://doi.org/10.1073/pnas.1012722107

Wallinga, J., 2002. Optically stimulated luminescence dating of fluvial deposits: a review. Boreas 31, 303-322. https://doi.org/10.1111/j.1502-3885.2002.tb01076

Wintle, A.G., 1973. Anomalous fading of thermo-luminescence in mineral samples. Nature 245, 143–144. https://doi.org/10.1038/245143a0 457

Wintle, A. G., 1997. Luminescence dating: laboratory procedures and protocols. Radiat. Meas. 09927, 769-817. https://doi.org/10.1016/S1350-4487(97)00220-5

Wintle, A.G., Huntley, D. J., 1982. Thermoluminescence dating of sediments. Quat. Sci. Reviews 1(1), 31-53.

Wintle, A.G., Huntley, D. J., 1980. Thermoluminescence dating of ocean sediments. Can. Jour. Ear. Sci. 17, 348-360)

Wünnemann, B., Hartmann, K., Altmann, N., Hambach, U., Pachur, H.-J., Zhang, H., 2007. 22. Interglacial and glacial fingerprints from lake deposits in the Gobi Desert, NW China. In: Sirocko, F., Claussen, M., Goni, M.F.S., Litt, T. (Eds.), The Climate of Past Interglacials. Elsevier., pp. 323–347 2007.

Chapter 2: Equipment and Methodology

2.1 Equipment

Initially, in the late 90s and early 2000s, home-made systems were used to conduct IR-RF research (Trautmann et al., 1998, 1999a; Schilles and Habermann, 2000; Erfurt et al., 2003), Today there are two ready-to-use automated systems available, namely the Risø TL/OSL reader (Lapp et al., 2012) and the Lexsyg readers (Richter et al., 2013). All luminescence measurements discussed in this dissertation were done on a prototype Risø TL/OSL DA-20 reader with automated detection and stimulation head (DASH) (Lapp et al., 2012) at the Leibniz Institute for Applied Geophysics in Hannover, Germany (Fig. 2.1.); with the exception of the IRPL measurements described in chapter 5 which were conducted on a Risø TL/OSL reader at the Danish Technical University, Department of Physics: Luminescence Physics and Technologies in Roskilde, Denmark.

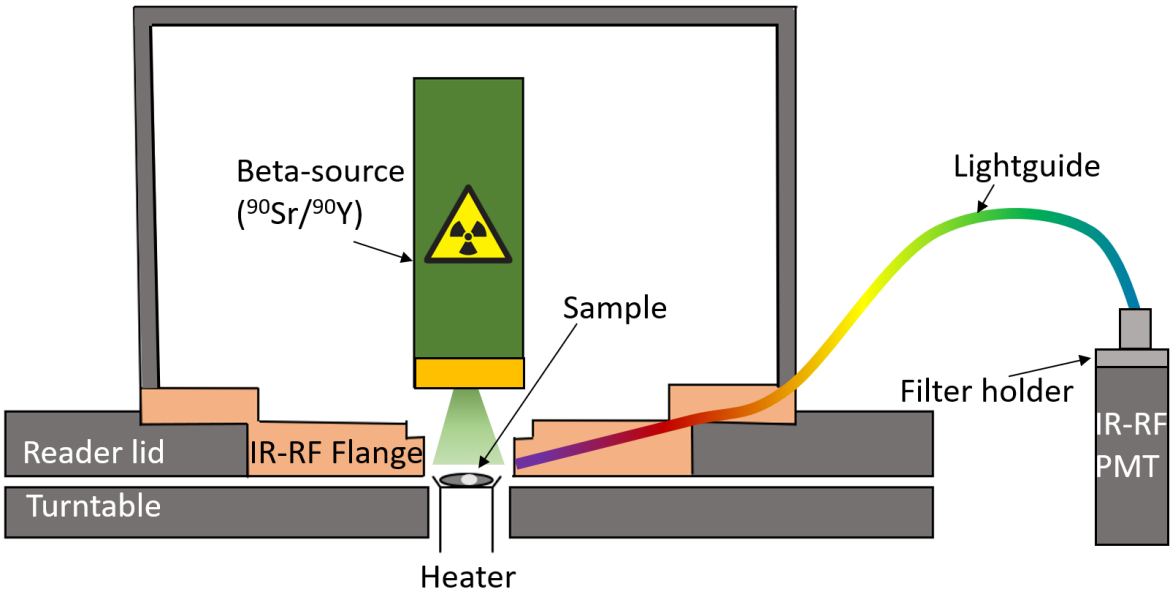

Fig. 2.1. Schematic diagram of the Risø OSL/TL reader with a focus on the equipment required for IR-RF measurements, redrawn from Lapp et al. (2012).

The reader is equipped with a ^{90}Sr/^{90}Y beta-source irradiation unit with a dose rate ranging from ~ 0.119 Gy/s to ~0.112 Gy for coarse-grains and ranging from ~ 0.0967 Gy/s to ~0.0947 Gy/s for polymineral fine grains (over three years of measurements) and was calibrated with Risø calibration quartz batch number 113. The infrared radiofluorescence response was detected using a Chroma D 900/100 interference filter (850 -945 nm). Aliquots were bleached using the ultraviolet LEDs operating at 90 % intensity housed in the Risø reader. X-ray fluorescence measurements were done using the XRF attachment coupled to the Risø reader.

2.2 Sample preparation

All samples were archived samples from the Leibniz Institute for Applied Geophysics in Hannover, coarse-grain (63 -150 µm), mid-grain (38 -63 µm) and polymineral fine-grain (4-11 µm) samples were prepared under subdued red-light conditions. All coarse grain samples were sieved to isolate the required grain size and underwent chemical treatments to remove carbonates, organic matter and clumping clays using hydrochloric acid, (HCL, 10 %) hydrogen peroxide (H_20_2, 30 %) and sodium oxalate (NaC_2O_4; 0.1 N), respectively. K-feldspar grains were then isolated using a two-step density separation process using sodium tungstate (Na_2WO_4) first at 2.62 g/cm^3 to separate the quartz and heavy minerals from the less dense feldspars then at 2.58 g/cm^3 to separate the alkaline feldspars grains from the plagioclase grains. Both density separation steps were a minimum of 3 hrs, while the density separation steps of the mid-grain samples were a minimum of 18 hrs to extract the K-feldspar mid-grain samples (< 2.58 g/cm^3) and the Na-feldspar mid-grain samples (2.58-2.62 g/cm^3). Coarse- and mid-grains were mounted to stainless steel disks using a thin layer of silicon oil as adhesive (small aliquots, 2.5 mm diameter). Polymineral fine-grain fractions (4-11 µm) were extracted with the use of a centrifuge through repeated cycles of washing and settling (Frechen et al., 1996). The fine-grains were (2 mg) mounted on aluminum discs using gravity settling from suspension in distilled water drops later evaporated in an oven at less than 50 ºC.

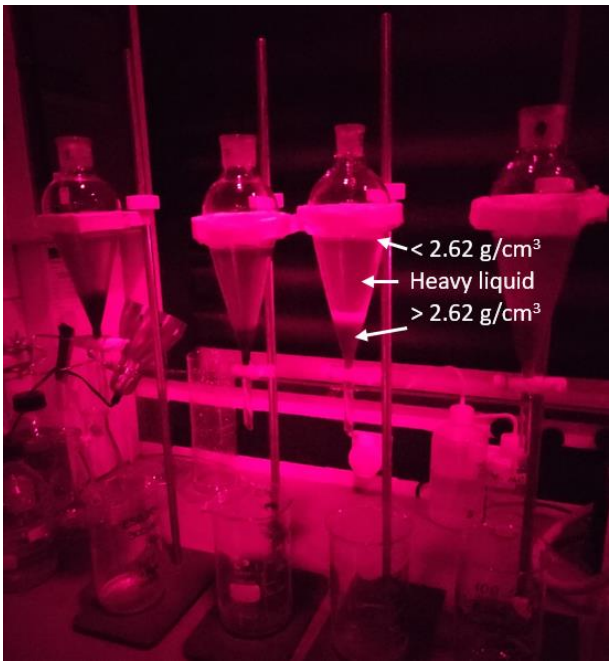

Fig. 2.2: Photo of the coarse grain density separation procedure.

2.3 Measurement parameters and equivalent dose determination

The IR-RF protocols used were largely based on the protocol developed by Frouin et al. (2017) with adaptions made to account for differences in readers, bleaching options and aliquot types (Table 2.1). A preheat was carried out first at 70 °C for 500 s, followed by continuous irradiation and measurement of the natural IR-RF signal for 5000 s. The sample was then bleached to fully reset the IR-RF signal, followed by a 1 hr pause to allow for the dissipation of bleaching induced phosphorescence (Erfurt and Krbetschek, 2003). Thereafter, a repetition of the same preheat parameters and a last continuous irradiation and measurement of the regenerated IR-RF signal for a minimum of 10 000 s (up to 30 000 s for older samples).

Table 2.1: The IR-RF dating protocol based on the RF_{70} protocol developed by Frouin et al. (2017) (Buchanan et al., 2022).

Step	IR-RF protocol	Observed
1	Preheat (70 °C, 500 s)	
2	Irradiation (70 °C, 5000 s)	Natural decay curve (RF_{nat})
3	Bleach (1500 s, *20 000 s)	
4	Pause 1 hr	
5	Preheat (70 °C, 500 s)	
6	Irradiation (70 °C, 20 000 s)	Regenerated decay curve (RF_{reg})

The IR-RF signal is described by an exponential decay curve, and IR-RF measurements generate two decay curves namely the natural and regenerated signal curves. The equivalent dose (D_e) was determined using the horizontal sliding method in which the natural curve is shifted on the dose (or x) axis until the curves overlap and the best fit is established. The horizontal distance the natural curve has shifted from its original position to the overlapped position describes the D_e. Murari et al. (2012) observed in their study focusing on dose recovery ratios that there is a change in sensitivity of the IR-RF signal induced by the bleaching step between the natural and regenerated measurements, which manifests as slight curve shape changes. As a result of this observation they recommend the inclusion of a vertical shift in the D_e determination procedure called the horizontal and vertical slide method.

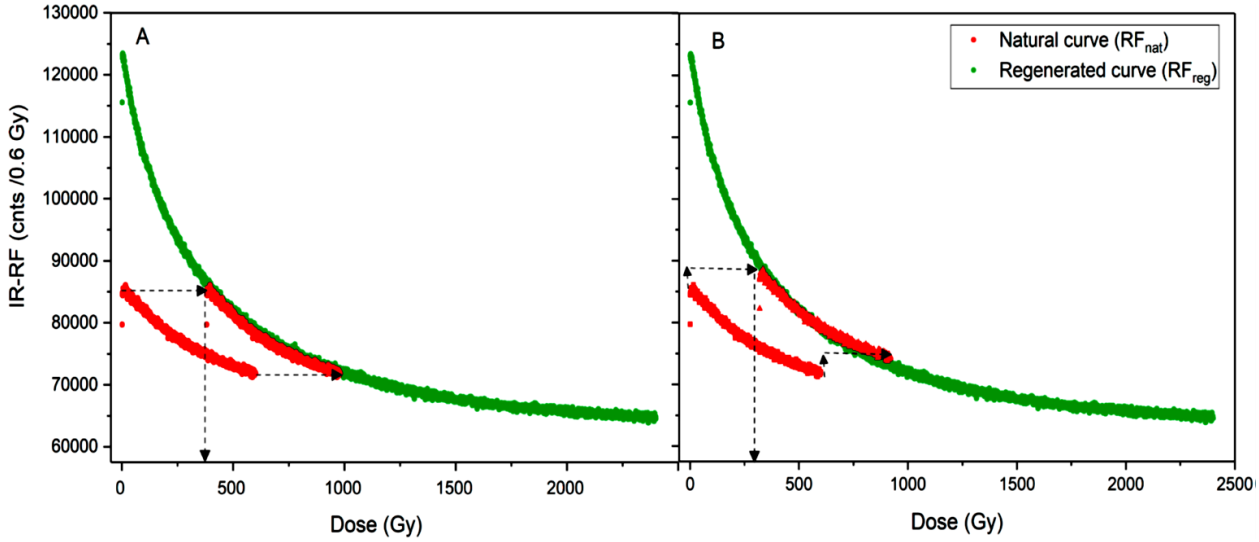

Fig 2.3: Example of the data output of the IR-RF signal and A) the 'horizontal sliding' method and B) the 'vertical and horizontal sliding' method; used to determine D_e for each aliquot (Buchanan et al., 2023).

An assessment of the samples' suitability for IR-RF dating was conducted through the employment of dose recovery tests to determine whether the sample can return a known given dose. Dose recovery tests were done by bleaching the sample, followed by a known dose irradiation step in with the dose is equivalent to the natural dose (Wallinga et al., 2000). There after the IR-RF measurement was measured using the same parameters as the equivalent dose measurements. The measured dose was then divided by the given dose, resulting in a dose recovery ratio. A dose recovery test is considered successful when the dose recovery ratio is within 10 % of unity. When dose recovery tests were unsuccessful (the dose regained was larger than acceptable), residual tests could be done to determine the residual dose retained by the sample. Additionally, in order to assess whether the bleaching step as sufficiently resetting the signal, bleachability tests were done in which different durations of beaching were compared. For more detailed descriptions of these tests refer to chapters 3,4 and 5.

References

Erfurt, G. & Krbetschek, M.R. 2003a: IRSAR-a single-aliquot regenerative-dose dating protocol applied to the infrared radiofluorescence (IR-RF) of coarse-grain K-feldspar. Ancient TL 21, 35-42.

Frechen, M., Schweitzer, U., Zander, A., 1996. Improvements in sample preparation for the fine grain technique. Ancient TL 14, 15–17.

Lapp, T., Jain, M., Thomsen, K.J., Murray, A.S., Buylaert, J.P., 2012. New luminescence measurement facilities in retrospective dosimetry. Radiat. Meas. 47, 803–808. http://doi.org/10.1016/j.radmeas.2012.02.006

Murari, M.K., Kreutzer, S., Fuchs, M., 2018. Further investigations on IR-RF: dose recovery and correction. Radiat. Meas. 120, 110–119.

Murari, K.M., Kreutzer, S., King, G., Frouin, M., Tsukamoto, S., Schmidt, C., Lauer, T., Klasen, N., Richter, D., Friedrich, J., Mercier, N., Fuchs, M., 2021. Infrared radiofluorescence IR-RF dating: a review. Quat. Geochronol. 64, 101155.

Richter A, Dornich K, 2013. Lexsyg - A new system for luminescence research. Geochron. 40(4): 220–228. https://doi.org/10.2478/s13386-013-0110-0

Schilles, T., Habermann, J., 2000. Radioluminescence dating: the IR emission of feldspar. Radiat. Meas. 32, 679–683. http://doi.org/10.1016/S1350-4487(00)00081-0

Trautmann, T., Krbetschek, M.R., Dietrich, A. Stolz, W., 1999. Feldspar radioluminescence; a new dating method and its physical background. Jour. of Lumin. 85, 45-58. https://doi.org/10.1016/S0022-2313(99)00152-0

Wallinga, J., Murray, A., Wintle, A., 2000. The single aliquot regenerative-dose (SAR) protocol applied to coarse grain feldspar. Radiat. Meas. 32, 529-533. https://doi.org/10.1016/S1350-4487(00)00091-3

Chapter 3:

Co-Author contributions.

This chapter was published in Radiation Measurements in 2022 and I am the first author. Archived (stored in Hannover) samples (60%) were used that were collected and partially prepared by Prof. Dr. Tsukamoto, Dr. Long and others both in China and in Hannover, Germany. A portion of (40 %) of the samples were prepared by me (K-feldspar) and Ms. Neda Rahimzadeh (quartz fine-grains). The main scientific idea frame work for the paper was outlined by Prof. Dr. Tsukamoto, while I added to and filled out the idea framework. I generated all of the luminescence data running luminescence experiments, with the support of Prof. Dr. Tsukamoto and Dr. Zhang. The regional dose rate data was generated by lab technicians for a previous study and regional dose rates calculated were generated by me using an R-script template written for general use by Dr. Zhang. The majority of analysis and interpretation was done by me, with the support of Prof. Tsukamoto and Dr. Zhang. I wrote the initial draft, which was reviewed by Prof. Dr. Tsukamoto, Dr. Zhang, and Dr. Long there after corrected/ edited by me and proof read by all authors.

Reference:

Buchanan, G.R., Tsukamoto, S., Zhang, J., Long, H., 2022. Testing the natural limits of infrared radiofluorescence dating of the Luochuan loess-palaeosol sequence, Chinese Loess Plateau. Radiat. Meas. 155. https://doi.org/10.1016/j.radmeas.2022.106797

Testing the natural limits of infrared radiofluorescence dating of the Luochuan loess-palaeosol sequence, Chinese Loess Plateau.

G.R. Buchanan [a],* , S. Tsukamoto [a] , J. Zhang [a] , H. Long [b]
[a] Leibniz Institute for Applied Geophysics, 30655, Hannover, Germany
[b] State Key Laboratory of Lake Science and Environment, Nanjing Institute of Geography and Limnology, Chinese Academy of Sciences (NIGLAS), Nanjing, 210008, China

Abstract

Testing the upper limit of infrared radiofluorescence (IR-RF) dating in nature is a critical step in developing our understanding of the signal and its potential. The Luochuan loess-palaeosol sequence on the Chinese Loess Plateau is a well-documented sequence spanning over 2.5 Ma, that has served as a proving ground for many trapped charge dating techniques, for example: feldspar post-infrared infrared stimulated luminescence (pIRIR), quartz electron spin resonance (ESR), and quartz violet stimulated luminescence (VSL). This study evaluates the IR-RF signal from coarse-grained feldspar on 10 samples from the loess-palaeosol sequence with depositional ages ranging from ~25 ka to ~900 ka. Initial work tested 6 samples using the RF_{70} protocol with a bleaching duration of 1500 s using UV-LEDs between the natural and regenerated IR-RF measurements which resulted in consistent and significant underestimation across all but the youngest sample. The bleaching duration was increased to 20 000 s and tested on 10 samples. The IR-RF ages of 5 samples younger than 300 ka (~1100 Gy) were consistent with the reference ages while the IR-RF ages for samples older than 300 ka were still significantly underestimated. Natural and laboratory dose response curves were constructed, and they revealed significantly different curves in the case of the shorter bleaching duration, but consistent curves in the case of the longer bleaching duration, confirming the importance of the selected bleaching duration. Furthermore, our study suggests that while the IR-RF signal of feldspar can be used successfully to date samples up to 1100 Gy (~300 ka at our site), it may not be possible to reach the theoretical laboratory-generated dating limit of 3500 Gy.

3.1. Introduction

Initially characterised by Trautmann et al. (1998), the infrared radiofluorescence (IR-RF) signal represents an alternative approach to conventional infrared stimulated luminescence (IRSL) of potassium-rich feldspars (K-feldspar), but instead uses continuous ionising irradiation to stimulate an infrared emission peaked at 1.43 eV (865 nm) (Trautmann et al., 1999; Erfurt and Krbetschek, 2003). This signal theoretically corresponds directly with and is proportional to the quantity of electrons being trapped, in previously empty traps, during irradiation (Trautmann et al., 1998), while IRSL signals are theorised to correspond to recombination pathways which are more complex. The IR-RF signal has advantages over other luminescence signals in that: 1) the required measurement time is generally shorter than that of conventional single aliquot regenerative dose (SAR) protocols, 2) there is a high resolution of data generated (many data points recorded) in the dose response curve, 3) there is the possibility that the IR-RF signal may not suffer from fading, and 4) the age range is expected to be larger due to the curves having better resolution (Murari et al., 2021). Erfurt and Krbetschek (2003b) showed that depending upon dose rates the dating limit of IR-RF could be around 1200–1500 Gy, while Murari et al. (2018) reported laboratory-generated equivalent doses up to ~3500 Gy using dose recovery experiments. However, there are a limited number of studies that have assessed this dating limit in nature. Recent work done on the IR-RF signal at elevated temperatures has seen the development of a new protocol, RF70, which shows promising results reporting equivalent dose measurements of up to 2000 Gy (Frouin et al., 2017). In this study we evaluate the RF70 signal from coarse-grained K-feldspar on samples that approach and pass the saturation dose outlined by Erfurt and Krbetschek (2003b) and compare the age results with independent age control.

The Luochuan loess-palaeosol sequence on the Chinese loess plateau is an excellent natural laboratory and testing ground with which to test trapped charge geochronology methodologies as it offers a continuous record of deposition in the region spanning more than 2.5 million years. An advantage of this sequence is the well-delineated independent age control developed by Ding et al. (2002) using orbital tuning of high-resolution grain size records and correlation with a composite marine $\delta^{18}O$ record. A plethora of geochronological studies have been done in the region including but not limited to: blue optically stimulated luminescence (OSL) (Chapot et al., 2012), thermally transferred (TT-) OSL (Chapot et al., 2016), violet stimulated luminescence (VSL) (Ankjærgaard et al., 2016; Rahimzadeh et al., 2021), fading corrected post-infrared infrared

stimulated luminescence (pIRIR225) and pulsed IRSL (Li et al., 2018), multiple elevated temperature (MET-) pIRIR (Li and Li, 2012; Zhang & Tsukamoto, 2022), and electron spin resonance (ESR) (Tsukamoto et al., 2018; Richter et al., 2020).

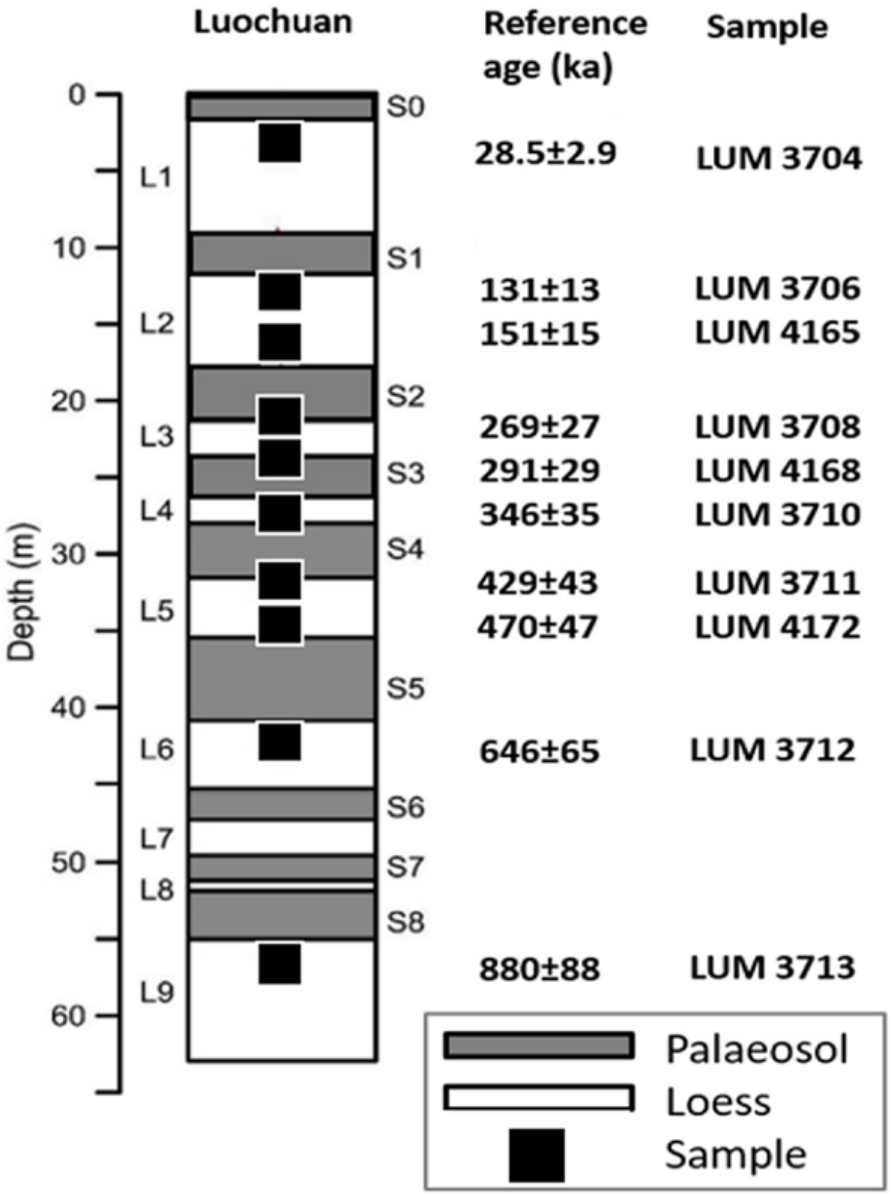

Fig. 3.1. Graphic representation of the Luochuan loess-palaeosol sequence illustrating the sample depth, relative position, and reference ages calculated from Ding et al. (2002).

3.2. Methodology

3.2.1. Sample preparation

Ten loess samples were collected from the Luochuan sequence in Potou village from units L1 to L9 as delineated by Ding et al. (2002) with ages ranging from ~25 ka (L1) to ~900 ka (L9) (Fig. 3.1.). The samples were collected by hammering light tight cylinders into exposed profiles, or as whole blocks depending upon how cemented the loess was. After initial sieving at the Nanjing Institute of Geography and Limnology, Chinese Academy of Sciences (NIGLAS) in China, the coarse fractions (>63 μm) of all the samples were prepared, stored and tested at the Leibniz Institute for Applied Geophysics in Hannover, Germany, under subdued red light. Seven of the samples (LUM3704, LUM3706, LUM3708, LUM3710, LUM3711, LUM3712 and LUM3713) were prepared in 2018 to extract the 63–100 μm K-feldspar grains. These seven samples were also used in Li et al. (2018), Tsukamoto et al. (2018) and Richter et al. (2020) to explore the IRSL properties of coarse-grained feldspar and the ESR properties of quartz, respectively. The other three samples (LUM4165, LUM4168 and LUM4172) were prepared in 2020 and the 63–150 μm fraction of K-feldspar grains were extracted due to a scarcity of feldspar in the samples. Raw samples were initially wet sieved to isolate the required grain size fraction. Thereafter, carbonates, organic matter, and clay particles were removed through the application of hydrochloric acid (HCl; 10 %), hydrogen peroxide (H_2O_2; 30 %) and sodium oxalate ($Na_2C_2O_4$; 0.1 N), respectively. Finally, heavy liquid separation was utilised to extract the K-feldspar grains (<2.58 g/cm3). Small aliquots (2.5 mm diameter) were prepared by mounting the K-feldspar grains on stainless-steel discs using a thin layer of silicone oil as adhesive.

3.2.2. Instrumentation and protocols

The IR-RF measurements were carried out on an automated Risø TL/ OSL DA-20 reader equipped with an automated detection and stimulation head (DASH) (Lapp et al., 2012). The IR-RF signal was stimulated using a $^{90}Sr/^{90}Y$ beta radiation source with a dose rate of approximately 0.119 Gy/s. The signal was detected through a Chroma D 900/100 interference filter (850–945 nm) and the bleaching was carried out using an ultraviolet (UV) LED operating at 90 % intensity (395–410 nm, 900 mW) and housed inside the Risø reader. The IR-RF protocol used was based on the protocol developed by Frouin et al. (2017) to detect the RF signal at 70 °C (RF_{70}), with some minor alterations due in part to the difference in the equipment as Frouin et al. (2017) used

a Lexsyg Research instrument (Richter et al., 2013). Initially, a preheat was done at 70 °C for 500 s which is shorter than the 900 s preheat outlined by Frouin et al. (2017) as thermal lag is less significant when using steel disks (Frouin et al. (2017) used steel cups). The preheat was followed by the natural IR-RF measurement, in which the sample was irradiated for 5000 s and the intensity of the IR-RF signal was measured. The sample was then bleached using the in-house UV LED followed by an hour-long pause to allow the phosphorescence generated by bleaching to subside (Erfurt, 2003). Initially, bleaching was done for 1500 s (a deviation from the 10800 s bleaching used by Frouin et al. (2017) due to different bleaching equipment) as suggested by Buylaert et al. (2012), and later it was extended to 20 000 s. Subsequent to the post-bleaching pause, a second preheat was done at 70 °C for 500 s and the regenerated IR-RF measurement took place. The sample was then irradiated for at least 10 000 s (up to 30 000 s for older samples) and the regenerated IR-RF signal was measured (Table 3.1).

Table 3.1: The IR-RF dating protocol based on the RF_{70} protocol developed by Frouin et al. (2017).

Step	IR-RF protocol	Observed
1	Preheat (70 °C, 500 s)	
2	Irradiation (70 °C, 5000 s)	Natural decay curve (RF_{nat})
3	Bleach (1500 s, *20 000 s)	
4	Pause 1 hr	
5	Preheat (70 °C, 500 s)	
6	Irradiation (70 °C, 20 000 s)	Regenerated decay curve (RF_{reg})

3.2.3. IR-RF D_e estimation

Every IR-RF measurement generates two exponential decay curves, the first and shorter of which is the natural signal (RF_{nat}) and the second and longer of which is the regenerated signal (RF_{reg}) (Fig. 3.2). In order to obtain the equivalent dose (D_e), we used the horizontal sliding method as outlined by Buylaert et al. (2012) in which the natural curve is horizontally shifted along the regenerated dose (or x-) axis until the two curves overlap (Fig. 3.2). The length of the horizontal shift from the original position to the new overlapping position is the De (Buylaert et al., 2012). This method of analysis was used as it does not rely

on the physical assumptions that constrain different models that may be used in other analyses such as extrapolation and interpolation. Additionally, the high number of individual data points used makes the sliding method statistically more robust (Buylaert et al., 2012). Analysis for the horizontal sliding method was done using the RLanalyse (version 1.30) software associated with the Risø readers. The vertical and horizontal sliding method of Murari et al. (2018) was also tested, and the analysis was done using the function analyse_IRSAR.RF from the R 'Luminescence' package (Kreutzer et al., 2017; Kreutzer, 2019).

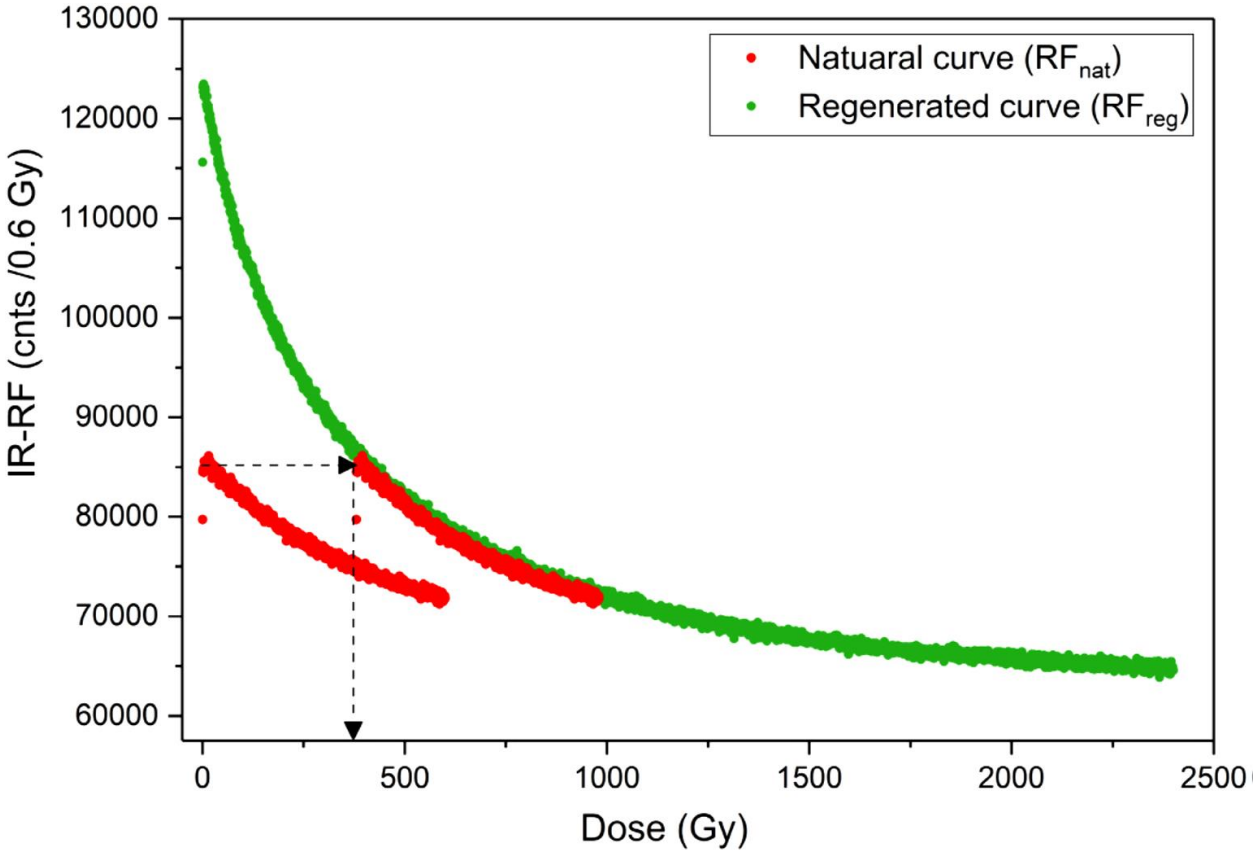

Fig. 3.2. Data output of the IR-RF signal and the horizontal sliding method used to determine the D_e for one aliquot. The smaller curve is the initial natural measurement curve, the larger curve in green is the regenerated measurement curve and the point at which the black arrowhead falls on the x-axis is the D_e

3.2.4. Environmental dose rates and expected ages

High resolution gamma spectrometry was used to determine radionuclide specific activities (Bq/kg) which were converted to concentrations of uranium (U, ppm), thorium (Th, ppm) and potassium (K, %) for all the samples (Table 3.2). The dose rate samples were stored for at least a month to ensure equilibrium buildup between ^{222}Rn and its daughter isotopes. Additionally, the water content was assumed to be 15 ± 5 % for all samples, in line with previous studies on the sequence (Li et al., 2018; Rahimzadeh et al., 2021). The cosmic dose rate was calculated following Prescott and Hutton (1994a). The radionuclide conversion factors and beta attenuation factors of Liritzis et al. (2013) and Gu´erin et al. (2012) were used, respectively. Following Kreutzer et al. (2018) the a-value was set to 0.07 ± 0.01. The internal dose rate was calculated with a K concentration of 12.5 ± 0.5 % (Huntley and Baril, 1997) and a^{87}Rb content of 400 ± 100 ppm (Huntley and Lamothe, 2001). The reference ages were calculated from Ding et al. (2002), which used orbital tuning of high-resolution grain size records and correlation with a composite marine δ^{18}O record to obtain the chronology of the sequence. It is worth mentioning that the chronology reported by Ding et al. (2002) was built upon relative dating techniques that require relative curve matching. While inherent assumptions are introduced when comparing relative and absolute ages, the large number of independent luminescence studies that have generated absolute age results that are consistent the Ding et al. (2002) chronology support its use in this instance. Because the reference ages provided by Ding et al. (2002) are on the boundaries of each depositional unit and our samples were collected from between these boundaries we interpolate the ages by assuming a constant accumulation rate between the boundary ages of each unit (Table 3.2). These assumptions prompt the assignment of a conservative uncertainty of 10 % which is in line with studies conducted by Ankjærgaard et al. (2016), Li et al. (2018), Richter et al. (2020) and Rahimzadeh et al. (2021).

Table 3.2: Summarising the radionuclide concentrations of U, Th and K, depths, dose rates, equivalent dose (Gy), age (ka), the expected dose rates and reference ages from Ding et al. (2002) and both the fading uncorrected and fading corrected results of Li et al. (2018) (using the $pIRIR_{225}$ signal).

							1500 s Bleach protocol 'horizontal slide'		**1500 s Bleach protocol 'horizontal & vertical slide'**		**20 000 s Bleach protocol**		**Ding et al. (2002)**		**Li et al. (2018)**	
Sample	LUM	Depth (m)	U (ppm)	Th (ppm)	K (%)	Dose rate (Gy/ka)	De (Gy)	Age (ka)	De (Gy)	Age (ka)	De (Gy)	Age (ka)	Expected Dose (Gy)	Ref age (ka)	$pIRIR_{225}$ Uncorr. (ka)	$pIRIR_{225}$ Corr. (ka)
L1(2)	3704	3.5	2.8±0.1	11.5±0.2	1.9±0.1	3.65±0.17					109±7	30±2	106±11	29±3	25±1	29±2
L2(1)	3706	11.9	2.3±0.1	10.1±0.2	1.6±0.1	3.06±0.16	380±36	124±12	654±42	214±14	394±24	129±8	401±40	131±13	109±6	146±8
L2(2)	4165	13.9	2.5±0.2	11.2±0.6	1.9±0.1	3.47±0.23					693±49	199±14	525±52	151±15		
L3(1)	3708	22.2	2.6±0.1	11.6±0.2	1.8±0.1	3.38±0.23	467±16	138±5	714±20	211±6	834±99	247±29	908±91	269±27	143±9	225±18
L3(2)	4168	23.1	2.2±0.1	11.1±0.6	1.8±0.1	3.29±0.23					1218±172	370±52	957±95	291±29		
L4(1)	3710	26.4	2.5±0.1	11.7±0.2	1.9±0.1	3.40±0.17	578±41	170±12	826±41	243±12	552±26	162±8	1176±119	346±35	164±9	246
L5(1)	3711	32.5	2.8±0.1	11.2±0.2	1.8±0.1	3.38±0.17	680±69	201±20	935±67	277±20	625±34	185±10	1448±145	429±43	177±9	>295
L5(2)	4172	34.9	2.4±0.1	11.5±0.7	1.9±0.1	3.45±0.23					1033±91	300±26	1620±162	470±47		
L6(1)	3712	42.6	2.5±0.1	11.2±0.2	1.8±0.1	3.30±0.17	759±71	230±21	991±61	300±18	765±46	232±14	2134±215	646±65	196±9	>290
L9(1)	3713	56.4	2.6±0.1	10.8±0.2	1.7±0.1	3.24±0.16	797±11	246±3	1047±9	323±3	833±38	257±12	2849±28	880±88	219±14	>305

3.3. IR-RF measurements and results

3.3.1. Age results

Employing the horizontal sliding method as described previously, D_e values were determined initially for six samples (LUM3706, LUM3708, LUM3710, LUM3711, LUM3712 and LUM3713) using the protocol with the shorter bleaching duration of 1500 s. Six aliquots of each sample were measured. The D_e results ranged from 380 ± 36 Gy (LUM3706) to 797 ± 11 Gy (LUM3713) (Table 2, Fig. 3.3), and the ages were then calculated by dividing the mean D_e of each sample by their respective dose rates. This resulted in all the samples except the youngest (LUM3706) significantly underestimating the reference ages of Ding et al. (2002) for all the samples except the youngest (LUM3706) (Table 2; Fig. 3.4, inset). These initial age data are similar to that of the fading uncorrected $pIRIR_{225}$ ages reported by Li et al. (2018) in which they showed significant underestimations relative to the reference ages (Table 2). While the $pIRIR_{225}$ signal is expected to fade and clearly does in the case of Li et al. (2018), there has been no clear evidence of fading in the IR-RF signal. An alternative explanation was tested; it was theorised that this consistent underestimation may be related to the bleaching time in the IR-RF protocol being insufficient. An incomplete bleach would result in a diminished IR-RF response as traps are already occupied and this does not allow the regenerated IR-RF curve to begin from a point of true zero (or highest initial IR-RF response). This would result in an underestimated D_e relative to a measurement with a complete bleach. Subsequently the bleaching time was increased to 20 000 s. Additionally four samples were collected from the upper (younger) part of the sequence (LUM3704, LUM4165, LUM4168, LUM4172) to test the IR-RF behavior in the expected dating range. The D_e results of the 20 000 s bleaching length protocol range from 109 ± 7 Gy (LUM3704) to 1218 ± 172 Gy (LUM4168), with the older samples (LUM3710, LUM3711, LUM4172, LUM3712, LUM3713) once again exhibiting underestimation, ranging from 552 ± 26 Gy (LUM3710) to 833 ± 38 Gy (LUM3713) (Table 2, Fig. 3.4). The calculated age results using the 20 000 s bleach are consistent with the reference ages for the younger samples (LUM3704 to LUM4168) up to approximately 300 ka indicating that the protocol using the longer bleaching time was successful for this age range (Fig. 3.4).

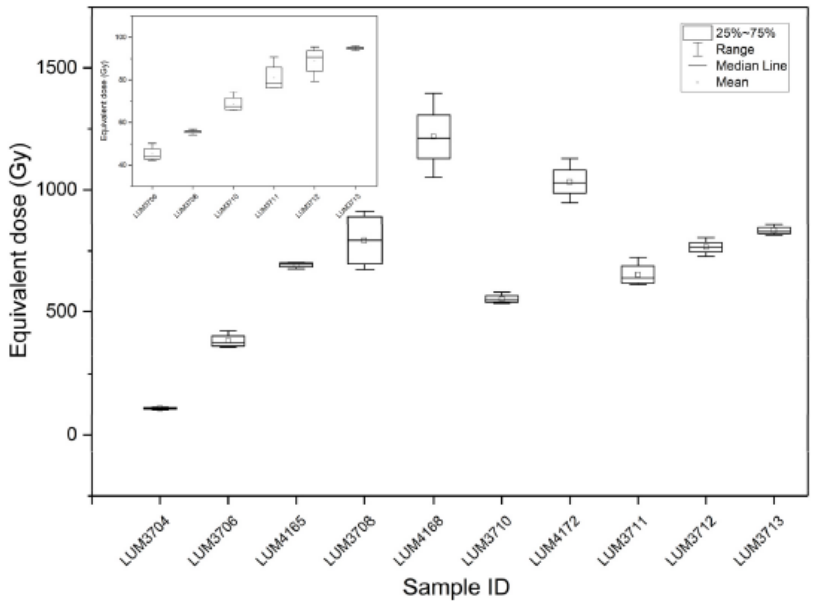

Fig. 3.3. Distribution of D_e results for each sample, the larger graph shows data for the 20 000 s bleaching protocol and the inset shows data for the 1500 s bleaching protocol.

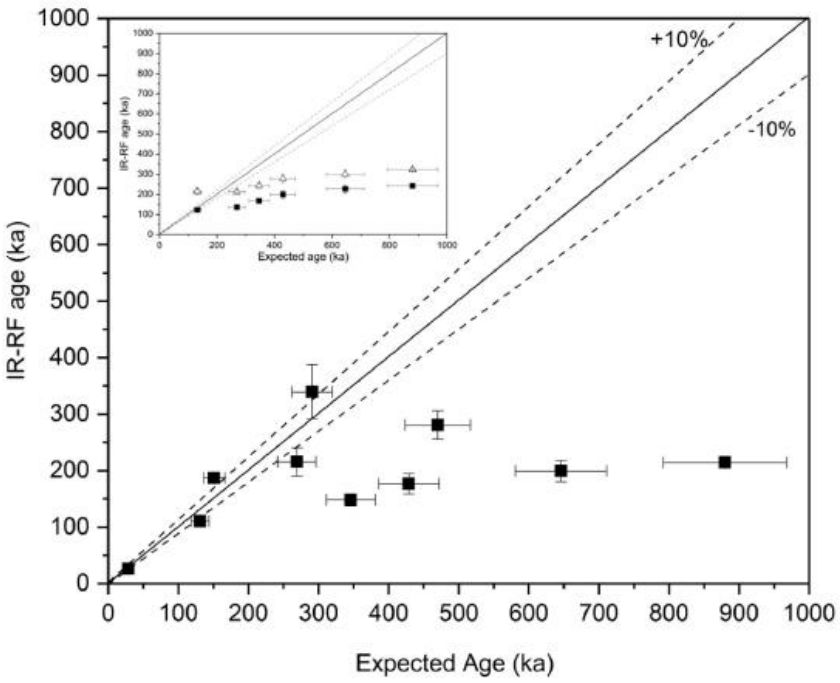

Fig. 3.4. Comparison of the IR-RF ages (ka) to the reference ages from Ding et al. (2002), in which the solid 1:1 line represents the reference ages and the dashed lines represent a ±10% error on either side of the reference ages. The inset graph shows results for the 1500 s bleaching duration measurement (solid squares) and the vertical and horizontal sliding method for D_e estimation (open triangles) and the main graph shows the results for the 20000 s bleaching protocol with the horizontal sliding method. The error bar is 1σ.

3.3.2. Dose recovery tests

Dose recovery tests were done to evaluate whether the protocol used can reliably measure D_e values. For each dose recovery measurement three aliquots were used for each sample and the result reported is the arithmetic mean of the three aliquots and the 1-σ standard error. Two sets of dose recovery tests were performed with different bleaching duration. In one set, the samples were initially bleached (zeroed) for 1500 s in the Risø reader with the UV LED, and then given doses. Subsequently, the IR-RF measurement was run to measure the D_e using the 1500 s bleaching duration. The dose recovery ratio was then calculated as a ratio of the measured dose divided by the given dose and a result of within 10% of unity was considered successful. The second set of dose recovery tests was a repetition of the first one but with a longer duration of 20 000 s for the initial (zeroed) bleaching step and the bleaching step within the protocol (between the natural and the regenerated curve). The results for samples LUM3704, LUM3706, LUM4165, LUM3708, LUM4168 are shown in Fig. 3.5. The dose recovery experiments with shorter bleaching gave dose recovery ratios of less than 0.9 for all except the youngest sample, which had a dose recovery ratio of 1.05 ± 0.08. Therefore, the dose recovery for the shorter bleaching duration was only successful for LUM3704 (Fig. 3.5a). The longer bleaching dose recovery experiment resulted in dose recovery ratios ranging from 0.92 ± 0.07 to 1.00 ± 0.10, and is therefore considered to be successful. These dose recovery results are consistent with the age results and suggest that these are analogous (Fig. 3.5b). One key observation is that while the average of the three aliquots for sample LUM4168 reflects a successful dose recovery, the spread of data on individual aliquots (grey dots) is large. The resulting large uncertainly is to be expected as the older samples are approaching the horizontal part of the IR-RF curve where miniscule changes in the signal detected will result in large differences in the D_e measured.

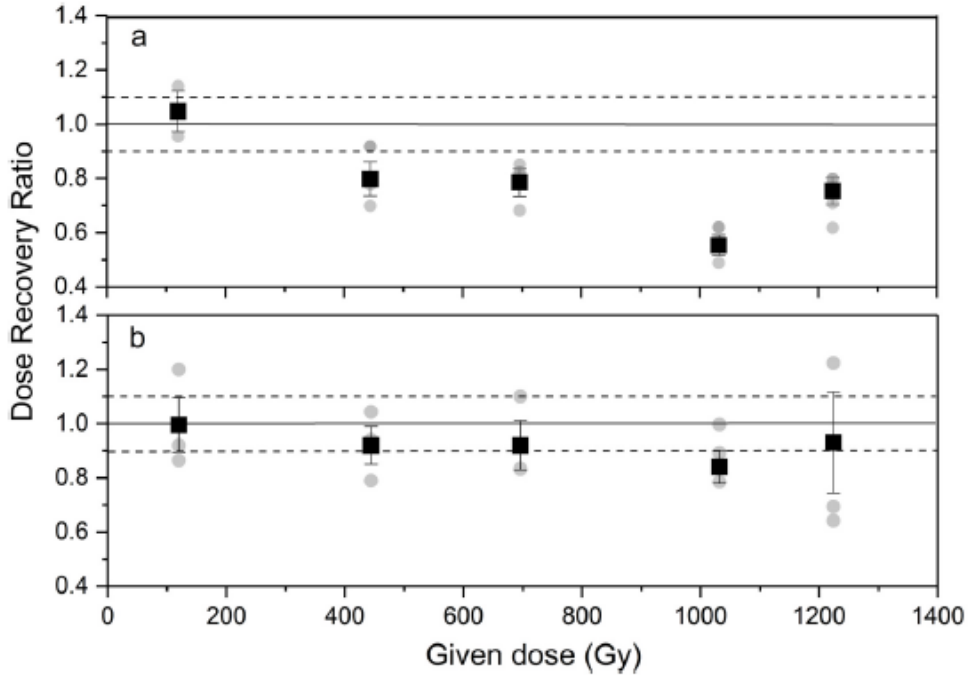

Fig. 3.5. a) Dose recovery ratios for samples LUM3704, LUM3706, LUM4165, LUM3708 and LUM4168 using the 1500 s bleaching duration; b) Dose recovery ratios for samples LUM3704, LUM3706, LUM4165, LUM3708 and LUM4168 using the 20 000 s bleaching duration. The solid line corresponds to the target of unity for the dose recovery to be successful, and the dashed lines are indicative of a 10 % margin. The grey circles are the individual aliquot results, and the black squares are the mean values. The error bar is 1σ.

3.3.3. Bleachability tests

Bleaching tests were done using the internally housed UV LED in the Risø reader to investigate the behavior of the IR-RF signal for a range of different bleaching durations. UV light has previously been evaluated and determined to be an effective bleaching wavelength by Frouin et al. (2015), who observed that direct photo eviction and excitation of trapped electrons was taking place at this wavelength. The bleaching test protocol begins with a preheat at 70 °C and natural RF measurement at 70 °C for 200 s followed by a bleach of 10 s, a pause, a preheat at 70 °C and then a second 200 s RF_{70} measurement. This cycle repeats through for bleaching durations of 50, 100, 200, 500, 1000, 1500, 3000, 5000, 8000, 10000, 20000 s. Following the last bleaching there is one last preheat at 70 °C and an IR-RF measurement at 70 °C for 25000 s. All the bleaching and testing cycles were done on every aliquot measured. Each 200 s measurement was then used in conjunction with the last regenerated curve to determine a D_e; these results were then normalised

to the natural first natural D_e measured (Fig. 3.6). The results show that the UV LEDs are extremely effective initially as the signal bleaches down to approximately 2% of the initial D_e for all samples after 1500 s and as such this should be sufficient to fully bleach the sample. After the 1500 s bleaching, the data fluctuates between 0 and 5% likely due to the sensitivity change as a result of the repetition of measurements. Note that in Fig. 3.6 the cumulative bleaching durations were plotted. The data suggest that there is no significant difference in the bleachability between the 1500 s and 20 000 s bleaching durations, which is in contradiction with the effect that these different bleaching duration settings have on age determination. This contradiction suggests that there is likely an alternative explanation for the observed effect such as uncorrected sensitivity changes during the IR-RF measurement.

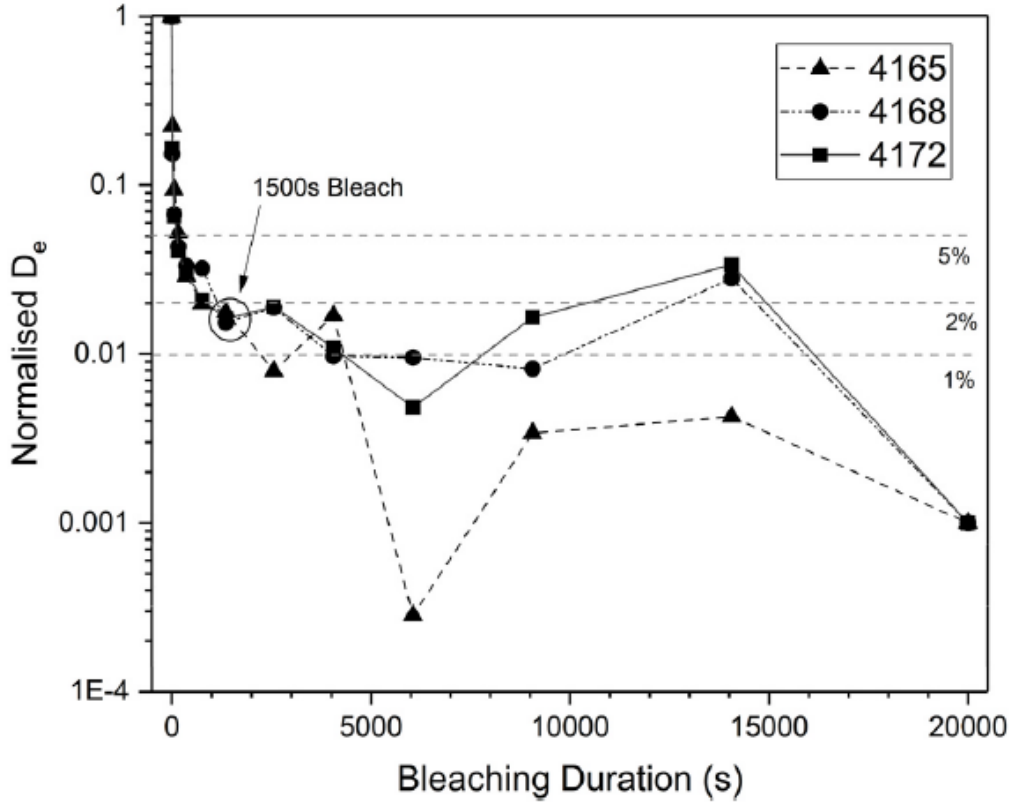

Fig. 3.6. Bleaching test results for three samples (LUM4165, LUM4168, LUM4172), note that a log scale was used on the y- axis. Bleaching was performed by the UV LEDs inside the Risø reader.

3.3.4. Correction for sensitivity change

Murari et al. (2018) observed differences in the IR-RF curve shapes between the first natural and the second regenerated curves; this was attributed to an induced sensitivity change during the bleaching between the two measurements. Because the bleaching tests show that residual doses were not the cause for the D_e difference between the 1500 s bleach and the 20 000 s bleach, sensitivity changes need to be considered. A correction for possible sensitivity changes occurring between the natural and regenerated IR-RF measurements was proposed, termed horizontal and vertical curve sliding (Murari et al., 2018). The corrected ages after the 1500 s bleach protocol were calculated using the function analyse_IRSAR.RF from the R 'Luminescence' package (Kreutzer et al., 2017; Kreutzer, 2019) (Table 2). All the corrected ages increased by ~30–70 %, with the larger relative increase occurring in the younger samples. Therefore, the age of the youngest sample (LUM3706) was overestimated significantly, the corrected age of LUM3708 increased to borderline consistent with the reference age, and the older sample ages were still underestimated (Fig. 3.4). In all the sample ages except that of LUM3706, the correction shows significant improvement for the short bleach and indicates that sensitivity change might be one reason for age underestimation. However, the large age overestimation of LUM3706 is a concern and the reason for this is unknown. Although the initial bleaching after natural curve measurement can induce sensitivity change, it was also found that all the curves measured subsequent to the regenerated curve have similar shapes, indicating that the bleaching steps after the regenerated curve induced negligible sensitivity change (Murari et al., 2018). This suggests that dose recovery tests, for which the aliquots have already been bleached once before the 'natural' curve measurement, will not be affected by the sensitivity change induced by bleaching. However, a clear underestimation in the dose recovery tests exists for the short bleach protocol, suggesting that the bleaching induced sensitivity change alone cannot account for the differences between the short and long bleach age results.

3.3.5. Comparison of the natural and laboratory dose response curves

The natural dose response curve (DRC) gives us information on how our dosimeter is theorised to have aged over time and a comparison of the natural DRC with the laboratory DRC allows us to gauge whether our measurements in the laboratory are approaching the natural processes involved. This comparison has been attempted on the Luochuan sequence using a number of different signals with varying degrees of success, namely: $pIRIR_{225}$ and pulsed IR at 50 °C (Li et al., 2018), OSL and TT-OSL (Chapot et al., 2012), VSL (Ankjærgaard et al., 2016; Ankjærgaard, 2019; Rahimzadeh et al., 2021) and ESR (Tsukamoto et al., 2018). These previous comparisons found that at different threshold doses the natural and laboratory DRCs deviate from one another and correspond to significant underestimations in age beyond this threshold dose. To construct the natural DRC for the IR-RF signal the initial natural IR-RF signal (average of the first 10 channels) of each aliquot was normalised to its highest regenerated IR-RF signal, and the mean renormalised natural signal was plotted against its expected D_e calculated from the reference age of each sample. To construct the laboratory DRC, the mean renormalised natural IR-RF signals (as described above) were plotted against the measured D_e values (Fig. 3.7). A single exponential curve was fitted to each data set derived after the initial equation used by Trautmann et al. (1999) (eqn. (1)):

$$\varphi_n(D_e) = \varphi_0 - \Delta\varphi n\ (1 - \exp(-D_e\lambda)) \quad (1)$$

where: φ_n is the normalised IR-RF signal, D_e is the equivalent dose, $\Delta\varphi_n$ is the dynamic range of the curve, λ is the decay parameter, 1λ is D_0: the characteristic value of the curve and φ_0 is the initial upper limit of the IR-RF signal (in this case has the value of 1 as the data is normalised).

In this study, the equation used by Trautmann et al. (1999) is simplified and used in the following form to highlight the value of the lower limit of the DRC's generated (y_0) (eqn.2):

$$\varphi_n(D_e) = \Delta\varphi_n \text{ x } \exp(-D_e\lambda) + y_0 \quad (2)$$

where: φn is the normalised RF signal, D_e is the equivalent dose, $\Delta\varphi_n$ is the dynamic range of the curve, λ is the decay parameter, 1λ is D_0: the characteristic value of the curve and y_0 approximates the lower limit of $\varphi_n(D_e)$.

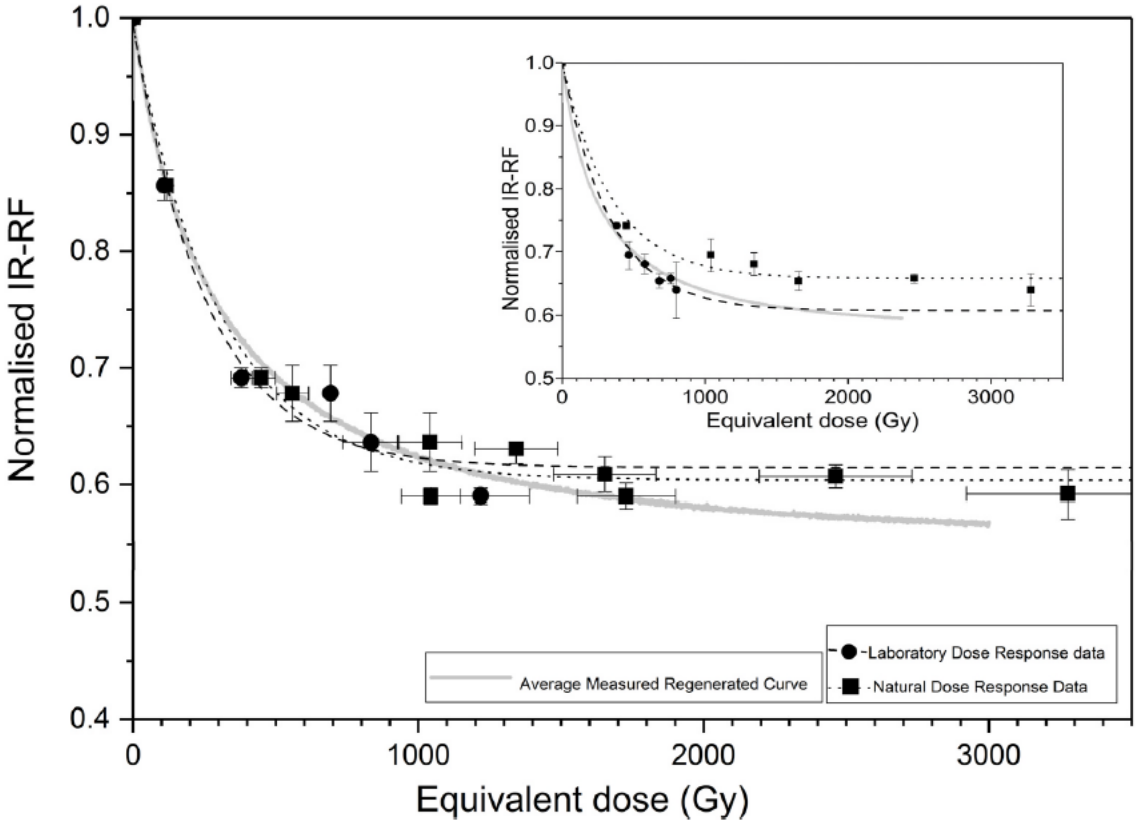

Fig. 3.7. Comparison of the natural DRC and the laboratory DRC, the main graph relates to the 20 000 s bleach protocol and the inset pertains to the 1500 s bleach protocol. Where the laboratory dose response data is shown with filled circles (curve: dots) and the natural dose response data is shown with filled squares (curve: dashes). The pale light grey curve depicts the average normalised measured regenerative curve.

A summary of the natural and laboratory DRC components for both the 1500 s bleach and the 20 000 s bleach protocol is provided in Table 3. Previous work has fitted IR-RF regenerated curves to stretched exponential curves (including a dispersion factor: β) (e.g., Erfurt and Krbetschek, 2003b) but this was done on direct IR-RF response data of a single aliquot. In our study, the IR-RF DRCs generated are average and normalised results and are a composite curve including all the samples measured. In the inset of Fig.3.7 the data show that with the 1500 s bleach protocol the laboratory DRC begins to significantly deviate from the natural DRC at approximately 400 Gy. This is in line with only sample LUM3706 showing an age result consistent with the reference age. For the 20 000 s bleach protocol only the samples younger than ~300 ka were included in the laboratory DRC for clarity. The overlap of the laboratory and natural DRCs of the 20 000 s bleach protocol suggests that up until the effect of saturation these curves are describing

similar processes (Fig. 3.7). The 20 000 s bleach protocol results in D_0 values of 305 ± 33 Gy and 262 ± 68 Gy for the natural and the laboratory DRCs, respectively (Table 3.3). Fig. 3.7 also shows the mean regenerated DRC, which starts to deviate from the natural and laboratory DRCs at ~1100 Gy. This suggests that the stretched exponential function, which is normally used to fit the IR-RF regenerative curve which is in essence a laboratory DRC, does not mimic the natural dose response as constructed in this study. Fig. 3.8 illustrates the properties of the natural DRC indicating the position of D_0 and illustrating that it is possible to date samples beyond $2D_0$. In this instance, we were able to date the sample at $4D_0$ however, the position of the sample (LUM4168) on the horizontal part of the curve suggests that at this point it is beyond the repeatable dating limit. Li et al. (2018) reported natural DRC D_0 values that are significantly higher ($pIRIR_{225}$: 452 ± 23 Gy and pulsed IR_{50}: 425 ± 30 Gy) than the IR-RF results. Regardless of this difference in D_0 values, there is agreement on the dating limits of the $pIRIR_{225}$ and RF_{70} signals of ~300 ka suggesting that this limit is likely a fundamental property of feldspar rather than a failure of the signal to date older material.

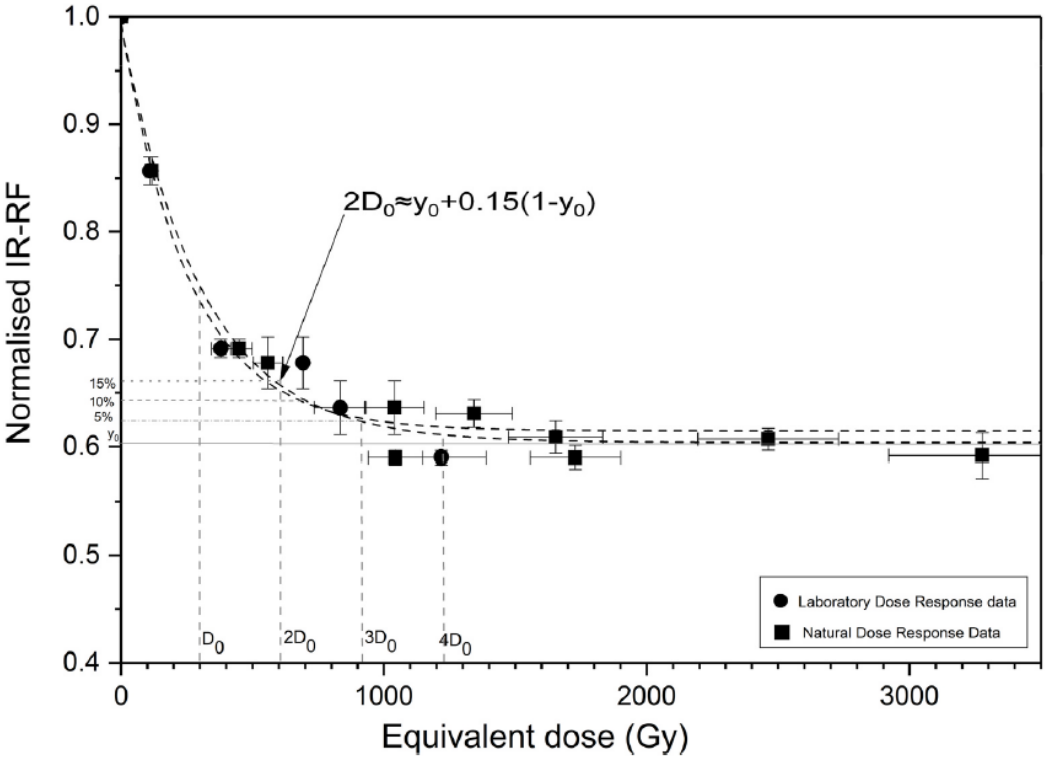

Fig. 3.8. Comparison of the natural and laboratory dose response curves illustrating the position of D_0-$4D_0$ defined proportionally in the same way that OSL and IRSL define $2D_0$ as 85% of the dynamic range of the curve.

Table 3.3: Summary of the natural and laboratory DRC components for both the 1500 s bleaching protocol and the 20 000 s bleaching protocol.

Component	**1500 s bleach protocol DRC**		**20 000 s bleach protocol DRC**	
	Natural	Laboratory	Natural	Laboratory
$\Delta\boldsymbol{\phi_n}$	0.388±0.018	0.430±0.014	0.389±0.016	0.379±0.032
$\boldsymbol{\lambda}$	3.28 x 10^{-3}	3.49 x 10^{-3}	3.28 x 10^{-3}	3.82 x 10^{-3}
$\frac{1}{\lambda}$, $\mathbf{D_0}$	305±42	286±27	305±33	261±68
$\boldsymbol{y_0}$	0.611±0.008	0.570±0.012	0.604±0.007	0.615±0.024

3.4. Conclusions

In this study, an attempt was made to test the RF_{70} signal on the Luochuan sequence using two distinct bleaching duration settings (1500 s and 20000 s). It was found that using the 1500 s bleaching duration all but the youngest sample yielded significantly underestimated ages. In contrast, while using the 20000 s bleaching duration protocol, the ages of samples younger than 300 ka were consistent with reference ages and the age results of the samples older than 300 ka underestimated the reference ages, indicating that these samples were beyond the dating limit. Dose recovery tests for the shorter bleach were unsuccessful while dose recovery tests using the longer bleach were successful. Bleaching tests did not show a significant difference in the bleachability of the samples at 1500 s and at 20000 s, leading us to consider sensitivity change to be a possible explanation. An attempt was made to correct for sensitivity using the vertical and horizontal sliding method which did improve the results for all but the youngest sample but age underestimation still existed for older samples. This suggests that there was an element of sensitivity change to account for, however unsuccessful dose recoveries for the short bleach indicated that sensitivity change alone cannot account for the differences. The natural and laboratory DRCs are consistent for samples younger than 300 ka using the longer bleaching duration; however, the shorter bleaching duration results in the DRCs diverging early and significantly. This study was able to define D_0 values of 305 ± 33 Gy and 262 ± 68 Gy for the average natural and laboratory DRCs respectively using a simple decaying exponential curve and in the case of the 20000 s protocol is able to date beyond $2D_0$. Though a sample with D_e at $4D_0$, was dated successfully, the natural IR-RF signal of this sample is on the horizontal part of the regenerative curve and individual aliquot data exhibit wide scatter indicating that it is possibly

beyond the limit of the datable age range. The upper limit of ~1100 Gy, observed in this study coincides where the natural DRC starts to deviate from the regenerated DRC. This suggests that the stretched exponential function, which is normally used to fit the IR-RF DRCs does not mimic the natural dose response. In conclusion, we can confirm that it is possible to date up to ~300 ka (~1100 Gy) using the IR-RF signal of feldspars in the Luochuan sequence but not the theoretical laboratory-generated dating limit of ~3500 Gy (~1000 ka). More work is needed to determine whether these theoretical dating limits are actually attainable in nature.

Declaration of competing interest

The authors declare that they have no known competing financial interests or personal relationships that could have appeared to influence the work reported in this paper.

Acknowledgements

We thank Petra Posimowski, Sonja Riemenschneider and Sabine Mogwitz for gamma spectrometry measurements and sample preparation. Jingran Zhang, Zhong He and Linhai Yang are thanked for their assistance in fieldwork and sample collection. This study was partly supported by the National Natural Science Foundation of China (No. 41977381). We would also like to thank the anonymous reviewer for their time, constructive comments, and helpful insights that have greatly improved the paper.

References

Ankjærgaard, C., 2019. Exploring multiple/aliquot methods for quartz violet stimulated luminescence dating. Quat. Geochronol. 51, 99–109.

Ankjærgaard, C., Guralnik, B., Buylaert, J.P., Reimann, T., Yi, S., Wallinga, J., 2016. Violet stimulated luminescence dating of quartz from Luochuan (Chinese loess plateau): agreement with independent chronology up to ~600 ka. Quat. Geochronol. 34, 33–46.

Buylaert, J.P., Jain, M., Murray, A.S., Thomsen, K.J., Lapp, T., 2012. IR-RF dating of sand-sized K-feldspar extracts: a test of accuracy. Radiat. Meas. 47, 759–765.

Chapot, M.S., Roberts, H.M., Duller, G.A., Lai, Z., 2016. Natural and laboratory TT-OSL dose response curves: testing the lifetime of the TT-OSL signal in nature. Radiat. Meas. 85, 41–50.

Chapot, M.S., Roberts, H.M., Duller, G.A.T., Lai, Z.P., 2012. A comparison of natural- and laboratory-generated dose response curves for quartz optically stimulated luminescence signals from Chinese Loess. Radiat. Meas. 47, 1045–1052.

Ding, Z.L., Derbyshire, E., Yang, S.L., Yu, Z.W., Xiong, S.F., Liu, T.S., 2002. Stacked 2.6- Ma grain size record from the Chinese loess based on five sections and correlation with the deep-sea δ18O record. Paleoceanography 17, 5-1–5-21.

Erfurt, G., Krbetschek, M.R., 2003a. Studies on the physics of the infrared radioluminescence of potassium feldspar and on the methodology of its application to sediment dating. Radiat. Meas. 37, 505–510.

Erfurt, G., Krbetschek, M.R., 2003b. IRSAR- a single-aliquot regenerative-dose dating protocol applied to the infrared radiofluorescence (IR-RF) of coarse-grain K-feldspar. Ancient TL 21, 35–42.

Frouin, M., Huot, S., Kreutzer, S., Lahaye, C., Lamothe, M., Philippe, A., Mercier, N., 2017. An improved radiofluorescence single-aliquot regenerative dose protocol for K-feldspar. Quat. Geochronol. 38, 13–24.

Frouin, M., Huot, S., Mercier, N., Lahaye, C., Lamothe, M., 2015. The issue of laboratory bleaching in the infrared-radiofluorescence dating method. Radiat. Meas. 81, 212–217.

Gu´erin, G., Mercier, N., Nathan, R., Adamiec, C., Lefrais, Y., 2012. On the use of the infinite matrix assumption and associated concepts: a critical review. Radiat. Meas. 47, 778–785.

Huntley, D.J., Baril, M.R., 1997. The K content of the K-feldspars being measured in optical dating or in thermoluminescence dating. Ancient TL 15, 11–13.

Huntley, D.J., Lamothe, M., 2001. Ubiquity of anomalous fading in K-feldspars and the measurement and correction for it in optical dating. Can. J. Earth Sci. 38, 1093–1106.

Kreutzer, S., Murari, M.K., Frouin, M., Fuchs, M., Mercier, N., 2017. Always remain suspicious: a case study on tracking down a technical artefact while measuring IR-RF. Ancient TL 35, 20–30.

Kreutzer, S., 2019. In: Kreutzer, S., Burow, C., Dietze, M., Fuchs, M.C., Schmidt, C., Fischer, M., Friedrich, J. (Eds.), analyse_IRSAR.RF%28%29: Analyse IRSAR RF Measurements. Function Version 0.7.5. Luminescence: Comprehensive Luminescence Dating Data Analysis. R package version 0.9.0.109. https://CRAN.R-project.org/package=Luminescence, 2019.

Kreutzer, S., Martin, L., Dubernet, S., Mercier, N., 2018. The IR-RF alpha-Efficiency of K-feldspar. Radiat. Meas. 120, 148–156.

Lapp, T, Jain, M, Thomsen J, K, Murray S, A, Buylaert, J, 2012. New luminescence measurement facilities in retrospective dosimetry. Radiat. Meas. 47 (9), 803–808.

Li, B., Li, S.H., 2012. Luminescence dating of Chinese loess beyond 130 ka using the non-fading signal from K-feldspar. Quat. Geochronol. 10, 24–31.

Li, Y., Tsukamoto, S., Long, H., Zhang, J., Yang, L., He, Z., Frechen, M., 2018. Testing the reliability of fading correction methods for feldspar IRSL dating: a comparison between natural and simulated-natural dose response curves. Radiat. Meas. 120, 228–233.

Liritzis, I., Stamoulis, K., Papachristodoulou, C., Ioannides, K., 2013. A re-evaluation of radiation dose-rate conversion factors. Mediterr. Archaeol. Archaeom. 13, 1–15.

Murari, M.K., Kreutzer, S., Fuchs, M., 2018. Further investigations on IR-RF: dose recovery and correction. Radiat. Meas. 120, 110–119.

Murari, K.M., Kreutzer, S., King, G., Frouin, M., Tsukamoto, S., Schmidt, C., Lauer, T., Klasen, N., Richter, D., Friedrich, J., Mercier, N., Fuchs, M., 2021. Infrared radiofluorescence IR-RF dating: a review. Quat. Geochronol. 64, 101155.

Prescott, J.R., Hutton, J.T., 1994a. Cosmic ray contributions to dose rates for luminescence and ESR dating: large depths and long-term time variations. Radiat. Meas. 23, 497–500.

Richter, D., Richter, A., Dornich, K., 2013. Lexsyg d a new system for luminescence research. Geochrono. 40, 220–228.

Richter, M., Tsukamoto, S., Long, H., 2020. ESR dating of Chinese loess using the quartz Ti centre: a comparison with independent age control. Quat. Int. 556, 159–164.

Rahimzadeh, N., Tsukamoto, S., Zhang, J., Long, H., 2021. Natural and laboratory dose response curves of quartz violet stimulated luminescence (VSL): exploring the multiple aliquot regenerative dose (MAR) protocol. Quat. Geochronol. 65, 101194.

Trautmann, T., Krbetschek, M.R., Dietrich, A., Stolz, W., 1998. Investigations of feldspar radioluminescence: potential for a new dating technique. Radiat. Meas. 29, 421–425.

Trautmann, T., Krbetschek, M.R., Dietrich, A., Stolz, W., 1999. Feldspar radioluminescence; a new dating method and its physical background. J. Lumin. 85, 45–58.

Trautmann, T., Dietrich, A., Stolz, W., Krbetschek, M.R., 1999b. Radioluminescence dating: a new tool for quaternary geology and archaeology. Naturwissenschaften 86, 441–444.

Tsukamoto, S., Long, H., Richter, M., Li, Y., King, G.E., He, Z., Yang, L., Zhang, J., Lambert, R., 2018. Quartz natural and laboratory ESR dose response curves: a first attempt from Chinese loess. Radiat. Meas. 120, 137–142.

Zhang, J., Tsukamoto, S., 2022. A simplified multiple aliquot regenerative dose protocol to extend the dating limit of K-feldspar pIRIR signal. Radiat. Meas. In this issue.

Chapter 4:

Co-Author contributions

The same samples were used in chapter 4 that were exclusively collected and partially prepared by Prof. Dr. Tsukamoto, Dr. Long and others both in China and in Hannover, Germany. All polymineral fine-grained samples were prepared by me and Ms. Neda Rahimzadeh. I prepared all mid-grain samples. The main scientific idea frame work for the paper was developed collaboratively by me and Prof. Dr. Tsukamoto, the comparison with mid-grains was my idea. I generated all of the of luminescence data running luminescence experiments, with the support of Prof. Dr. Tsukamoto and Dr. Zhang. The regional dose rate data was generated by lab technicians for a previous study and regional dose rates calculated were generated by me using an R-script template written for general use by Dr. Zhang. I performed all XRF measurements and analysis. The majority of analysis and interpretation was done me, with the support of Prof. Dr. Tsukamoto and Dr. Zhang. I wrote the initial draft, which was reviewed by Prof. Dr. Tsukamoto, Dr. Zhang, and Dr. Long there after corrected/ edited by me, and proof read by all authors.

Reference:

Buchanan, G.R., Tsukamoto, S., Zhang, J., Long, H., 2023. Testing infrared radiofluorescence dating on Polymineral fine-grains from the Luochuan loess-palaeosol sequence, Chinese loess plateau. Quat. Geochron. 79. http://doi.org/10.1016/j.quageo.2023.101485

Testing infrared radiofluorescence dating on polymineral fine-grains from the Luochuan loess-palaeosol sequence, Chinese Loess Plateau.

G.R. Buchanan [a,b,*] , S. Tsukamoto [a] , J. Zhang [a] , H. Long [c]
[a] Leibniz Institute for Applied Geophysics, Geochronology section, 30655, Hannover, Germany
[b] Eberhard Karl's University Tübingen, Terrestrial Sedimentology, 72076, Tübingen, Germany
[c] State Key Laboratory of Lake Science and Environment, Nanjing Institute of Geography and Limnology, Chinese Academy of Sciences (NIGLAS), Nanjing, 210008, China

Abstract

In the past infrared radiofluorescence (IR-RF) dating has been focused on coarse-grain potassium feldspar (K-feldspar). However, polymineral fine-grains (4–11 μm) have proven to be successful dosimeters when dating using conventional infrared stimulated luminescence (IRSL). In this study, we investigated the potential of IR-RF signals generated from polymineral fine-grains for dating on 6 loess samples (~30–480 ka) from the well documented Luochuan loess-palaeosol sequence on the Chinese Loess Plateau. Both the natural and regenerated IR-RF signals from the polymineral fine-grains were uncharacteristically flat with little or no dynamic range using either a bleaching duration of 1500 s or 20000 s between the measurements. X-ray fluorescence (XRF) analyses showed that the polymineral fine-grains were dominated by quartz and Na-feldspars. K-feldspar and Na-feldspar mid-grain (38–63 μm) sample sets were further prepared, measured and compared. The IR-RF signals from the K-feldspar mid-grains exhibited the characteristic exponentially decaying signal, while the IR-RF signals from the Na-feldspar mid-grains were flat with little dynamic range, indicating that the Na-feldspar dominates the polymineral fine-grain IR-RF signal. The polymineral fine-grain ages (both bleaching settings) were consistent with reference ages up to 300 ka (~1000 Gy), however, due to the flat nature of the curves the uncertainties were large. The consistency of the results using the two bleaching durations indicates that the bleaching duration has a less significant role in the IR-RF dating with polymineral fine-grains than in the coarse grains. Of the mid-grain ages, the IR-RF ages of Na-feldspar mid-grains were consistent with the reference ages up to 360 ka (~1200 Gy) while those of the K-feldspar mid-grains were consistent with the reference ages up to 200 ka (~600 Gy). Dose recovery tests were undertaken on all samples, however, where the dose recovery ratios were considered the most successful (K-feldspar mid-grains) the dating results were the least successful, suggesting that dose recovery tests in this way may be a less useful predictor of the dating performance of the IR-RF dating. IR-RF dating of polymineral fine-grains was possible up to 300 ka for Chinese loess, despite the uncharacteristically flat signals.

4.1. Introduction

Infrared radiofluorescence (IR-RF) dating was initially proposed by Trautmann et al. (1998) as a suitable dating method for K-feldspar. It was termed by Erfurt and Krbetschek (2003b) and further developed by e.g. Frouin (2014), Frouin et al. (2015, 2017), Huot et al. (2015), Kreutzer et al. (2017) and Murari et al. (2018). IR-RF dating is an alternative approach to conventional infrared stimulated luminescence (IRSL) dating of potassium-rich feldspars (K-feldspar), in which continuous ionising radiation stimulates an infrared emission with a peak at 1.43 eV (865 nm) (Trautmann et al., 1999a, b; Erfurt and Krbetschek, 2003a, b). It is theorised that this signal is a direct measurement of the quantity of electrons being trapped, in previously empty traps, during irradiation. In contrast, IRSL signals are theorised to correspond to more complex recombination pathways. IR-RF has the potential to date older materials with greater accuracy due to the high resolution of data generated (many data points recorded) in the dose response curve. Other advantages include that the required measurement time of IR-RF dating is generally shorter than that of conventional single aliquot regenerative dose (SAR) protocols of IRSL dating and that IR-RF has not yet been proven to suffer from fading (Murari et al., 2021). A number of investigations have attempted to evaluate the upper dating limit of IR-RF. Erfurt and Krbetschek (2003b) showed that the dating limit of IR-RF could be approximately 1200–1500 Gy depending upon dose rates. Frouin et al. (2017) investigated IR-RF signals at elevated temperatures, developed the RF_{70} protocol, and reported equivalent dose (D_e) measurements up to 2000 Gy. While dose recovery experiments undertaken by Murari et al. (2018) reported laboratory-generated equivalent doses of up to ~3500 Gy, Buchanan et al. (2022) assessed the dating limit in nature and reported D_es of up to 1200 Gy using an extended bleaching (using the UV LED housed in the Risø reader) duration between the natural and regenerated measurements of 20000 s. Additionally, recent work done by Kreutzer et al. (2022) observed an absolute limit of 1200 Gy and that samples beyond this limit consistently underestimate relative to a given dose; which confirms the observations of Erfurt and Krbetschek (2003b) and Buchanan et al. (2022).

Previous investigations of the IR-RF signal have largely focused on coarse-grained K-feldspar (for example: 63–150 μm), but a few investigations have been done on polymineral grains with varying results (Schilles, 2002; Kreutzer et al., 2018; Coussot et al., 2019). Schilles (2002) was the first to successfully investigate the application of IR-RF dating to polymineral fine-grains on young samples up to 45 Gy (~15 ka), concluding that there was great potential for IR-RF dating

on polymineral fine-grains. Recent work done by Coussot et al. (2019) applied IR-RF dating to polymineral mid-grains (40–60 μm) successfully on two older samples with equivalent doses between 690 and 820 Gy (~260–290 ka). Further, testing of the IR-RF signal on polymineral fine-grains allows for broadening the range of applicable environmental settings, that are dominated by fine-grain sediments, for example loess dominated deposits (Murari et al., 2021). There is some concern that the mixture of minerals could complicate the situation as quartz which is likely to be a dominant mineral (40–50 %) does emit RF in the IR region (though <735 nm) (Schmidt et al., 2015); however, the standard detection window of the IR-RF signal (850–945 nm) should not be affected by the quartz IR-RF peak. An expected additional concern is the retention of a larger percentage of Na-feldspars (10–15 %) than K-feldspars (<5 %) that has been observed in polymineral fine-grains (Tsukamoto et al., 2012). Buylaert et al. (2012) observed that when IR-RF was applied to coarse-grained quartz and Na-feldspar, the dose response curves were essentially flat and did not conform to the expected exponential decay curve shape. Therefore, depending upon the minerals present, the IR-RF signal generated from polymineral fine-grains could potentially be significantly different to that of coarse-grained K-feldspar.

This study tested the IR-RF dating method of polymineral fine-grains on 6 loess samples (~30–480 ka) from the well documented Luochuan loess-palaeosol sequence on the Chinese Loess Plateau, and compared these results with two mid-grain sample sets dominated by K- and Na-feldspar from the same samples, respectively.

The Luochuan loess-palaeosol sequence on the Chinese Loess Plateau is an ideal testing ground and serves as a natural laboratory offering a continuous record of deposition spanning more than 2.5 million years and a well-delineated independent age control developed by Ding et al. (2002). A large number of geochronology studies have been done in the region in order to test the various luminescence signals including but not limited to: blue optically stimulated luminescence (OSL) (Chapot et al., 2012), thermally transferred (TT-) OSL (Chapot et al., 2016), violet stimulated luminescence (VSL) (Ankjærgaard et al., 2016; Rahimzadeh et al., 2021), fading corrected post-infrared infrared stimulated luminescence ($pIRIR_{225}$) and pulsed IRSL (Li et al., 2018), multiple elevated temperature (MET-) pIRIR (Li et al., 2018; Zhang and Tsukamoto, 2022; Zhang et al., 2022), electron spin resonance (ESR) (Tsukamoto et al., 2018; Richter et al., 2020) and IR-RF of coarse-grained K-feldspar (Buchanan et al., 2022). Recent work done by Zhang et

al. (2022) established an alternative absolute geochronology for the central Chinese Loess Plateau extending back 350 ka and resolving the boundary discrepancies between different orbitally tuned age models.

4.2. Samples

Six samples were collected from units L1-L5 of the Luochuan loess-palaeosol sequence in Potou village with reference ages ranging from 29 ka (L1; LUM3704) to 470 ka (L5; LUM4172) (Ding et al., 2002, Fig. 4.1). The samples were collected (by horizontally hammering light tight cylinders into exposed profiles) and thereafter prepared, tested, analysed and catalogued under subdued red light at the Leibniz Institute for Applied Geophysics in Hannover, Germany. Three of these samples (LUM3704, LUM3707 and LUM 3710) were initially prepared in 2018 to extract the 63–100 μm K-feldspar and quartz grains. These samples were used in Li et al. (2018), Tsukamoto et al. (2018) and Richter et al. (2020) to evaluate the IRSL and ESR properties of K-feldspar and quartz respectively. The other three samples (LUM4165, LUM4168 and LUM4172) were prepared in 2020 and coarse (63–150 μm) K-feldspar grains were extracted as well as polymineral fine-grains (4–11 μm). Rahimzadeh et al. (2021) used all six samples and Buchanan et al. (2022) used five samples (LUM3704, LUM3710, LUM4165, LUM4168 and LUM4172) to evaluate the VSL and IR-RF properties of polymineral fine-grains and coarse-grained K-feldspar respectively.

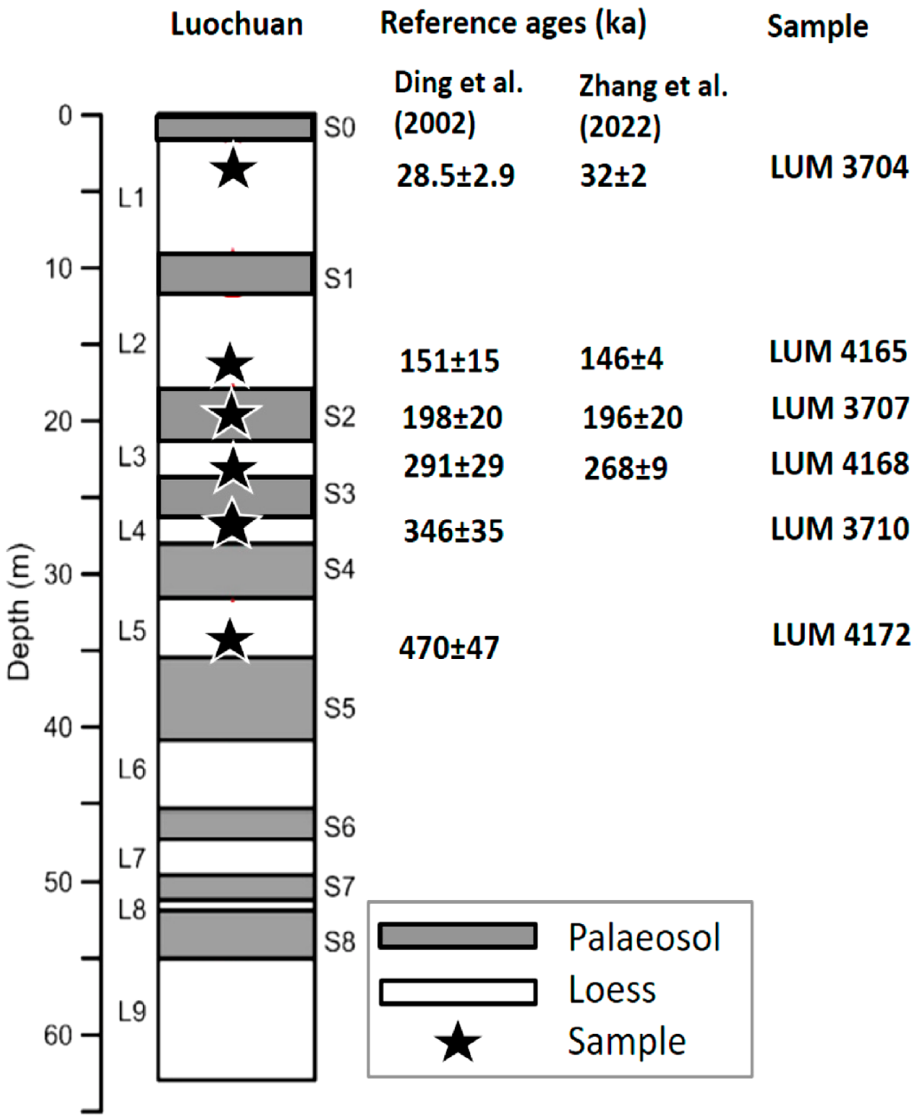

Fig. 4.1. Graphic representation of the Luochuan loess-palaeosol sequence illustrating the sample depths, relative positions, reference ages calculated from Ding et al. (2002) and the age model of Zhang et al. (2022) (Modified after Buchanan et al. (2022)).

The reference ages used were calculated from the astronomical age model generated by Ding et al. (2002), which is in line with the majority of the geochronology work done on this sequence (e.g., Tsukamoto et al., 2018; Richter et al., 2020; Rahimzadeh et al., 2021.) The chronology reported by Ding et al. (2002) was built upon relative dating techniques by first correlating high resolution median grain size records of five different sedimentary sequences on the Chinese Loess Plateau, namely: Baoji, Lingtai, Jingchuan, Puxian and Pingliang. Most sections

showed near continuous deposition across the Quaternary, with only minor hiatuses within single sections. These sections were compared and adjusted to the theoretical variations in precession and obliquity of the Earth (using paleomagnetic reversal as time controls on each sequence), these orbital timescale grain size records were then averaged to form a regional stacked loess grainsize (or Chiloparts) archive of the Pleistocene (Ding et al., 2002). This regional Chiloparts record was applied to the Luochuan sequence which is in close proximity to the sequences used (Ding et al., 2002).

The comparison of relative and absolute dating techniques introduces inherent assumptions that were deemed acceptable due to the large volume of work within the luminescence dating community that has generated absolute ages that are consistent with the Ding et al. (2002) chronology. The reference ages reported by Ding et al. (2002) were taken from the boundaries of each depositional unit. Our samples were taken from between these boundaries and we interpolated the ages by assuming a constant accumulation rate within each unit. A conservative uncertainty of 10 % was assigned to account for these assumptions, in line with previous studies conducted by Ankjærgaard et al. (2016), Li et al. (2018), Richter et al. (2020), Rahimzadeh et al. (2021) and Buchanan et al. (2022).

Recent work done by Zhang et al. (2022) established an absolute geochronology model for the central Chinese Loess Plateau extending back to 350 ka and is broadly in agreement with the Ding et al. (2002) age model except in the case of the L3/S3 boundary where there is a significant difference. The reference ages of our samples were also read from the age-depth model of Zhang et al. (2022) using the relative positions of our samples within each unit. The Ding et al. (2002) age model has been preferred in this study as it spans the whole age range of the sample set, and it is entirely independent of luminescence techniques and was previously used with regards to the coarse-grained IR-RF study (Buchanan et al., 2022). However, the Zhang et al. (2022) age model has been included for comparison and it is reassuring that these relative and absolute age models are largely in agreement.

4.3. Methodology

4.3.1. Sample preparation

Polymineral fine-grains as well as K-feldspar and Na-feldspar mid-grains (38–63 μm) were prepared. Initially the samples were chemically treated with hydrochloric acid (HCl; 10%), hydrogen peroxide (H_2O_2; 30%) and sodium oxalate (NaC_2O_4; 0.1 N) in order to eliminate carbonates, organic material and clay aggregates, respectively. The mid-grain fraction was then extracted through wet sieving and separated using heavy liquid density separation (for a minimum of 18 hr) to extract the K-feldspar mid-grains (<2.58 g/cm3) and the Na-feldspar mid-grains (2.58–2.62 g/cm3). The mid-grains were mounted on stainless steel disks using a thin layer of silicon oil as adhesive to make small aliquots (2.5 mm in diameter). The polymineral fine-grain fraction (4–11 μm) was extracted using repeated cycles of settling and washing using a centrifuge (Frechen et al., 1996). The fine-grains were mounted on to aluminium discs through gravity setting from suspension in distilled water drops followed by evaporation of the water in an oven (<50 ◦C). The laboratory standard used is 2 mg per aliquot.

4.3.2. Instrumentation

All IR-RF measurements were carried out on an automated Risø TL/ OSL DA-20 reader equipped with an automated detection and stimulation head (DASH) (Lapp et al., 2015). The IR-RF signal was stimulated using a $^{90}Sr/^{90}Y$ beta radiation source with a dose rate of 0.0967 Gy/s for the fine-grains and 0.119 Gy/s for coarse-grains. The signal was detected through a Chroma D 900/100 interference filter (850–945 nm) and the bleaching was carried out using an ultraviolet (UV) LED operating at 90 % intensity (395–410 nm, 900 mW) and housed inside the Risø reader. Additionally, the X-ray fluorescence (XRF) measurements were carried out using the XRF attached to the Risø reader.

4.3.3. Signal measurement protocols

The IR-RF protocol used was based on the protocol developed by Frouin et al. (2017) to measure the IR-RF signal at 70 °C (RF_{70}), with the adaptions outlined by Buchanan et al. (2022) to account for the differences in measuring equipment, bleaching capabilities and aliquot types. Initially a preheat was carried out at 70 °C for 500 s, followed by continuous irradiation for 5000

s and the intensity of the natural IR-RF signal was measured. The sample was then bleached using the built-in UV LEDs inside the Risø reader for 1500 s (Buylaert et al., 2012) or 20 000 s (Buchanan et al., 2022). Bleaching was followed by an hour-long pause to allow bleaching induced phosphorescence to dissipate (Erfurt and Krbetschek, 2003b). Thereafter, a second preheat was carried out at 70 °C for 500 s, followed by continuous irradiation for 20 000 s and the intensity of the regenerated IR-RF signal was measured (Table 1). Two sets of measurements were done on the polymineral fine-grains using bleaching duration settings of 1500 s and 20 000 s on 6 aliquots for all 6 samples. Both the K-feldspar and the Na-feldspar mid-grain sample sets were measured using the bleaching duration of 1500 s on 6 aliquots for all 6 samples.

Table 4.1: Protocol used based on the RF_{70} protocol developed by Frouin et al. (2017).

Step	IR-RF protocol	Observed
1	Preheat (70 °C, 500 s)	
2	Irradiation (70 °C, 5000 s)	Natural decay curve (RF_{nat})
3	Bleach (UV LED, 90 %, 1500 s or 20 000 s)	
4	Pause 1 hr	
5	Preheat (70 °C, 500 s)	
6	Irradiation (70 °C, 20 000 s)	Regenerated decay curve (RF_{reg})

4.3.4. XRF measurements

XRF measurements were done on all samples using the XRF attachment of the TL/OSL reader, and grain size fractions, using molybdenum cups. One cup was used per sample. Each cup was filled to approximately half its volume with the entire base covered and the surface made as flat as possible using a spatula. The measurement time was 60 s, at 10 kV, 30 μA, over 1024 channels and with a spectrometer gain of 120. Each cup was measured three times and an average of the three measurements was calculated. This measurement generated a quartz content percentage and the percentages of the K-, Na-, and Ca-feldspar in the sample. The results were evaluated using the XRFanalyse V. 1.30 developed for the XRF attachment for the Risø reader.

4.3.5. IR-RF D_e estimation

All IR-RF measurements generate a natural (RF_{nat}) and a regenerated (RF_{reg}) signal in the form of two exponential decay curves (Fig. 4.2). In order to estimate the equivalent dose (D_e) we fit the natural curve to the regenerated curve and the horizontal distance travelled of the natural curve along the dose (or x-) axis is the D_e. This can be achieved in a number of ways, for example: shifting the natural curve, interpolation and extrapolation (Murari et al., 2021). With all measurements we made use of the 'horizontal sliding' method as outlined by Buylaert et al. (2012). The 'horizontal and vertical sliding' method as outlined by Murari et al. (2018) was also used to attempt to account for sensitivity changes where the dynamic range of the measurements made this possible. These sliding methods of analysis were favoured as they do not rely on the physical assumptions that constrain the models that use extrapolation and interpolation; and the high number of individual data points used makes the sliding methods more robust statistically (Buylaert et al., 2012). The D_es were calculated using the average of 6 aliquots and all measurements were analysed using the 'horizontal sliding' method, except the K-feldspar mid-grains which were analysed using both the 'horizontal sliding' and the 'horizontal and vertical sliding' methods as these results were the only results with sufficient vertical dynamic range. The 'horizontal sliding' method was analysed using the RLanalyse (version 1.30) software associated with the Risø reader. The 'vertical and horizontal sliding' method was analysed using the function analyse_IRSAR.RF from the R 'Luminescence' package (Kreutzer et al., 2017; Kreutzer, 2019).

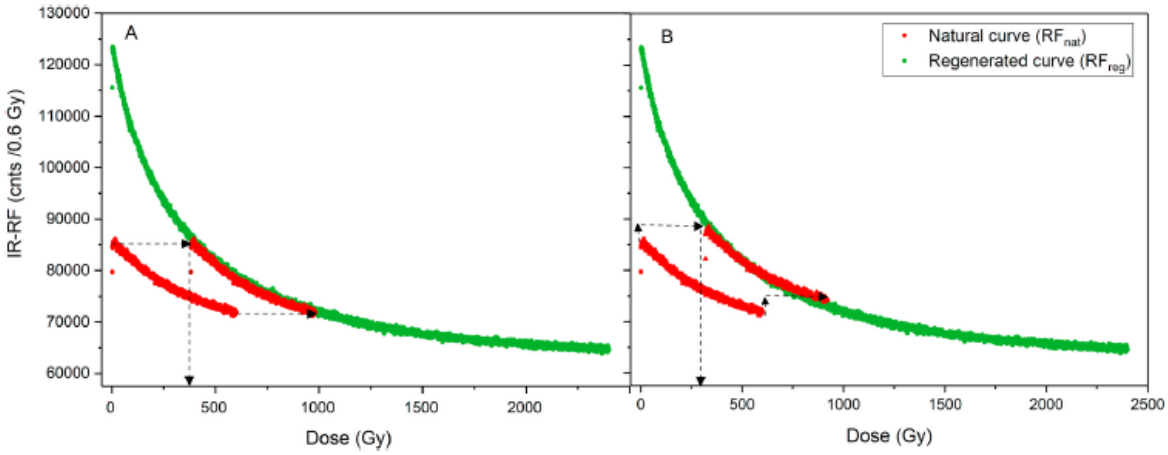

Fig. 4.2. Example of the data output of the IR-RF signal and A) the 'horizontal sliding' method and B) the 'vertical and horizontal sliding' method; used to determine D_e for each aliquot. The red curve is the natural curve and the green curve is the regenerated curve, with the point at which the arrowhead falls on the x-axis is the De. (Modified after Buchanan et al., 2022).

4.3.6. Environmental dose rates

Radionuclide specific activities (Bq/kg) were determined by high resolution gamma spectrometry and converted to concentrations of uranium (U, ppm), thorium (Th, ppm) and potassium (K, %) for all samples. Samples were stored for at least a month to ensure equilibrium between 222Rn and its daughter isotopes before the gamma spectrometry measurements. In line with previous studies on this sequence, the water content was estimated to be 15 ± 5 % for all samples. The cosmic dose rates were calculated following Prescott and Hutton (1994). The radionuclide conversion factors from Liritzis et al. (2013), and beta and alpha attenuation factors from Gu´erin et al. (2012) and Brennan et al. (1991) were used, respectively. The a-value of 0.07 ± 0.01 was used following Kreutzer et al. (2018). The internal dose rate was calculated with a K concentration of 12.5 ± 1.0 % (Huntley and Baril, 1997) and a ^{87}Rb content of 400 ± 100 ppm (Huntley and Hancock, 2001) for the K-feldspar mid-grains. The internal dose rate for the Na-feldspar mid-grains was calculated using the measured K content by the XRF measurement (see 3.4).

4.3.7. Dose recovery tests

Dose recovery tests were done by bleaching the aliquots (3 aliquots per sample) for durations equal to the in-measurement bleaching durations of 1500 s or 20 000 s, using the UV LEDs housed inside the Risø reader. The samples were then irradiated with doses that approximate the expected doses and were measured using the IR-RF protocols used for D_e determination. The given dose was then divided by the measured dose, and a successful dose recovery gives a ratio within 10% of unity.

4.3.8. Bleaching tests

Bleaching tests were done by running an IR-RF measurement on 3 aliquots per sample at 70 °C for 100 s, beginning with an initial natural measurement and thereafter at bleaching intervals of 10, 50, 100, 200, 400, 600, 800, 1000, 1500, 2000 s using the UV LED housed in the Risø TL/OSL reader. Three aliquots were measured and averaged over 20 data points (over the full 100 s, 5 s/channel) and these results were normalised against the highest average IR-RF signal. Every IR-RF measurement step used during every bleaching test cycle adds a dose of ca. 10 Gy (100 s

irradiation), which is then bleached out in the following step. A dose of 10 Gy is of little significance when compared with the Des of the samples, while, as the bleaching cycles approach full bleaching the 10 Gy could be expected to be more significant. However, the later bleaching cycles that approach full bleaching are significantly longer than the early cycles. Therefore, it was assumed that the additional 10 Gy is fully bleached out early during the longer bleaching steps and so is of no significance to the final result.

4.4. Results and discussion

4.4.1. IR-RF signal characteristics

The immediate and glaring observation was that all the polymineral fine-grain IR-RF curves were uncharacteristically flat with little vertical dynamic range (Fig. 4.3). Fig. 4.4 compares the regenerated IR-RF curves of polymineral fine-grains (Fig. 4A), K-feldspar and Na-feldspar mid-grains (Fig. 4.4B) for sample LUM 4165. Similarly, the Na-feldspar mid-grain IR-RF curves were flat with little vertical dynamic range (Fig. 4.4B). In contrast, the K-feldspar mid-grain IR-RF curves exhibited the expected characteristic exponential decay. The observations of Buylaert et al. (2012) that the IR-RF signals generated from coarse-grained Na-feldspar and quartz were flat, as well as our observations of the flat nature of the IR-RF curves of the Na-feldspar versus the characteristic curves from the K-feldspar, lead to the hypothesis that the flat IR-RF curve of the polymineral fine-grains was likely due to the abundance of quartz and Na-feldspar. XRF measurements were undertaken to discern the different feldspar chemistry and quartz concentrations of the three sample sets.

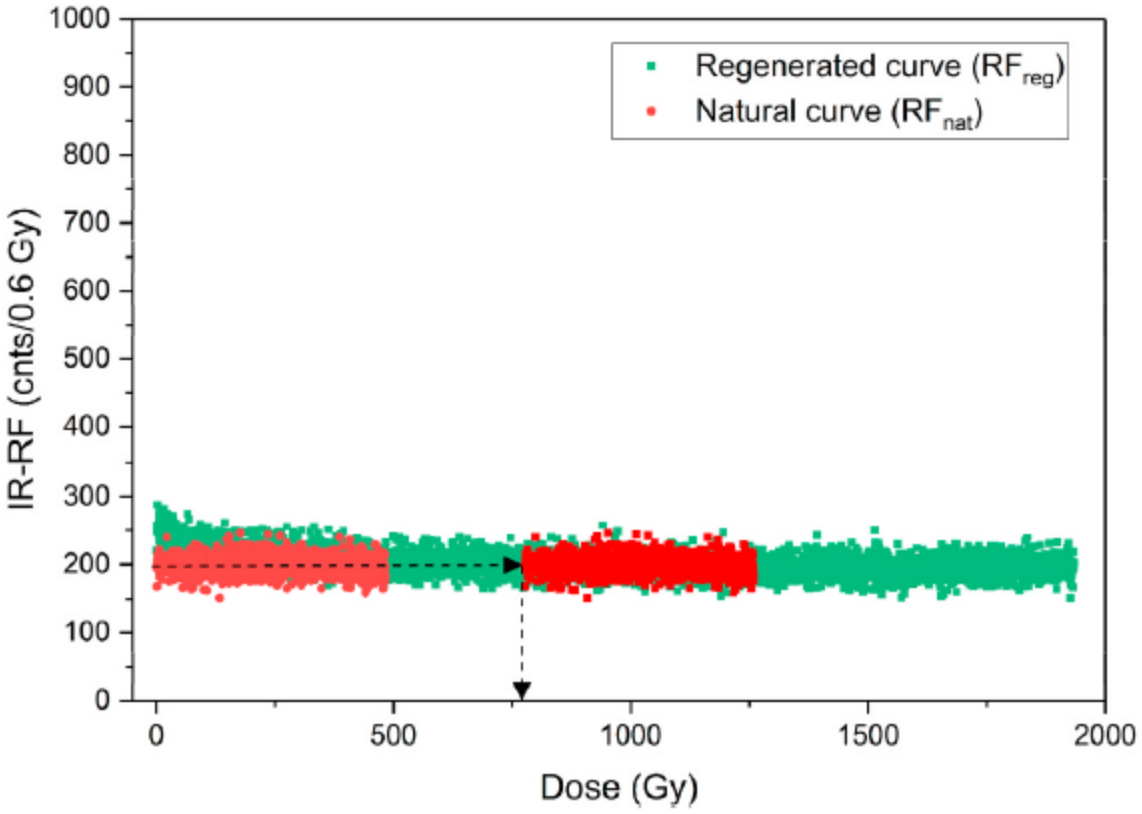

Fig. 4.3. An example of the data output of the IR-RF signal from a polymineral fine-grained sample (LUM4165) of one aliquot. The smaller curve (red) is the natural curve and the larger curve (green) is the regenerated curve, with the point at which the arrowhead falls on the x-axis is the D_e.

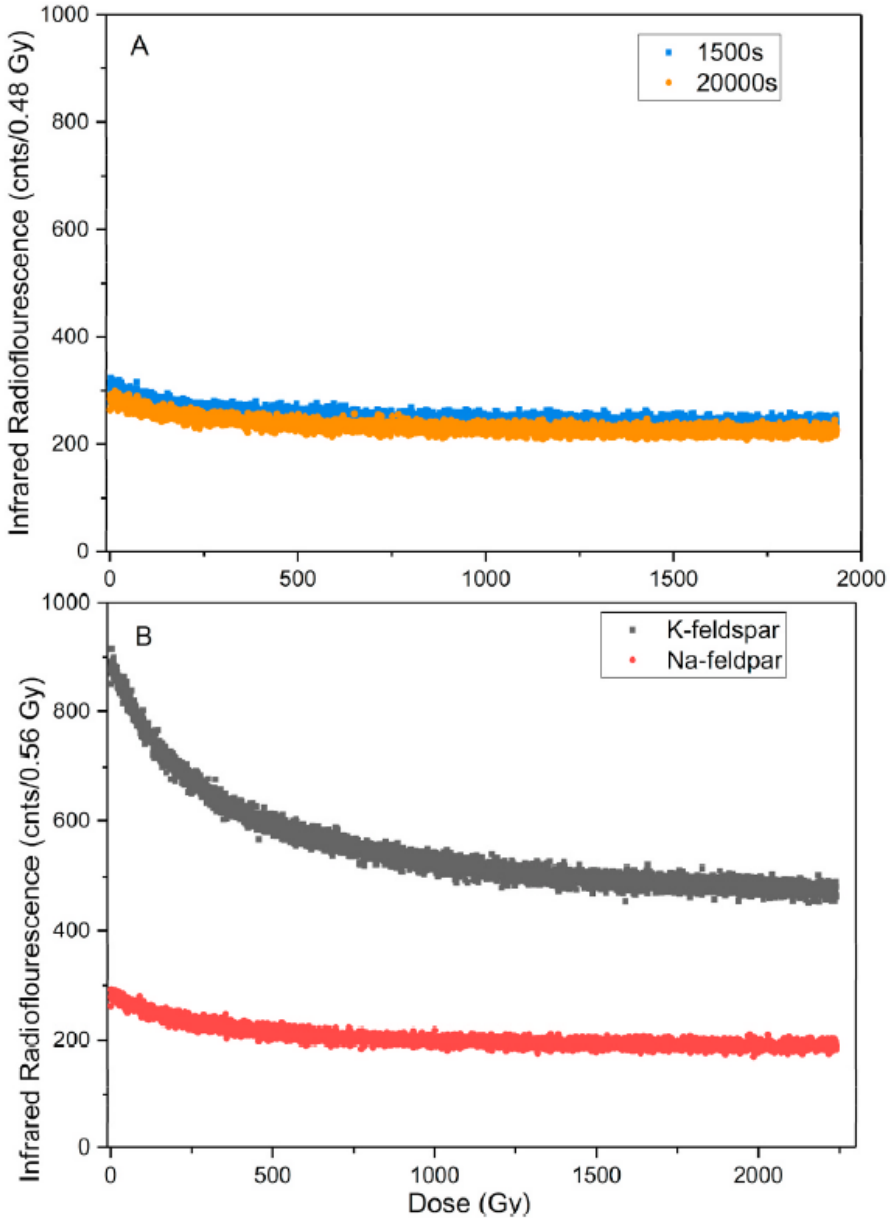

Fig. 4.4. Shape and intensity of the regenerated IR-RF curves (LUM 4165) for: A) the polymineral fine-grains (blue curve: 1500 s bleach and orange curve: 20 000 s bleach) and B) the K-feldspar (black curve) and Na-feldspar mid-grains (red curve).

4.4.2. XRF results

The XRF attached to the Risø reader is focused on the quartz and feldspar chemistry percentages (Na-, K- or Ca-rich feldspars) present in the samples as the majority of other likely minerals were previously removed using chemical treatments. All XRF results were summarized in Table 4.2. The quartz percentages of the polymineral fine-grains range from 46 to 49 % while the quartz percentages of the K-feldspar and Na-feldspar mid-grain samples range from 4 to 10 %

and from 37 to 46 %, respectively. With regards to the feldspar chemistry, the K-feldspar mid-grain samples were dominated by K-feldspar ranging from 84 to 88 %, with minor Na-feldspar ranging from 12 to 16 % and negligible Ca-feldspar, less than 1 % (Fig. 4.5). The Na-feldspar mid-grain samples had a larger proportion of Na-feldspar ranging from 51 to 65 %, less K-feldspar ranging from 30 to 43 % and negligible Ca-feldspar 4–6 % (Fig. 4.5). The polymineral fine-grain samples fall between the two mid-grain samples for K- and Na-feldspar contents ranging from 52 to 63 % and from 28 to 38 %, respectively (Fig. 4.5). The measured K content for the Na-feldspar mid-grain ranged from 4 to 6 % (average: 5.22 ± 0.26 %), for the K-feldspar mid-grain ranged from 11.7 to 12.4 % (average: 11.98 ± 0.24 %) and for the polymineral fine-grains ranged from 7 to 9 % (average: 7.79 ± 0.21 %) (Table 2). The mean K content of the Na-feldspar mid-grains was used to calculate the internal dose rate. The K content calculated from the XRF results for the K-feldspar mid-grains is consistently lower than the standard 12.5 ± 1.0 % traditionally used to calculate the dose rate in coarse-grained K-feldspar. We tested the sensitivity of this change on our dose rate calculation and found that substituting in the measured K contents did not change the dose rates within the reported precision.

The similarly dominant proportions of quartz and a significant proportion of Na-feldspar in both the polymineral fine-grains and in the Na-feldspar mid-grains, an average sum of over 63% and 73% respectively, was likely the cause for their equally flat IR-RF responses. This is in line with Buylaert et al. (2012)'s observations of the IR-RF signal from coarse-grained Na-rich feldspars and quartz. While quartz does emit an RF signal in the IR range (below 735 nm) (Schmidt et al., 2015), the bulk of a quartz response would not have been detected in this study as our detection window is between 850 and 945 nm. However, it is possible that the long-wavelength tail of a quartz emission could overlap with and be detected in the IR-RF detection window as such a peak cannot be completely excluded when using long-pass filters (Krbetschek et al., 2000). This red peak increases with growing irradiation dose which would likely counter any decreasing of the IR peak that we are attempting to measure (Krbetschek et al., 2000). Additionally, it is important to be cognizant of the fact that the polymineral fine-grain samples likely contain other minerals (e.g. micas such as muscovite and biotite) that would not be removed during preparation but may be contributing to the K content analysed by the XRF. Tsukamoto et al. (2012), in a comparative study of the IRSL signal stability of aeolian polymineral fine-grain samples, found that the K-feldspar percentage was less than 5% using both X-ray diffractometry (XRD) as well as scanning

electron microscopy-energy dispersive X-ray (SEM-EDX). The result is confirmed by Meyer et al. (2013) which used the quantitative evaluation of minerals by scanning electron microscopy (QEMSCAN) on polymineral fine-grain samples from interglacial lacustrine deposits (K-feldspar~ 2–4 %). While different original lithologies and depositional environments would likely result in different mineral assemblages, these studies suggest that our XRF results likely over-estimated the K-feldspar contents in the polymineral fine-grains.

Where the feldspar percentages indicate the proportion of feldspar that is either Na– Ca or K- feldspar, they add up to 100%. Note that the quartz percentages reported using the XRF analysis software are an estimate of quartz contamination and may potentially include mica and other silicate contents.

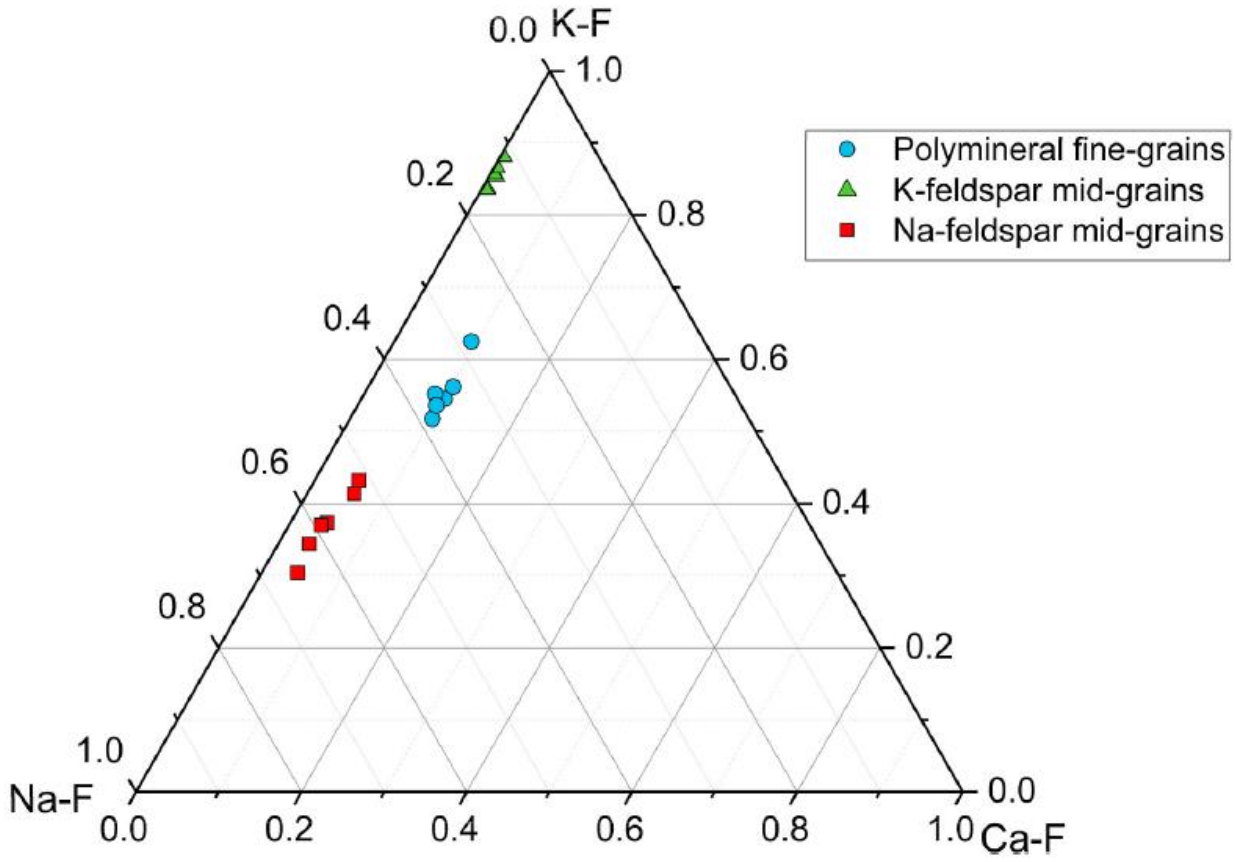

Fig. 4.5. Ternary diagram illustrating the feldspar chemistry of the polymineral fine-grains (blue circles), K-feldspar mid-grains (green triangles) and the Na-feldspar mid-grains (red squares).

Table 4.2 Quartz percentages and relative Na-, K-, and Ca feldspar percentages.

LUM	Polymineral fine-grains					K-feldspar mid-grains					Na-feldspar mid-grains				
	Quartz (%)	Na-feldspar (%)	K-feldspar (%)	Ca-feldspar (%)	K (%)	Quartz (%)	Na-feldspar (%)	K-feldspar (%)	Ca-feldspar (%)	K (%)	Quartz (%)	Na-feldspar (%)	K-feldspar (%)	Ca-feldspar (%)	K (%)
3704	45.5	35.4	54.5	10.1	7.6	7.3	13.8	85.5	0.8	12.0	36.9	58.2	37.3	4.5	5.2
4165	48.2	33.6	56.2	10.3	7.9	10.2	13.9	85.8	0.3	12.0	46.0	52.9	41.4	5.7	5.8
3707	48.6	28.2	62.5	9.3	8.7	6.8	13.1	86.6	0.2	12.1	39.4	59.2	37.0	3.9	5.2
4168	47.2	38.3	51.8	10.0	7.2	7.3	15.7	83.8	0.5	11.7	43.6	65.3	30.4	4.3	4.3
3710	49.3	36.2	55.2	8.6	7.7	4.4	15.9	83.7	0.4	11.7	43.2	51.4	43.2	5.4	6.0
4172	48.8	36.9	53.6	9.5	7.5	8.8	11.5	88.2	0.3	12.4	45.5	61.8	34.4	3.8	4.8

4.4.3. D_e and age results

Notwithstanding the flat nature of all the polymineral fine-grains and the Na-feldspar mid-grains regenerated IR-RF curves, it was possible to acquire D_e results as well as calculate and compare their ages with the reference chronology. The polymineral fine-grain D_es for the 1500 s and the 20 000 s bleaching duration measurements ranged from 251 ± 41 to 961 ± 247 Gy and from 208 ± 68 to 1099 ± 198 Gy, respectively (Table 4.3; Fig. 4.6A and B). The D_es of the two different bleaching durations were consistent with each other within error. There were large uncertainties in both measurements, which were due to the flat nature of the curves and the difficulty with fitting near-horizontal curves, as a slight difference in the intensity of the IR-RF signal resulted in a large difference in D_e (Fig. 4.3). The K-feldspar mid-grain results ranged from 130 ± 14 to 741 ± 51 Gy and from 394 ± 18 to 1000 ± 19 Gy using the 'horizontal sliding' and the 'horizontal and vertical sliding' methods, respectively (Table 3; Fig. 4.6C). These two sets of ages were not consistent with each other, with the 'horizontal and vertical sliding' method consistently and significantly generating higher D_e results across all samples. Both of the K-feldspar result sets have relatively small uncertainties relative to the polymineral fine-grains. The Na-feldspar mid-grain results range from 137 ± 23 to 1238 ± 182 Gy, and the uncertainties broadly increase with sample age (Table 3; Fig. 4.6D). Additionally, two K- and Na-feldspar mid-grain samples (LUM4168 and LUM3710) samples were measured using the bleaching duration of 20 000 s, all 4 D_es increased significantly relative to the shorter bleaching results (the 'horizontal sliding' results) (Table 4.3). Where, horiz: horizontal and vert.: vertical; the horizontal slide was used unless otherwise stated. All reported errors are at 1 sigma, calculated using the standard deviation of the average values divided by the square root of the number of aliquots measured.

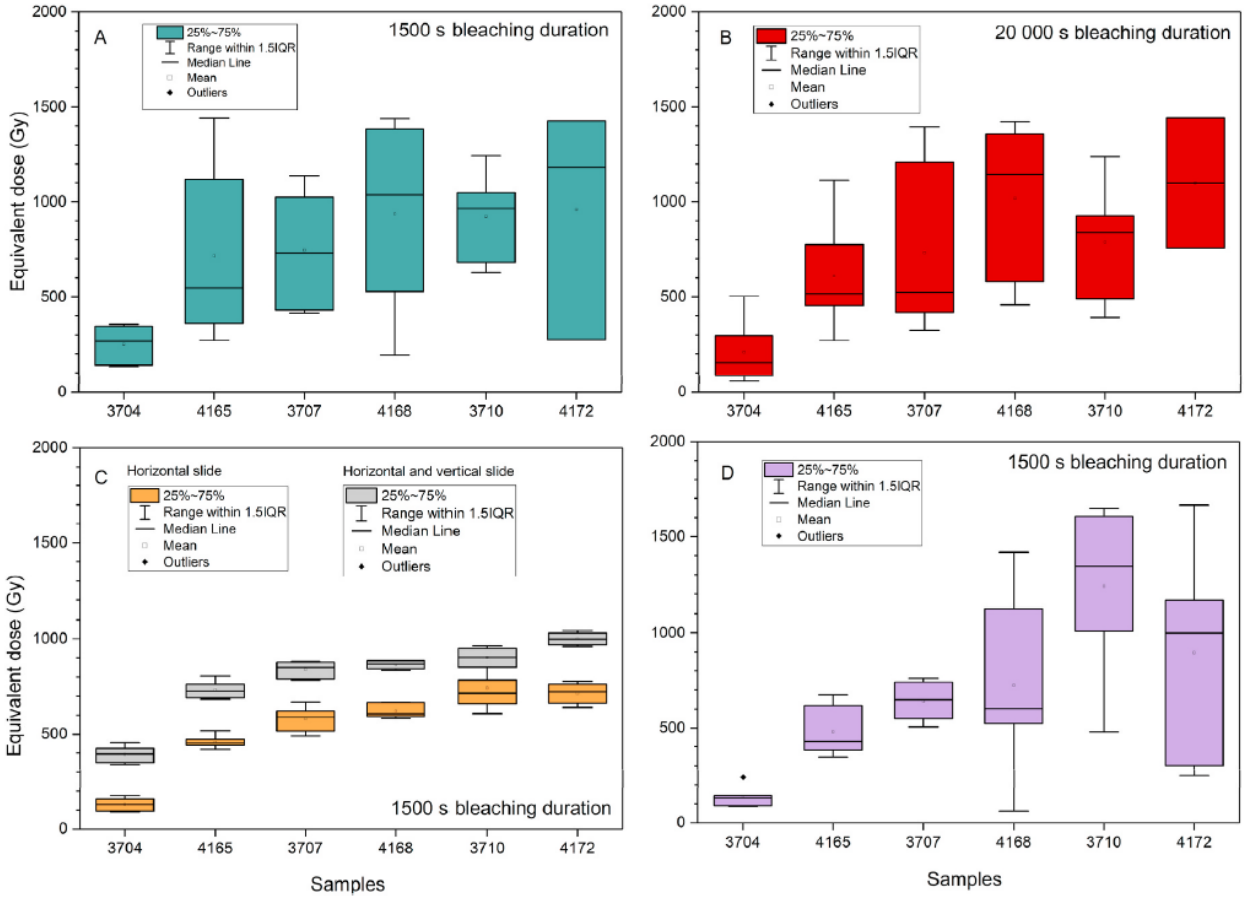

Fig. 4.6. Distribution of the D_e results of A) the polymineral fine-grains (bleaching duration 1500 s), B) the polymineral fine-grains (bleaching duration 20000 s), C) K feldspar mid-grains ('horizontal sliding' and the 'vertical and horizontal sliding' method) and D) Na-feldspar mid-grains.

The age results were calculated by dividing the De results by the corresponding dose rates for each sample (Table 4.3). With the exception of the youngest sample (LUM3704) the polymineral fine-grain age results were consistent (within 1 sigma) with the reference chronology of Ding et al. (2002) up to 300 ka with both bleaching durations, however, the protocol with the 20 000 s bleach performed marginally better (Fig. 4.7) as sample LUM3704 was consistent with the reference chronology within 2 sigma but the shorter bleaching duration age for this sample was outside the 2 sigma range. The older samples (LUM3710 and LUM4172) underestimate relative to the reference ages. The K-feldspar mid-grain age results for the 'horizontal sliding' method were consistent with the reference chronology up to 200 ka and underestimate the ages for samples older than 200 ka (LUM4168, LUM3710 and LUM4172). In contrast, the 'horizontal and vertical sliding' method increased the ages of all the samples which resulted in the samples younger than

200 ka overestimating (LUM3704 and LUM4165), samples from 200 to 300 ka consistent (LUM3707 and LUM4168) with and the samples older than 300 ka underestimating (LUM3710 and LUM4172) the reference chronology (Fig. 4.7). The Na-feldspar mid-grain ages are consistent with the reference chronology up to 350 ka, with the oldest sample (LUM4172) underestimated. Where the two reference ages of Ding et al. (2002) and Zhang et al. (2022) deviate slightly at sample LUM4168 (L3 unit) all the samples show better consistency with the Zhang et al. (2022) reference ages (Table 4.3). Of the two mid-grain samples that were measured using a 20 000 s bleaching duration, the "horizontal slide" K-feldspar mid-grain ages increased to being consistent (within 1 sigma) with the reference ages and the Na-feldspar mid-grains significantly overestimate (Table 4.3). This suggests that bleaching duration plays a more significant role in the mid-grains than in the polymineral fine-grains, and that larger bleaching durations while useful in dating K-feldspar mid-grains are not useful when dating Na-feldspar mid-grains.

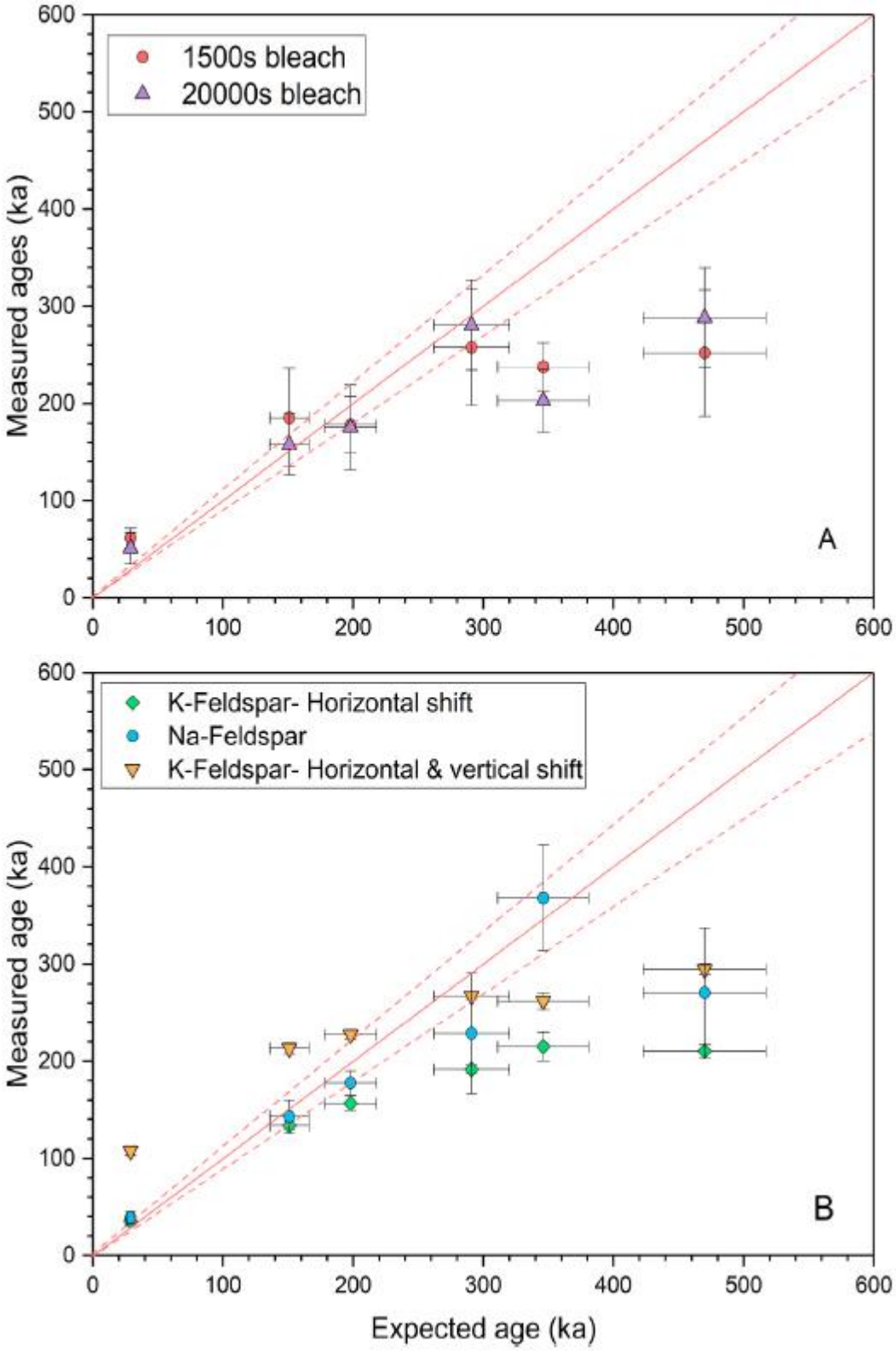

Fig. 4.7. Age results for: A) the polymineral fine-grains (1500 s and 20000 s bleaches) and B) the mid-grains (1500 s bleach), the solid red line represents the age control of Ding et al. (2002) and the dashed lines represent a 10 % error.

Table 4.3 Summary of the equivalent doses, ages calculated and age control.

	Polymineral fine-grain				**K-feldspar mid-grain**						**Na-feldspar mid-grain**				**Ding et al. 2002**	**Zhang et al., 2022**
LUM	1500 s Bleach		20000 s Bleach		1500 s Bleach		1500 s Bleach (vert. & horiz.)		20000 s Bleach		1500 s Bleach		20000 s Bleach			
	D_e (Gy)	Age (ka)	D_e (Gy)	Age (ka)	D_e (Gy)	Age (ka)	D_e (Gy)	Age (ka)	D_e (Gy)	Age (ka)	D_e (Gy)	Age (ka)	D_e (Gy)	Age (ka)	Age (ka)	Age (ka)
3704	251±41	65±11	208±68	54±18	130±14	36±4	394±18	108±5			137±23	39±7			29±3	32±2
4165	714±195	196±53	608±121	167±33	459±14	134±4	732±19	213±5			480±55	144±17			151±15	146±4
3707	745±121	188±31	733±184	185±46	579±28	157±8	840±19	227±5			642±46	178±13			198±20	196±8
4168	935±217	272±63	1018±169	296±49	621±16	192±5	864±10	267±3	853±32	264±10	722±196	230±62	1944±85	619±27	291±29	268±9
3710	922±95	251±26	787±126	214±34	741±51	215±15	902±29	262±8	1488±263	432±76	1238±182	370±54	1875±159	560±47	346±35	
4172	961±247	266±68	1099±198	304±55	714±22	210±7	1000±19	295±6			897±221	272±67			470±47	

Where, horiz.: horizontal and vert: vertical; the horizontal slide was used unless otherwise stated.

Table 4.4 Gamma spectrometry and dose rates of the polymineral and mid-grain fractions.

Sample	**LUM**	**Depth (m)**	**U (ppm)**	**Th (ppm)**	**K (%)**	**Dose rates (Gy/ka)**		
						Polymineral fine-grain	K-feldspar mid-grain	Na- feldspar mid-grain
L1(2)	3704	3.5	2.8±0.1	11.5±0.2	1.9±0.1	3.87±0.18	3.65±0.19	3.55±0.18
L2(2)	4165	13.9	2.5±0.2	11.2±0.6	1.9±0.1	3.65±0.18	3.43±0.19	3.34±0.18
S3	3707	18.3	2.8±0.1	13.8±0.2	2.1±0.1	3.96±0.18	3.69±0.19	3.60±0.18
L3(2)	4168	23.1	2.2±0.1	11.1±0.6	1.8±0.1	3.44±0.17	3.24±0.18	3.14±0.17
L4(1)	3710	26.4	2.5±0.1	11.7±0.2	1.9±0.1	3.67±0.18	3.44±0.19	3.35±0.18
L5(2)	4172	34.9	2.4±0.1	11.5±0.7	1.9±0.1	3.61±0.18	3.40±0.19	3.30±0.18

4.4.4. Dose recovery tests

The dose recovery ratios for the polymineral fine-grains using the 1500 s bleaching duration showed that the three youngest samples (LUM3704, LUM4165 and LUM3707) have a large spread of data with the average dose recovery ratios far exceeding 1, however, with increasing age the spread of data decreases and the dose recovery ratios approach 1 (Fig. 4.8A). The polymineral fine-grain results for the 20 000 s beach duration showed a similar trend for younger samples having a larger spread of data, significantly exceeding 1 and trend towards 1 with increasing age (Fig. 4.8B). However, the age of the oldest sample (LUM4172) was underestimated. For mid-grain samples, the dose recovery results of K-feldspar (horizontal slide) are all largely within 10% uncertainly; however, the oldest sample (LUM4172) marginally underestimates (Fig. 4.8C); while the Na-feldspar dose recovery results show less consistency with large uncertainties and two samples overestimating significantly, three samples within 10% of 1 and LUM4172 marginally underestimating (Fig. 4.8D). Additionally, dose recovery tests were done on the K-feldspar mid-grains with the horizontal and vertical slide method. For the younger samples (LUM3704 and LUM4165), both results overestimate in similar proportions to the D_e over-estimations previously mentioned showing that in these two instances the dose recovery test was able to predict the over-estimation. This is an issue with the horizontal and vertical slide method that was observed by Murari et al. (2018). The older samples all showed dose recovery results in saturation using the horizontal and vertical slide method. The fact that the K-feldspar mid-grain dose recovery measurements using the horizontal slide method performed better than the others while simultaneously the D_e and age determinations performed worse indicates that the dose recovery measurements were not a useful predictor of whether an IR-RF measurement will determine the age successfully. This could be due to the observation of Murari et al. (2018) that there is a sensitivity change between the natural and regenerated measurements (due to the initial bleaching of the natural signal) and thereafter no sensitivity change between subsequent measurements. Therefore, the initial bleaching of the samples during the dose recovery tests could have already altered the sample, and so we were not actually successfully recreating the natural aging process when performing dose recovery tests on the IR-RF signal. This could potentially be overcome with the use of a modern analog sample, such as was used by Murari et al. (2018) where they illustrate the problem of sensitivity change between the natural and regenerative measurements. However, caution should be taken to select a truly representative analogue as the

IR-RF signal is a direct measurement (is not normalised with a test dose in the way that IRSL signals are) and thus the individual intensities can vary significantly sample to sample within the same sequence. The poor performance of the dose recovery tests was, however, not observed in IR-RF signals from coarse-grained K-feldspar (Buchanan et al., 2022), suggesting that the effect of this may be larger in fine- and mid-grains. An additional observation is that the extremely large overestimation in the youngest sample occurred in samples that were rich in Na-feldspar and quartz (but not in the K-feldspar mid-grains), which suggested that this trend may be specific to the composition of these samples.

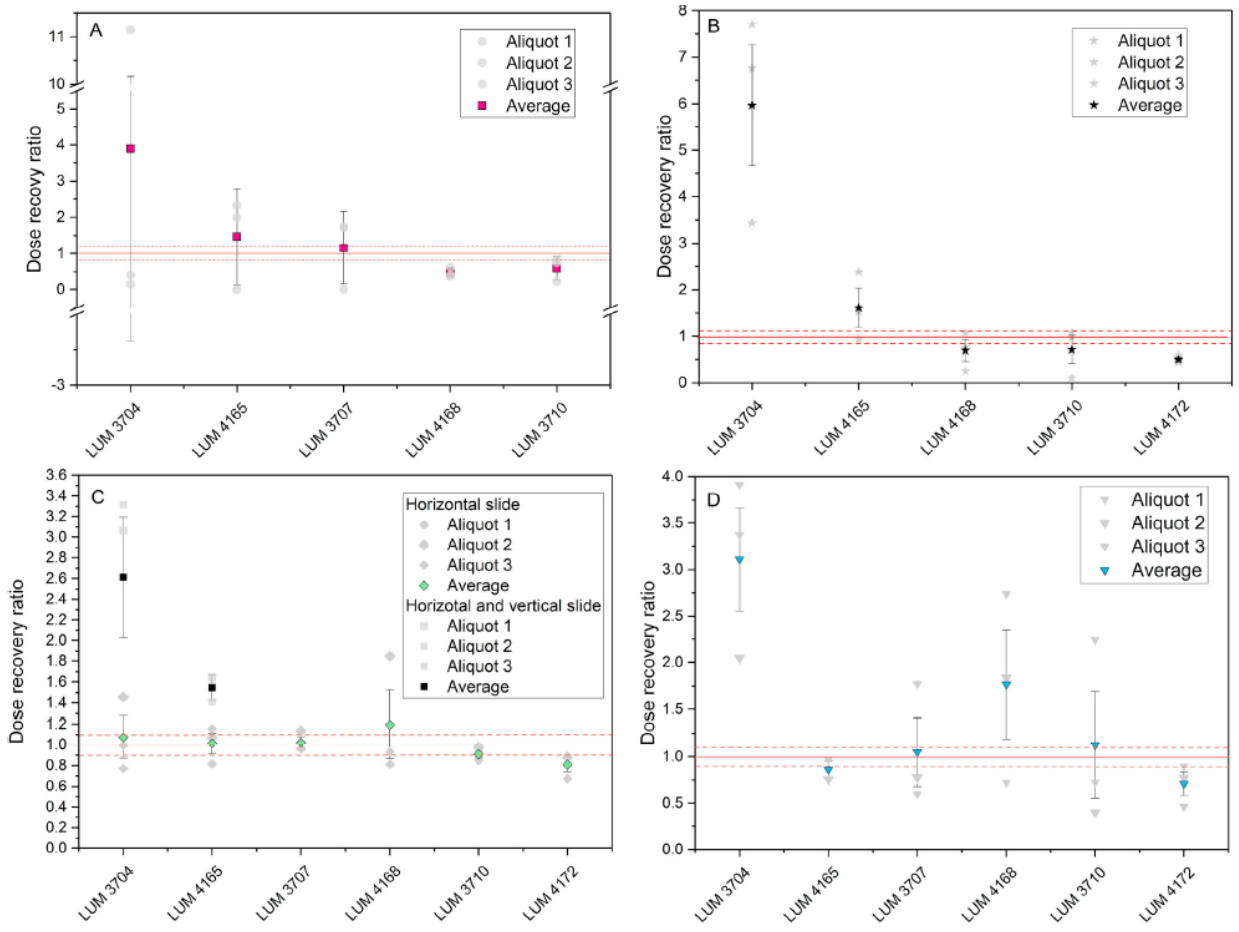

Fig. 4.8. Dose recovery test results where a dose recovery ratio of 1 (red solid line) within 10% (the red dashed line) is considered successful. A) Polymineral fine-grains (1500 s bleach), B) Polymineral fine-grains (20000 s bleach), C) K-feldspar mid-grains, and D) Na-feldspar mid-grains. The samples are ordered in increasing age from left to right.

4.4.5. Bleaching tests

All samples were successfully bleached to within 5% of the fully bleached signal. Both mid-grain K-feldspar and Na-feldspar bleaching tests appear to plateau out at approximately 160 s while the polymineral fine-grains bleaching tests plateau at approximately 60 s (Fig. 4.9). The polymineral fine-grains graph is misleading, wrongly suggesting that the degree to which the polymineral fine-grains were bleached was less than the mid-grains, which is not the case. In order to ensure that the bleaching results of different samples (with different natural signal intensities) is independent of D_e we normalised the results. The results were normalised to the last measurement (most bleached measurement), and this measurement is the most likely to suffer from sensitivity changes (and possibly over bleaching, ie. a more intense bleach than it would experience in nature) due to repeated bleaching cycles. These bleaching results, while subtle, reinforce the previous D_e results suggesting that the bleaching behavior of the different grain sizes is significantly different and that the IR-RF signal bleaches out earlier or easier in the polymineral fine-grains. It was also observed that the errors on the average result (3 aliquots measured) are different for the different data sets. The polymineral fine-grain error bars are the largest (~15 %) followed by the Na-feldspar mid-grain errors (~10 %) and the smallest errors in the K-feldspar mid-grain bleaching data; likely due once again to the shape of the curve and the low dynamic range in the IR-RF signals from the polymineral fine-grains and Na-feldspar mid-grains. This is in line with Buchanan et al. (2022) where it was found that coarse-grains required a significantly longer bleaching duration.

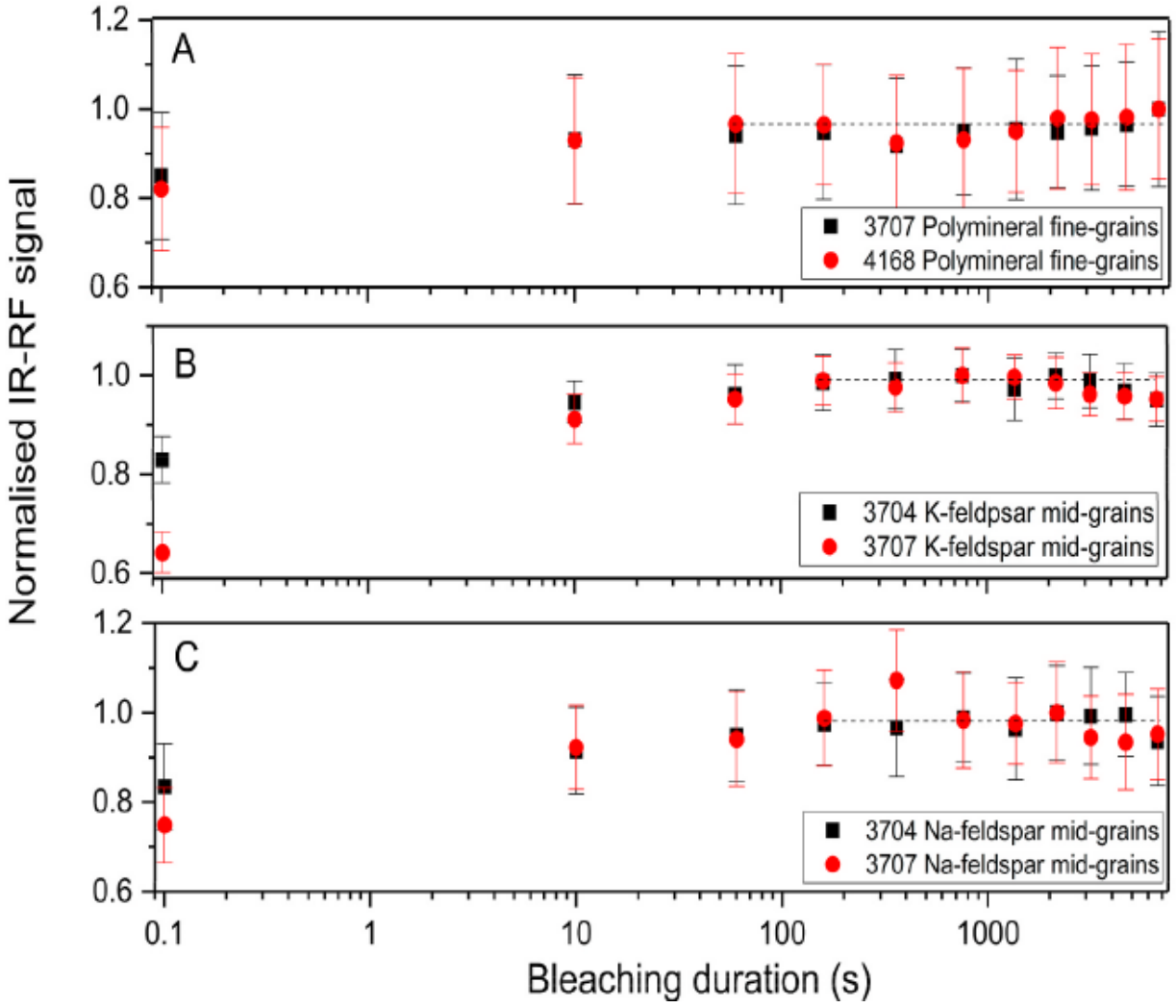

Fig. 4.9: Bleaching test results of: A) polymineral fine grains of LUM3707 and LUM4168, B) K-feldspar mid-grains of LUM3704 and LUM3707, C) Na-feldspar mid-grains of LUM3704 and LUM3707. Note that these are cumulative measurements. Dotted lines show approximate suggested plateaus. These results are an average of 3 aliquots.

4.5. Conclusions

In this study we tested IR-RF dating on polymineral fine-grains from the Luochuan loess-palaeosol sequence using two different bleaching duration settings (1500 s and 20 000 s) between the natural and the regenerated curves, and compared them with mid-grain sample sets of K-feldspar and Na-feldspar rich grains. The polymineral IR-RF curves did not exhibit the characteristic decreasing exponential curve shape but were unexpectedly flat, as were the curves of the Na-feldspar mid-grains; in contrast the K-feldspar mid-grain curves exhibited the

characteristic IR-RF curve shape. We attribute the flattened nature of the curves to the dominance of Na-feldspar and quartz in the polymineral samples.

The polymineral fine-grain ages (both bleaching durations) were consistent with the reference ages of Ding et al. (2002) up to 300 ka, while older samples underestimate. The K-feldspar mid-grain ages are consistent with the reference ages up to 200 ka when using the 'horizontal sliding' method to obtain the D_e. When an attempt was made to account for sensitivity changes the 'vertical and horizontal sliding' method was considered. This increased all ages of the samples and resulted in age overestimation of the samples younger than 200 ka, and consistency with reference ages in samples between 200 and 300 ka and underestimation in samples older than 300 ka. While the Na-feldspar samples are consistent with the reference ages up to 350 ka, with the 'horizontal sliding' method.

The sample set with the most successful dose recovery tests gave the poorest dating results (K-feldspar mid-grains) and the sample set with the least successful dose recovery tests gave the best dating results (Na-feldspar mid-grains, polymineral fine-grains), suggesting that in the case of polymineral fine-grains and mid-grains, dose recovery tests were a less useful indicator of whether IR-RF dating of a sample will be successful than in the case of coarse-grained K-feldspar.

The observation that the polymineral fine-grain ages generated by both bleaching durations is consistent with the reference ages suggests that the influence of bleaching duration is less significant in polymineral fine-grains than has been observed in coarse grains previously (Buchanan et al., 2022). However, when the K-feldspar mid-grains are bleached over a longer period (20 000 s), ages of the samples that were previously underestimated (1500 s bleach) increased to being consistent with the reference ages. Additionally, the bleaching tests show that the polymineral fine-grains bleach out earlier than the mid-grains, suggesting that grain size is a significant factor when determining a suitable bleaching duration.

Despite the uncharacteristic regenerated curve shapes, polymineral fine-grains are a suitable dosimeter for IR-RF dating up to 300 ka. While the presence of quartz and Na-feldspar in polymineral fine-grains can alter the shape of the regenerated IR-RF curve, this should not exclude the use of polymineral fine-grains in IR-RF dating. The dating of polymineral fine-grains does not require the long bleaching times of the coarse-grained K-feldspars, which suggests that IR-RF dating of polymineral fine-grains may be suitable for depositional environments that exhibit partial

bleaching in coarse-grains, e.g. water lain sediments. Dose recovery tests should not solely be relied upon to evaluate the reliability of a dosimeter; reference ages and comparisons of different methods are also useful alternative tools to do so.

Declaration of competing interest

The authors declare the following financial interests/personal relationships which may be considered as potential competing interests: Hao Long reports financial support was provided by National Natural Science Foundation of China.

Data availability

Data will be made available on request.

Acknowledgements

We thank Sonja Riemenschneider, Sabine Mogwitz and Petra Posimowski for their assistance with sample preparation and gamma spectrometry. Jingran Zhang, Zhong He and Linhai Yang are thanked for their assistance with sample collection and fieldwork. This study was partly supported by the National Natural Science Foundation of China (No. 41977381). Heartfelt thanks also go to the two anonymous reviewers and editor, whose comments and suggestions have improved this paper tremendously.

References

Ankjærgaard, C., Guralnik, B., Buylaert, J.-P., Reimann, T., Yi, S.W., Wallinga, J., 2016. Violet stimulated luminescence dating of quartz from Luochuan (Chinese loess plateau): agreement with independent chronology up to ~600 ka. Quat. Geochronol. 34, 33–46.

Brennan, B.J., Lyons, R.G., Phillips, S.W., 1991. Attenuation of alpha particle track dose for spherical grains. Int. J. Radiat. Appl. Instr. Part D 18, 249–253.

Buchanan, G.R., Tsukamoto, S., Zhang, J., Long, H., 2022. Testing the natural limits of infrared radiofluorescence dating of the Luochuan loess-palaeosol sequence, Chinese Loess Plateau. Radiat. Meas. 155.

Buylaert, J.P., Jain, M., Murray, A.S., Thomsen, K.J., Lapp, T., 2012. IR-RF dating of sand-sized K-feldspar extracts: a test of accuracy. Radiat. Meas. 47, 759–765.

Coussot, C., Liard, M., Kreutzer, S., Mercier, N., 2019. S´equence de Comblement d'un Pal´eovallon en Contexte de Plateau (290-10 ka) : La Coupe de Courville-sur-Eure (Eure-Et-Loir, France). Quaternaire 30 (2), 167–183.

Ding, Z.L., Derbyshire, E., Yang, S.L., Yu, Z.W., Xiong, S.F., Liu, T.S., 2002. Stacked 2.6- Ma grain size record from the Chinese loess based on five sections and correlation with the deep-sea δ18O record. Paleoceanography 17, 5-1-5-21.

Erfurt, G., Krbetschek, M.R., 2003a. Studies on the physics of the infrared radioluminescence of potassium feldspar and on the methodology of its application to sediment dating. Radiat. Meas. 37, 505–510.

Erfurt, G., Krbetschek, M.R., 2003b. IRSAR- a single-aliquot regenerative-dose dating protocol applied to the infrared radiofluorescence (IR-RF) of coarse-grain K-feldspar. Ancient TL 21, 35–42.

Frechen, M., Schweitzer, U., Zander, A., 1996. Improvements in sample preparation for the fine grain technique. Ancient TL 14, 15–17.

Frouin, M., 2014. Les feldspaths comme support pour la datation par luminescence de gisements archeologiques et de sequences quaternaires d'Aquitaine PhD thesis Universite Bordeaux Montaigne, p. 390. France.

Frouin, M., Huot, S., Kreutzer, S., Lahaye, C., Lamothe, M., Philippe, A., Mercier, N., 2017. An improved radiofluorescence single-aliquot regenerative dose protocol for K-feldspar. Quat. Geochronol. 38, 13–24.

Frouin, M., Huot, S., Mercier, N., Lahaye, C., Lamothe, M., 2015. The issue of laboratory bleaching in the infrared-radiofluorescence dating method. Radiat. Meas. 81, 212–217.

Huntley, D.J., Baril, M.R., 1997. The K content of the K-feldspars being measured in optical dating or in thermoluminescence dating. Ancient TL 15, 11–13.

Huntley, D.J., Hancock, R.G.V., 2001. The Rb contents of the K-feldspar grains being measured in optical dating. Ancient TL 19, 43–46.

Krbetschek, M.R., Trautmann, T., Dietrich, A., Stolz, W., 2000. Radioluminescence dating of sediments: methodological aspects. Radiat. Meas. 32, 493–498.

Kreutzer, S., Murari, M.K., Frouin, M., Fuchs, M., Mercier, N., 2017. Always remain suspicious: a case study on tracking down a technical artefact while measuring IR-RF. Ancient TL 35, 20–30.

Kreutzer, S., 2019. Luminescence: comprehensive luminescence dating data analysis. In: Kreutzer, S., Burow, C., Dietze, M., Fuchs, M.C., Schmidt, C., Fischer, M., Friedrich, J. (Eds.), analyse_IRSAR.RF( ): Analyse IRSAR RF Measurements. Function Version 0.7.5. R package version 0.9.0.109. https://CRAN.R-project.or g/package=Luminescence.

Kreutzer, S., Martin, L., Dubernet, S., Mercier, N., 2018. The IR-RF alpha-Efficiency of K-feldspar. Radiat. Meas. 120, 148–156.

Kreutzer, S., Mercier, N., Lamothe, M., 2022. Infrared-radiofluorescence: dose saturation and long-term signal stability of a K-feldspar sample. Radiat. Meas. 156, 106818.

Lapp, T., Kook, M., Murray, A.S., Thomsen, K.J., Buylaert, J.-P., Jain, M., 2015. A new luminescence detection and stimulation head for the Risø TL/OSL reader. Radiat. Meas. 81, 178–184.

Li, Y., Tsukamoto, S., Long, H., Zhang, J., Yang, L., He, Z., Frechen, M., 2018. Testing the reliability of fading correction methods for feldspar IRSL dating: a comparison between natural and simulated-natural dose response curves. Radiat. Meas. 120, 228–233.

Liritzis, I., Stamoulis, K., Papachristodoulou, C., Ioannides, K., 2013. A re-evaluation of radiation dose-rate conversion factors. Mediterr. Archaeol. Archaeom. 13, 1–15.

Murari, M.K., Kreutzer, S., Fuchs, M., 2018. Further investigations on IR-RF: dose recovery and correction. Radiat. Meas. 120, 110–119. Murari, K.M., Kreutzer, S., King, G., Frouin, M., Tsukamoto, S., Schmidt, C., Lauer, T., Klasen, N., Richter, D., Friedrich, J., Mercier, N., Fuchs, M., 2021. Infrared radiofluorescence IR-RF dating: a review. Quat. Geochronol. 64, 101155.

Prescott, J.R., Hutton, J.T., 1994. Cosmic ray contributions to dose rates for luminescence and ESR dating: large depths and long-term time variations. Radiat. Meas. 23, 497–500.

Rahimzadeh, N., Tsukamoto, S., Zhang, J., Long, H., 2021. Natural and laboratory dose response curves of quartz violet stimulated luminescence (VSL): exploring the multiple aliquot regenerative dose (MAR) protocol. Quat. Geochronol. 65, 101194.

Richter, M., Tsukamoto, S., Long, H., 2020. ESR dating of Chinese loess using the quartz Ti center: a comparison with independent age control. Quat. Int. 556, 159–164.

Schilles, T., 2002. Die Infrarot-Radiolumineszenz von Feldsp¨aten und ihr Einsatz in der Lumineszenzdatierung. . PhD thesis. Ruprechts-Karls-Universit¨at Heidelberg, Germany, pp. 1–149.

Schmidt, C., Kreutzer, S., DeWitt, R., Fuchs, M., 2015. Radiofluorescence of quartz: a review. Quat. Geochronol. 27, 66–77.

Trautmann, T., Krbetschek, M.R., Dietrich, A., Stolz, W., 1998. Investigations of feldspar radioluminescence: potential for a new dating technique. Radiat. Meas. 29, 421–425.

Trautmann, T., Krbetschek, M.R., Dietrich, A., Stolz, W., 1999a. Feldspar radioluminescence; a new dating method and its physical background. J. Lumin. 85, 45–58.

Trautmann, T., Dietrich, A., Stolz, W., Krbetschek, M.R., 1999b. Radioluminescence dating: a new tool for quaternary geology and archaeology. Naturwissenschaften 86, 441–444.

Tsukamoto, S., Long, H., Richter, M., Li, Y., King, G.E., He, Z., Yang, L., Zhang, J., Lambert, R., 2018. Quartz natural and laboratory ESR dose response curves: a first attempt from Chinese loess. Radiat. Meas. 120, 137–142.

Tsukamoto, S., Jain, M., Murray, A., Thiel, C., Schmit, E., Wacha, L., Dohrmann, R., Frechen, M., 2012. A comparative study of the luminescence of polymineral fine grains and coarse-grained K- and Na-rich feldspars. Radiat. Meas. 47, 903–908.

Zhang, J., Tsukamoto, S., 2022. A simplified multiple aliquot regenerative dose protocol to extend the dating limit of K-feldspar pIRIR signal. Radiat. Meas. 157.

Zhang, J., Hao, Q., Li, S.-H., 2022. An absolutely dated record of climate change over the last three glacial–interglacial cycles from Chinese loess deposits. Geol. 50, 1116-112

Chapter 5:

Co-Author contributions.

This chapter is a manuscript in preparation, with expected submission in 2024. Archived (stored in Hannover) samples were used that were collected and prepared by Dr. Thiel for a previous study. The initial scientific idea was outlined by Dr. Thiel (when she was supervising the PhD work), and evolved over time with Prof. Dr. Tsukamoto's guidance. I generated the majority of luminescence data running luminescence experiments, with the support of initially Dr. Thiel and thereafter Prof. Dr. Tsukamoto and Dr. Zhang. One sample was measured with the IRPL dating method by Dr. Jain at the Technical University of Denmark (DTU) Risø Campus laboratory in Denmark due to an addition of the sample to the study after I had completed the initial measurement and I had returned to Hannover. The regional dose rate data was generated by lab technicians for a previous study and I generated and recalculated the regional dose rates using an R-script template written for general use by Dr. Zhang. The majority of analysis and interpretation was done by me, with the support of Prof. Dr. Tsukamoto and Dr. Zhang. I wrote the initial drafts, which were reviewed by Prof. Dr. Tsukamoto, thereafter corrected/ edited by me and will be reviewed and proof read by all authors.

Preliminary authors: Buchanan, G.R, Tsukamoto, S., Zhang, J., Jain, M., and Thiel, C

Intended Journal: Quaternary Geochronology

Early insights comparing the infrared radiofluorescence (IR-RF) and infrared photoluminescence (IRPL) signals for dating: A case study from Sardinia.

G. R. Buchanan [a, b], S. Tsukamoto [a, b], J. Zhang [a], M. Jain [c], C., Thiel [d]

[a] Leibniz Institute for Applied Geophysics, Section 3: Geochronology, 30655, Hannover, Germany

[b]University Tübingen, Terrestrial Sedimentology, 72076, Tübingen, Germany

[c]Department of Physics, Technical University of Denmark, DTU Risø Campus, Denmark

[d]Federal Institute for Geoscience and Natural Resources, 30655, Hannover, Germany

Abstract

The role of feldspar as a dosimeter using infrared stimulated luminescence has long been hampered by the observation of anomalous fading resulting in the underestimation of obtained ages when using dating techniques that measure recombination. We investigated and compared luminescence dating techniques that make use of the principal trap and are theorised to have a reduced effect of fading: infrared radiofluorescence (IR-RF; at room temperature: RF_{RT}, and at 70 °C: RF_{70}) and the novel infrared photoluminescence (IRPL; $IRPL_{880}$ and $IRPL_{955}$). Four coarse grained coastal samples from Sardinia (~133 ka to 234 ka) were measured and compared with reference ages determined by Thiel et al. (2010). Bleaching tests were done on the IR-RF signals to evaluate their bleachability, as well as dose recovery tests to evaluate the validity of the measurement protocol of the IR-RF signals. The IRPL signals exhibited large recuperation percentages which increased with successive IRPL-IRSL cycles, therefore two IRPL cycles were compared: the first and last. The two younger samples (~133 ka -136 ka) show good correlation for all ages with reference ages generally within 1σ and only a few within 2σ. The older samples (SG_3: ~189 ka, SG_4: ~ 234 ka) show reasonable correlation within 2 σ, however the range of the 2σ uncertainty is wider and more varied than the younger samples. Of the two IR-RF signals, the RF_{RT} signal appears to perform better in these samples, likely doe to resetting issues of the RF_{70} signal. Of the IRPL signals the $IRPL_{955}$ performed slightly better with regards the recuperation and the first IRPL cycle (before the preheat) was preferred for the same reason.

5.1. Introduction

Optically stimulated luminescence (OSL) makes use of the natural dosimeters of quartz and feldspar to establish absolute geochronologies in sedimentary sequences deposited during the Quaternary (Duller, 1996). This widely accepted dating method determines the depositional age of the sediment, the time elapsed since the last exposure to the surface and thus the bleaching effect of sunlight. Quartz and feldspar exhibit different luminescence properties, advantages and disadvantages. The infrared stimulated luminescence (IRSL) signal of feldspar saturates at a slower rate than the signal generated using the quartz OSL signal and thus allows for the dating of older sediments relative to the quartz methods. The IRSL signal suffers from an instability termed anomalous fading which is due to the quantum tunneling of electrons (Spooner, 1994; Huntley and Lian, 2006). This instability can be accounted for by using both elevated temperature signals that have demonstrated lower fading rates: a) the post-infrared IRSL (hereafter $pIRIR_a$ where the subscript is the post IR stimulation temperature) and the multi-elevated temperature IRSL signals (MET-pIRIR) and are less affected by anomalous fading (Thomsen et al., 20011; Li and Li, 2011); and b) post measurement fading correction models (Huntley and Lamothe, 2001, Kars et al., 2008, Lamothe et al., 2003). While the pIRIR methods, i.e. $pIRIR_{225}$ (Buylaert et al., 2009) and $pIRIR_{290}$ (Thiel et al., 2011), exhibit increasingly stable signals, they have been observed to exhibit evidence (non-zero g-values) that they may suffer from minor fading (Li et al., 2014; Li et al., 2018). Luminescence dating methods that make use of the principal trap have been brought to the fore as alternative non-fading dating options, namely: infrared radiofluorescence (IR-RF) (Trautmann et al., 1998; Erfurt and Krbetschek, 2003) and infrared photoluminescence (IRPL) (Prasad et al., 2017; Kumar et al., 2018). A recent investigation by Kumar et al. (2022), reports observations that fading is primarily a result of changes in the recombination efficiency due to the loss of available traps at the recombination centre and that a direct loss of electrons in the principal trap is minor in comparison. This suggests that the use of IRPL and IR-RF dating could gain main stream importance in the future.

Trautmann et al. (1998) proposed infrared radiofluorescence (IR-RF) as an alternative method that makes use of an infrared luminescence signal stimulated by continuous irradiation (β or γ). It is theorized, that this signal does not suffer from fading as the signal obtained is emitted while electrons are entering the traps rather than when previously trapped electrons are released from the traps, additionally recombination is not a concern. Erfurt and Krbetschek (2003)

developed an infrared radiofluorescence single aliquot protocol (IRSAR) measurement at room temperature (RF_{RT}) and demonstrated its utility. Buylaert et al. (2012a) however, compared IR-RF dating of coastal marine and colluvial sediments with independent age control which resulted in an overestimation of samples aged 20-45 ka and underestimation of samples aged ~128 ka. The failure of IR-RF to return ages comparable with independent age control set back interest in the IR-RF signal until Frouin et al. (2017) developed a modified IR-RF protocol (RF_{70}) during which preheats and measurements were conducted at 70° C. This modified protocol keeps shallow unstable traps related to Fe^{3+} empty, and showed good correlation between RF_{70}, $pIRIR_{290}$ and OSL signals (where available) with samples ranging from ~ 0 ka to ~194 ka, within 2σ with the exception of one sample that significantly over estimated.

IRPL is a novel, new optical dating method pioneered by Prasad et al. (2017). Similar to IRSL, IRPL was measured using a SAR based protocol for dating sediments (Kumar et al., 2021). Where IRSL is based on anti-Stokes photon emissions (associated with recombination centres) and is destructive, IRPL is non-destructive and makes use of Stokes photon emissions (Prasad et al., 2017). Essentially the IRPL protocol results in the excitation of electrons within the principal trap and is potentially a stable component that may exhibit little to no fading (Prasad et al., 2017; Kumar et al., 2022). Two IRPL signals have been observed ($IRPL_{880}$ and $IRPL_{955}$; the subscript denotes the emission wavelength in nm), compared and investigated as to whether the IRPL signals and the IR-RF signals make use of the same traps (Kumar et al., 2018). Kumar et al. (2021) compared the IR-RF results obtained by Buylaert et al. (2012a) with both IRPL signals, and observed that the IRPL signal performs better than the IR-RF signal in those samples and they attribute the underestimation observed by Buylaert et al. (2012) to sensitivity changes. Kumar et al. (2018) showed that the signals likely originate in the same defects but that the IRPL stimulation likely probes specific defects while the IR-RF signal may have contributions from other defects, e.g. the Fe^{3+}, leading to a more mixed response.

The objective of this study is to compare the suitability of new and innovative luminescence dating methods that make use of the principal trap in feldspar; IR-RF (RF_{RT} and RF_{70}) and IRPL ($IRPL_{880}$ and $IRPL_{955}$). The suitability of these methods is ascertained by comparing the obtained ages with chronologically controlled samples, the ages of which are published in Thiel et al. (2010) and were obtained using conventional OSL and fading corrected $pIRIR_{225}$ signals.

5.2. Materials and methods

5.2.1. Samples and their previous age assignments:

Four samples were measured in this study, these samples were taken on the western coast line of Sardinia at the San Giovanni di Sinnis sequence (Fig. 5.1). Samples SG_1 and SG_3 were taken at the Northern San Giovanni outcrop and samples SG_2 and SG_4 were taken from the adjacent southern San Giovanni out crop. For more information on the sampling location, depositional environment and geological setting see: Lecca and Carboni (2007), Andreucci et al. (2009), Coltorti et al. (2010) and Thiel et al. (2010).

All four of the samples were dated by Thiel et al. (2010) using conventional OSL (quartz) and fading corrected $pIRIR_{225}$ (K-feldspar) methods which are considered to be a reliable reference age. Samples SG_1 and SG_2 were taken from carbonate rich laminated sandstone, which are interpreted by Coltorti et al. (2010) as being from the same stratigraphic unit and aeolian in nature. While in contrast Lecca and Carboni (2007) interpret SG_1 as being a result of aeolian deposition and SG_2 as a part of the foreshore environment. Sample SG_3 derives from a carbonate-rich sandstone unit that contains coarse quartz pebbles, and sample SG_4 derives from cemented fine sands that contain shell debris. Luminescence dating done by Thiel et al. (2010) revealed that the San Giovanni sections were deposited before and during marine isotope stage (MIS). Samples SG_1 and SG_2 were dated to MIS 5e (Thiel et al., 2010; Passuci et al., 2014), specifically 119±11 and 115±11 ka respectively using OSL on quartz. The samples taken from the underlying units, SG_3 and SG_4, were dated to be 182±10 ka and 223±16 ka respectively using the fading corrected $pIRIR_{225}$ signal of K-feldspar (Thiel et al., 2010) and later interpreted to fall within MIS 7 to MIS 6 (Passuci et al., 2014) (Table 5.1). In the case of the younger samples both OSL dates and the sedimentological correlation of multiple investigations point to MIS 5e with confidence. In the case of SG_3 the fading corrected $pIRIR_{225}$ age of 182±10 ka (Thiel et al., 2010) is on the border between MIS 6 and MIS 7 additionally there is an OSL age of 186±13 ka reported by Andreucci et al. (2009), this unit was interpreted to be MIS 7 due to the presence of a middle (inaccessible) unit between SG_1 and SG_3, the middle unit is correlated with MIS 6 though stratigraphic (and high stand) and sedimentological characteristic comparison (Lecca and Carboni, 2007; Andreucci et al., 2009; Passuci et al., 2014). In the case of SG_4, underlying SG_2, there is less confidence in the age as it is older than the OSL limit. The fading corrected $pIRIR_{225}$ age reported by Thiel et al. (2010) falls well within the range for MIS 7, even the OSL minimum age

(>209 ka) falls within MIS 7, however the sedimentological (and high stand) correlations of Lecca and carboni (2007), Andreucci et al. (2009), Passuci et al. (2014) interpret this unit to be MIS 6. These same four samples (the quartz fraction) were used by Rahimzadeh et al. (2023) in their investigation of the quartz violet stimulated luminescence (VSL) signal.

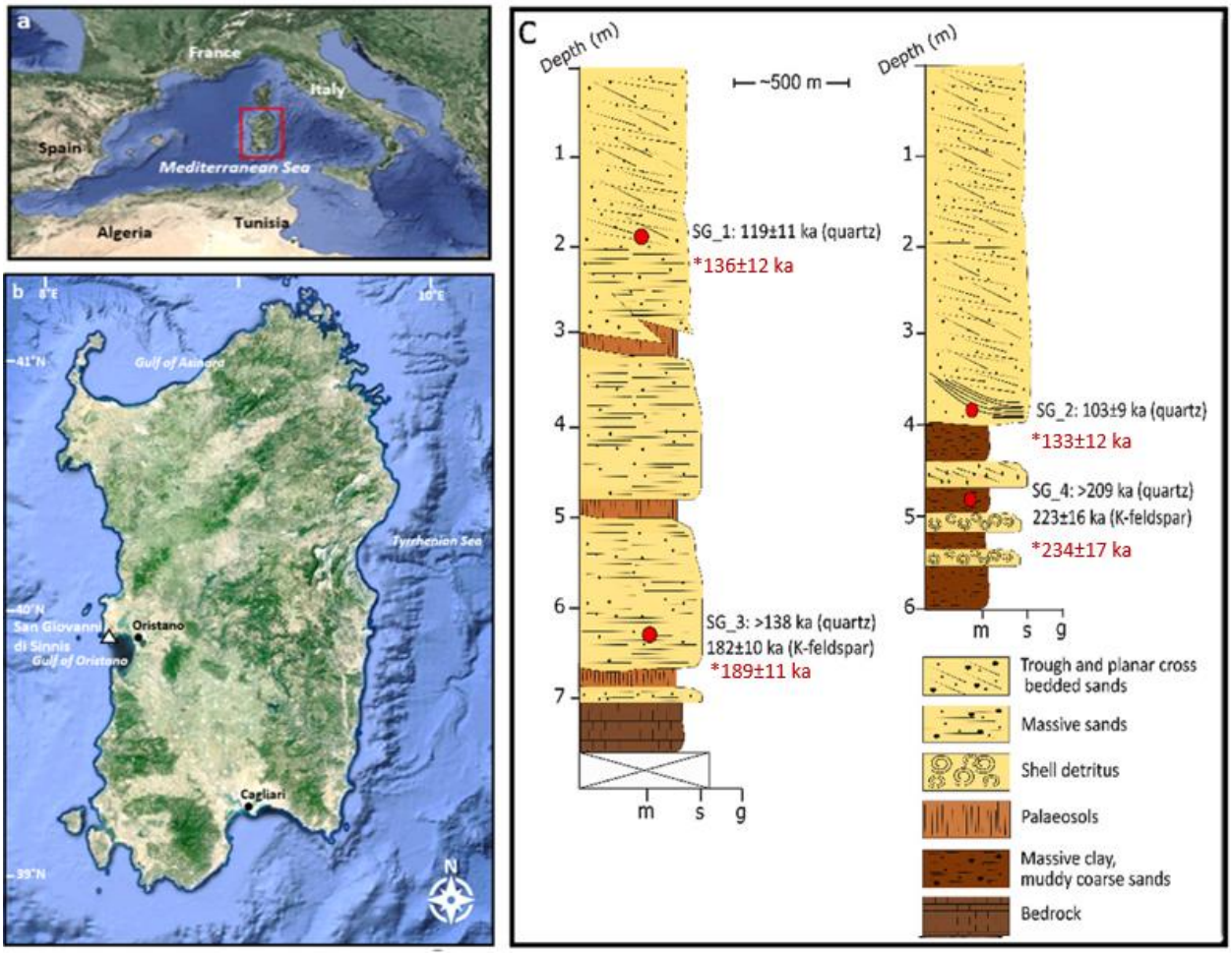

Fig. 5.1: a) Satellite image of the Mediterranean Sea indication the location of Sardinia (red rectangle); b) satellite image of Sardinia illustrating the location of the sampling site at San Giovanni di Sinis (white triangle); c) stratigraphic logs of the sections studied (modified after Rahimzadeh et al., 2023 (originally modified after Coltorti et al., 2010)). Note the ages in black are the original ages from Thiel et al. (2010), starred (*) ages in red are the recalculated reference ages. (Images a and b, are Landsat imagery obtained using Google Earth Pro.)

The regional dose rates were determined using high-resolution gamma spectrometry and the total dose rates are summarized in Table 1. As samples SG_1 and SG_2 only have quartz ages and dose rates published, the K-feldspar dose rates for all samples were recalculated using the data published in Thiel et al. (2010). The dose rates were recalculated using the conversion factor of

Guérin et al. (2011) and beta attenuation factors of Aitken (1985). The recalculated dose rates were consistently lower than the original dose rates which is attributed to an error in the calculation spreadsheet used by Thiel et al. (2010) and the use of more recent conversion rates in our study. As all other factors such as water content, elevation, location, depth etc. were kept consistent with Thiel et al. (2010). Therefore, all the ages published in Thiel et al. (2010) were recalculated in order to be able to compare the data sets. The expected recalculated ages are as follows: SG_1: 136±12 ka; SG_2: 133±12 ka; SG_3: 189±11 ka; and SG_4: 234±17 ka (Table 1). The independently recalculated dose rates and resulting new reference ages agree with the recalculated results in Rahimzadeh et al. (2023).

Table 5.1: Dose rates and ages from Thiel et al. (2010) and recalculated dose rates and new expected ages used for comparison in this study.

Sample	Thiel et al. (2010)				This Study		
	Dose rates		Ages		Recalculated dose rates		Expected Ages
	Quartz	K-feldspar	Quartz	K-feldspar	Quartz	K-feldspar	
SG_1	1.09±0.11	n.a.	119±11	n.a.	0.95±0.04	1.61±0.19	136±12[a]
SG_2	0.71±0.08	n.a.	115±11	n.a.	0.55±0.02	1.19±0.18	133±12[a]
SG_3	1.81±0.13	2.41±0.13	>138	182±10	1.62±0.06	2.29±0.20	189±11[b]
SG_4	1.00±0.11	1.60±0.11	>209	223±16	0.92±0.05	1.57±0.20	234±17[b]

[a]: Quartz ages

[b]: Fading corrected $pIRIR_{225}$ K-feldspar ages

5.2.2. Instrumentation

All samples measured are the same as those measured by Thiel et al. (2010), detailed information on the preparation of these samples is available in Thiel et al. (2010). The K-feldspar grains were mounted as small aliquots (diameter of 2.5 mm) on stainless-steel discs using silicone spray as adhesive. A Risø TL/OSL DA-20 reader equipped with an automated detection and stimulation head (DASH) was used for IR-RF measurements (Lapp et al., 2015), at the Leibniz Institute for Applied Geophysics laboratory in Hannover, Germany. The IR-RF signal was stimulated using the $^{90}Sr/^{90}Y$ beta radiation source (with a dose rate of approximately 0.119 Gy/s), detected by a Chroma D 900/100 interference filter (band pass: 850-945 nm) and bleached by a powerful UV LED (395 nm, 10 W). IRPL measurements were done at the Technical University of Denmark, Risø campus laboratory, in Roskilde, Denmark, on a Risø TL/OSL reader equipped with an automated detection and stimulation head (DASH) (Lapp et al., 2015) and an IRPL attachment (Kook et al., 2018) with a $^{90}Sr/^{90}Y$ beta radiation source (with a dose rate of approximately 0.22

Gy/s). The IRPL signal was stimulated using a ~1.49 eV (830 nm) laser (PM tubes Hamamatsu H7421-50 and Hamamatsu H10330C-25) and detected using band pass interference filters transmitting 880 nm (FWHM 10 nm) and 950 nm (FWHM 50 nm), the same system used and described by Kumar et al. (2021). Three of the samples (SG_1, SG_2 and SG_3) were measured using the IRPL signal in 2019 (dose rate: 0.22 Gy/s) and one sample (SG_4) was measured later (dose rate: 0.205 Gy/s).

5.2.3. Measurement protocols and signals

5.2.3.1 IR-RF

IR-RF, initially developed by the Freiberg research group (Trautmann et al., 1999; Krbetschek et al., 2000; Erfurt and Krbetschek, 2003a) has been presented as a method that does not exhibit anomalous fading and thus could potentially extend the dating range of K-feldspar relative to IRSL (Wagner et al., 2010). As a result of being stimulated by continuous beta radiation, K-feldspar emits luminescence in the infrared band, the intensity of which is measured over time (5000 s; e.g. Frouin et al., 2017) and the result of which is a natural decay curve as the potential for electrons to fill traps decreases over time. The sample is then bleached to zero out the signal, followed by an hour pause to eliminate bleaching induced phosphorescence and a second laboratory decay curve is generated over a significantly longer time (10 000 s; e.g. Frouin et al., 2017) than the natural curve (Table 5.2). The equivalent dose (D_e) was determined by fitting the natural curve to the laboratory curve using the horizontal slide method, and taking the distance traveled from zero to the new position as the equivalent dose. In the case of systematic underestimation, it was recommended by Murari et al. (2018) to overcome sensitivity change with the use of the horizontal-vertical slide method to determine D_e. However, as systematic underestimation was not observed either in the age determination or the dose recoveries, in this case, it was not deemed necessary.

In this paper the protocols developed by Erfurt and Krbetschek (2003) (RF_{RT}) and Frouin et al. (2017) (RF_{70}) were compared (Table 5.2). The main differences between these protocols is: 1) that the protocol put forward by Frouin et al. (2017) includes a preheat and measurement at 70 °C while the Erfurt and Krbetschek (2003) is measured at room temperature (Table 5) and 2) the length of bleaching time. Frouin et al. (2017)'s protocol measures samples at elevated temperature in order to stabilise the signal by keeping very shallow traps empty over the measuring process.

As these protocols were measured on a Risø TL/OSL reader, the bleaching intensity, duration and light frequency set-ups were significantly different. The Risø TL/OSL readers have a built-in UV bleaching light (395 nm) while the Erfurt and Krbetschek (2003) protocol makes use of solar light (for 0.5 hr) and the Frouin et al. (2017) protocol used very specific bleaching settings to simulate natural terrestrial sunlight using the simulator integrated into the *Lexsyg* system (365 nm at 10 mW/cm^2, 462 nm at 63 mW/cm^2, 525 nm at 54 mW/cm^2, 590 nm at 37 mW/cm^2, 623 nm at 115 mW/cm^2 and 850 nm at 96 mW/cm^2) for 3 hrs. Due to these different bleaching options the bleachability of the samples was investigated first with a solar simulator (Hönle SOL2), which was found to be logistically problematic with the transport of aliquots between the Risø TL/OSL reader and the solar simulator in different laboratories resulting in the loss of grains. As a result, all bleaching within the IR-RF measurements was done using the built in UV LED in the Risø TL/OSL reader as initially tested by Buylaert et al. (2012a).

Dose recovery and residual tests were undertaken for both protocols. The dose recoveries were done as described above, by bleaching the samples, giving them a dose approximating the expected dose and then running the IR-RF measurements in order to ascertain whether the expected doses are recoverable. Residual dose tests entailed the bleaching of the sample followed by running the IR-RF measurements, allowing an evaluation of whether there is a residual dose remaining after the 4 hours of bleaching. A series of bleaching tests were done using the built-in bleaching light of the reader. The bleaching tests consisted of a natural curve measurement (100 s) followed by a series of alternating bleaching and measuring phases with increasingly long bleaching durations (10 s, 50 s, 100 s, 200 s, 400 s, 600 s, 800 s, 1000 s, 1200 s, 1400 s and 1600 s) followed by a final regenerated curve (10000 s). The bleaching tests were single rather than multiple aliquot tests; i.e.: all phases of the bleaching tests were done on each aliquot. Each D_e (essentially a residual dose) was determined by using the horizontal slide method comparing each differently bleach "natural curve" with the same final regenerated curve.

Table 5.2 Protocol for the measurement of the RF_{70} and RF_{RT} signals as developed by Frouin et al. (2017) and Erfurt and Krbetschek (2003) respectively.

RF_{70}	RF_{RT}	Observed
Preheat (70 °C/ 900 s)		
IR-RF (70 °C/ 5 000 s)	IR-RF for 5 000 s	Natural decay curve
Bleach 0.5 hrs	Bleach for 0.5 hrs	
Pause 1 hr	Pause 1hr	
Preheat (70 °C / 900 s)		
IR-RF (70 °C/ 10 000 s)	IR-RF for 10 000 s	Regen. decay curve

5.2.3.3 IRPL

The non-destructive nature of IRPL allows one to insert IRPL measurements between IRSL measurement in a sequence and allows for the comparison of IRPL and IRSL results at different temperatures and after the destructive measurement of each IRSL measurement evacuates shallow traps (Kumar et al., 2021). The protocol used is a coupled IRPL-IRSL SAR protocol and includes both the 950 nm ($IRPL_{950}$) emission discovered by Prasad et al. (2017) and the 880 nm ($IRPL_{880}$) emission observed by Kumar et al. (2018). These IRPL emissions are measured at room temperature, after a preheat at 320 °C and thereafter alternating with and in-between the $IRSL_{50}$, $IRSL_{90}$, $IRSL_{130}$ and $IRSL_{290}$ signals (Table 5.3). The protocol used in this study is the same as 'protocol A', investigated by Kumar et al. (2021). In order to create the growth curve with which to compare the natural dose, steps 1-20 were then repeated with laboratory doses on the aliquot of 40 Gy, 80 Gy, 180 Gy, 260 Gy, 520 Gy (older samples), and a repeat of 0 Gy and 60 Gy (Fig, 5.7). The calculated D_e for each temperature step signal when graphed on axes of D_e vs temperature would be expected to trend toward a plateau (the over-all D_e of the sample) with increased temperature.

Table 5.3: Protocol developed by the Risø research group for IRPL measurements (modified after Kumar et al., 2021).

Step	IRPL	Observed
1	Dose	
2	Pause 100s	
3	IRPL at 880nm	Lx_{1a}; Tx_{1a}
4	IRPL at 950nm	Lx_{1b}; Tx_{1b}
5	Preheat (320 °C/ 60 s)	
6	IRPL at 880nm	Lx_{2a}; Tx_{2a}
7	IRPL at 950nm	Lx_{2b}; Tx_{2b}
8	IRSL (50 °C/ 100 s)	Lx_3; Tx_3
9	IRPL at 880nm	Lx_{4a}; Tx_{4a}
10	IRPL at 950nm	Lx_{4b}; Tx_{4b}
11	IRSL (90 °C/ 100 s)	Lx_5; Tx_5
12	IRPL at 880nm	Lx_{6a}; Tx_{6a}
13	IRPL at 950nm	Lx_{6b}; Tx_{6b}
14	IRSL (130 °C/ 100 s)	Lx_7; Tx_7
15	IRPL at 880nm	Lx_{8a}; Tx_{8a}
16	IRPL at 950nm	Lx_{8b}; Tx_{8b}
17	IRPL (290 °C/ 100s) (effective clean out bleach)	Lx_9; Tx_9
18	IRPL at 880nm	
19	IRPL at 950nm	
20	Test dose (84 Gy), there after repeat steps 2-18	

5.3. Measurement performance, equivalent dose and age determinations

5.3.1 IR-RF

The initial, striking observation in a comparison of the two IR-RF signals (across all samples) is that the RF_{RT} exhibits a significantly brighter signal (~ 3x larger), an indication that the RF_{70} signal makes up approximately one third of the total signal at room temperature and that an elevated temperature measurement excludes a large portion of the available IR-RF traps (Fig 5.2). These measurements were done within a month of one another and so this difference in intensity cannot be accounted for with source decay or changes in the efficiency of the detection unit. As it is observed for all samples it was likely a result of the preheat and measurement temperature at 70 °C and the loss of signal intensity directly illustrated the portion of thermally unstable traps that were avoided when the IR-RF signal was measured at elevated temperature.

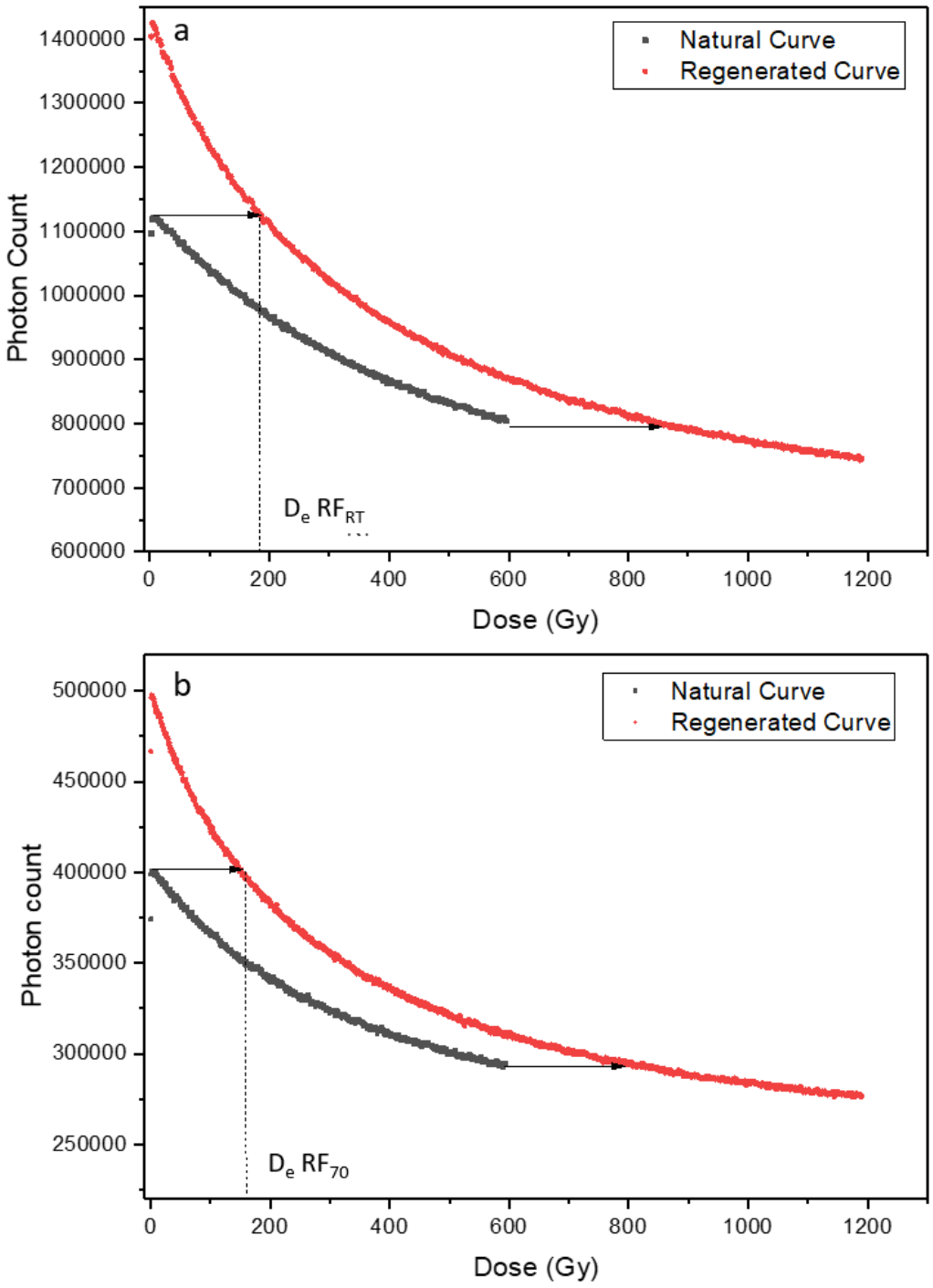

Fig. 5.2: Representative decay curves of a single aliquot of the a) RF_{RT} and b) RF_{70} measurements on sample SG_2. Showing the natural measurement curve (black) and the regenerated curve (red), and the horizontal shift method used to determine D_e.

The D_e results of samples SG_1, SG_2 and SG_3 all show the same trend, that the D_e results generated by the RF_{RT} signal were consistently larger than the D_e results of the RF_{70} signal. In contrast the D_e results for sample SG_4 were larger for the RF_{70} signal (table 5.4). In a comparison of the regenerated IR-RF curves of the two signals (normalised to account for the differences in intensity), observed that the RF_{RT} signal decays to a larger extent than the RF_{70} signal (Fig. 5.3). This is in line with findings from Frouin et al., (2017) stating that RF_{70} bleaches more slowly relative to lower temperature IR-RF. The shape of these regenerated curves is consistent with this reversal in the trend with regards to SG_4 in that a sample exhibiting a normalised intensity of less than 0.6, the RF_{70} protocol over estimates relative to the RF_{RT} protocol. Both IR-RF protocols overestimate D_e values in comparison with the Thiel at al., (2010) results, SG_1 and SG_2 to a lesser extent than SG_3 and SG_4, this is due to the reported D_e results of SG_3 and SG_4 being fading uncorrected. The ages generated by both the IR-RF signals are consistent with the expected ages (within 1σ) for all but one sample, the RF_{70} signal age overestimates for sample SG_4 (but still consistent within 2σ).

Table 5.4: RF_{70}, RF_{RT} D_e (Gy) and age (ka) values compared with the reference ages.

D_e (Gy)				**Ages (ka)**		
Sample	RF_{70}	RF_{RT}	Expected D_e	RF_{70}	RF_{RT}	Reference
SG_1	221±8	247±14	218±19[a]	137±5	153±9	136±12
SG_2	177±22	191±10	157±14[a]	149±18	161±8	132±12
SG_3	411±7	458±20	398±6[b]	177±3	197±9	189±11
SG_4	427±23	357±55	325±8[b]	279±15	233±36	233±17

[a]: Originally quartz D_e values published by Thiel et al., (2010) recalculated to reflect the expected Feldspar D_e values

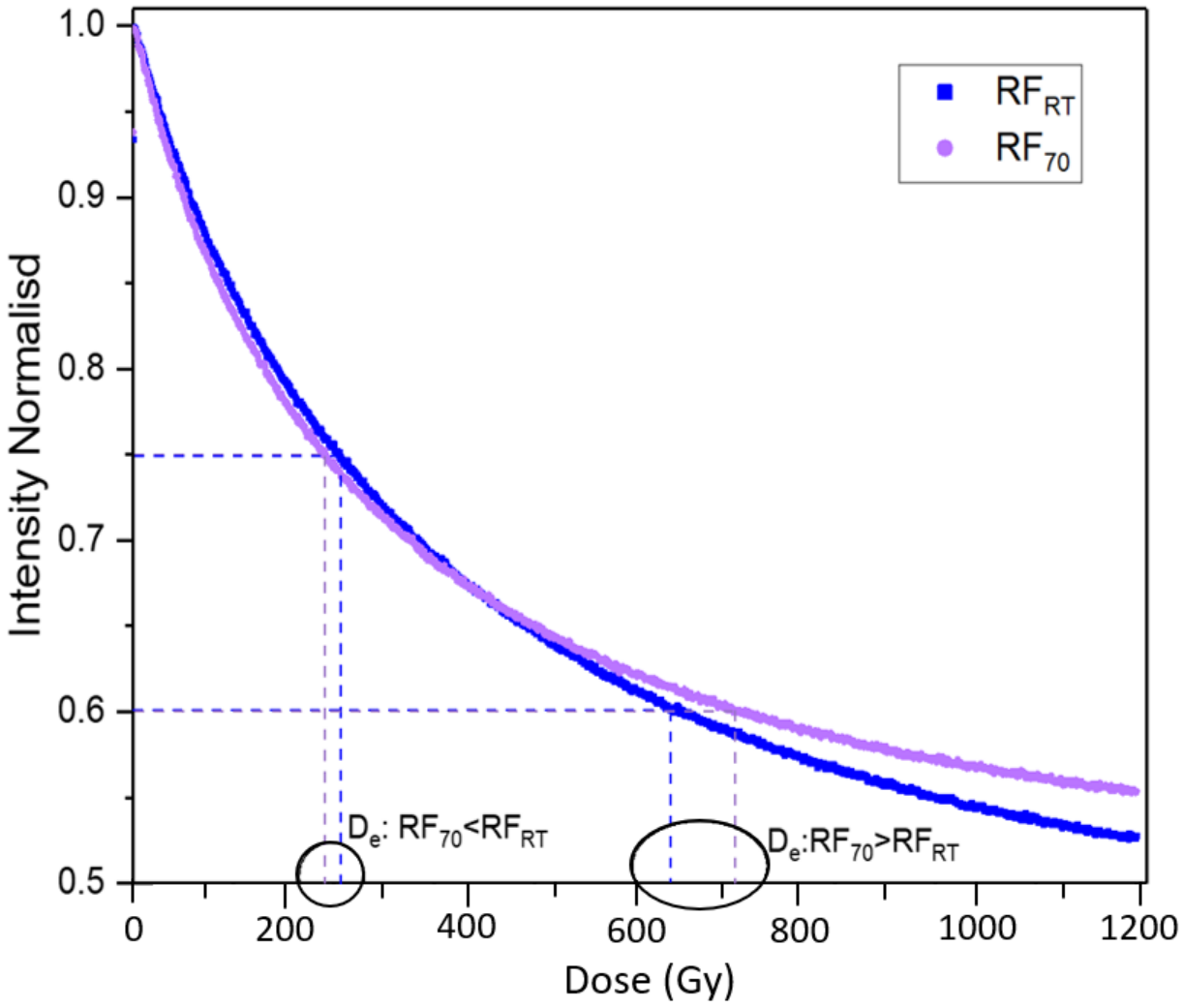

Fig. 5. 3: Comparison of the regenerated normalized curves of the two IR-RF protocols, the purple curve represents the RF_{70} signal and the blue curve represents the RF_{RT} protocol.

The results of the bleaching test illustrate that the signal is sufficiently (~5 % of the D_e) bleached after 1800 s confirming that the bleaching time could be modified to 0.5 hr for both protocols which is a bleaching setting put forward by Buylaert et al. (2012) as being sufficient when using the UV LED in the Risø reader (Fig. 5.4).

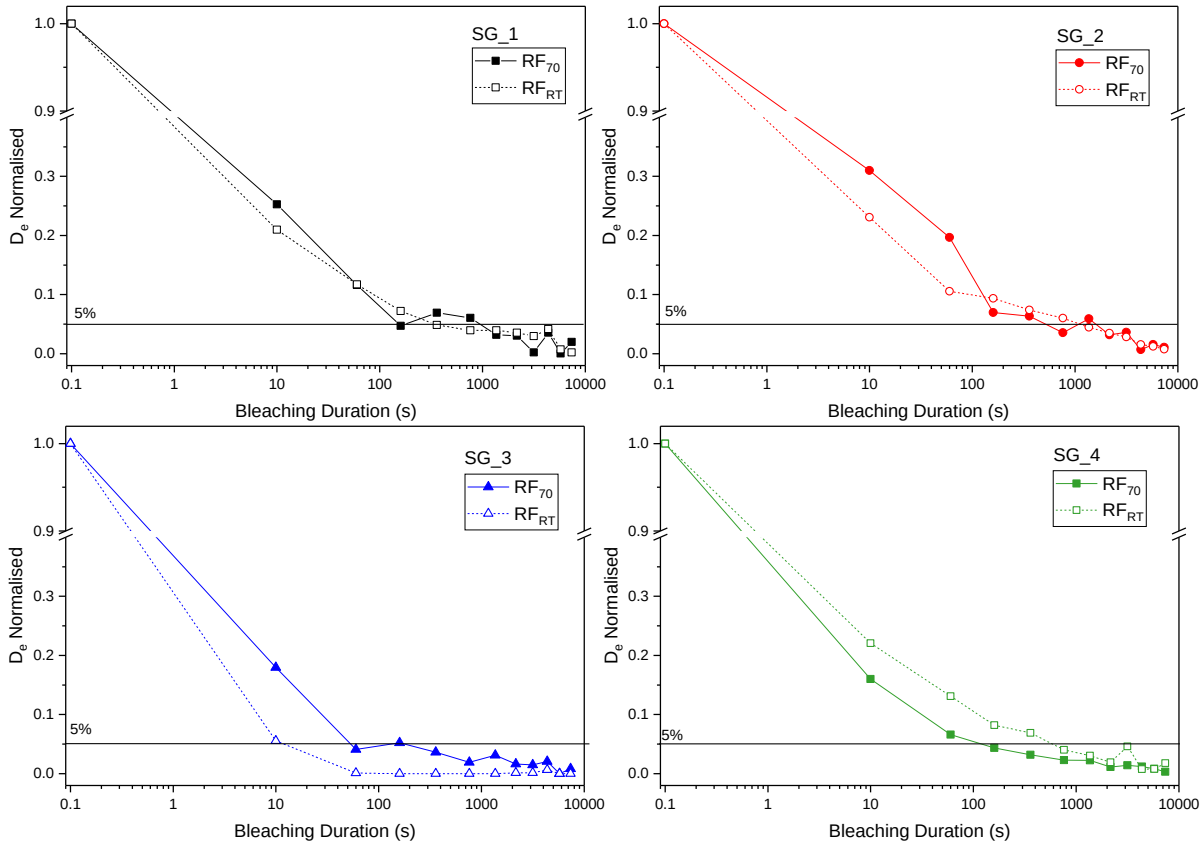

Fig. 5.4: Bleaching test results for each of the samples using the RF_{70} and RF_{RT} signals, solid lines represent the RF_{70} signal and the dotted lines represent the RF_{RT} signal.

All dose recovery results for the RF_{RT} protocol fall within the acceptable 10% ranging from 0.94±0.06 to 1.07±0.00 and the RF_{70} protocol results of SG_1 to SG_3 fall within the accepted 10% ranging from 1.07±0.09 to 1.10±0.04 however, in the case of SG_4 the dose recovery reflects a significant overestimation of 1.27±0.12 (Table 5.5, Fig. 5.5), which is consistent with the observed overestimation of D_e using the RF_{70} protocol. With regards to residual dose percentages the RF_{RT} protocol shows a relatively constant residual percentage ranging from 13±1% to 15±1 % while in contrast the RF_{70} protocol residual percentage ranges from 11±3 % to 17±2 % and increases with an increase in D_e (Table 5.5). This suggests that the signal measured using RF_{70} protocol is increasingly difficult to bleach with increased age. This high residual and the corrected dose recovery ratio for SG_4 accounts for the large overestimation in the age.

Table 5.5: Residual corrected dose recovery ratios and the residual percentages.

Sample	RF_{70}		RF_{RT}	
	Dose Rec.	Residual (%)	Dose Rec.	Residual (%)
SG_1	1.08±0.09	11±3	1.07±0.00	13±1
SG_2	1.07±0.09	14±2	1.01±0.05	15±1
SG_3	1.10±0.04	15±1	1.01±0.05	14±3
SG_4	1.27±0.12	17±2	0.94±0.06	14±3

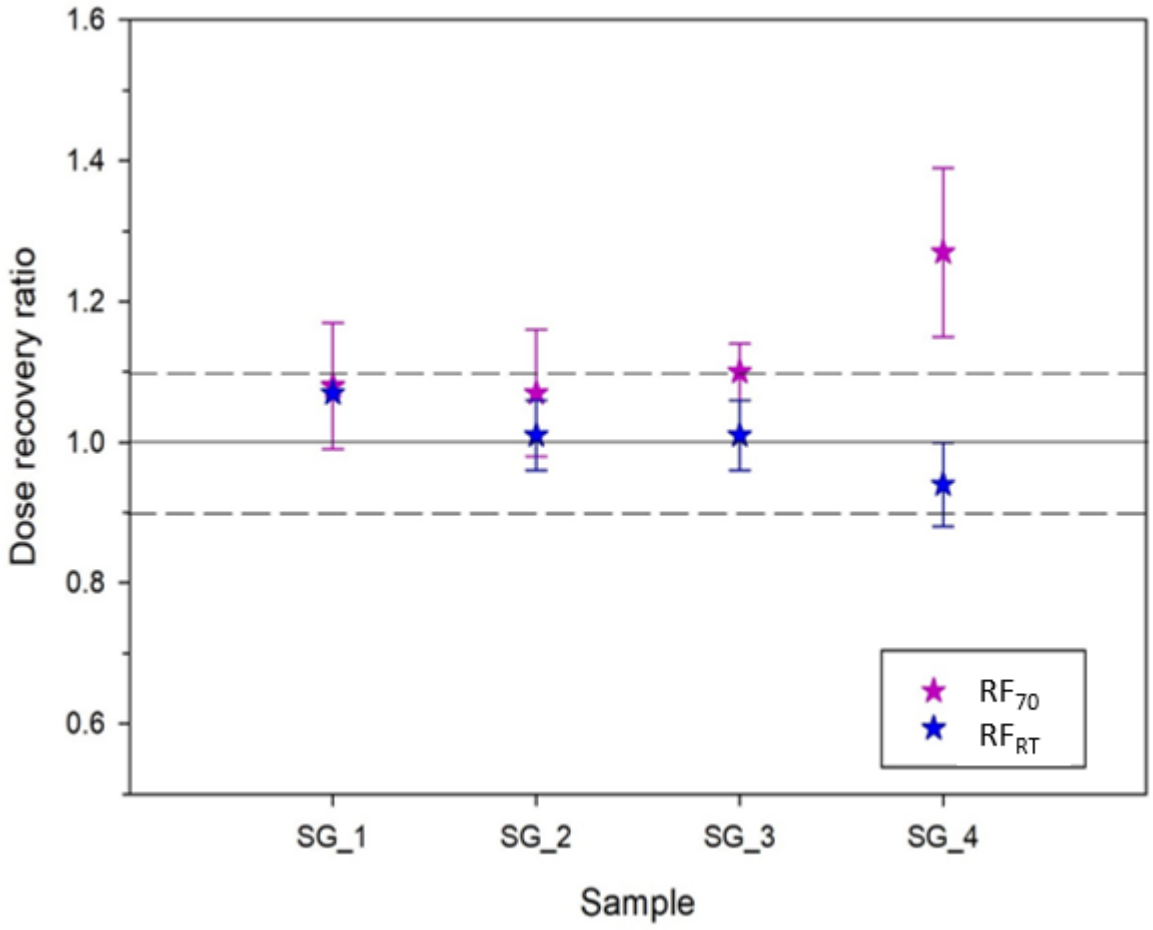

Fig. 5.5: Residual corrected dose recovery test results of the RF_{70} and the RF_{RT} signals, the solid black like represents a successful ratio and the dashed lines the acceptable 10% error. The samples are in order of increasing age.

5.3.2. IRPL

The IRPL protocol generated two sets of IRPL signals ($IRPL_{880}$ and $IRPL_{955}$) and a set of IRSL signals at a range of temperatures. The $IRPL_{880}$ and $IRPL_{955}$ signals exhibit good fits with the single exponential growth curve and nearly identical dose response curve shapes with only some minor deviations at doses larger than 500 Gy (Fig. 5.6). However, they do not go through the origin, which resulted in elevated recuperation ratios theorised to be linked with incomplete resetting of the IRPL signal.

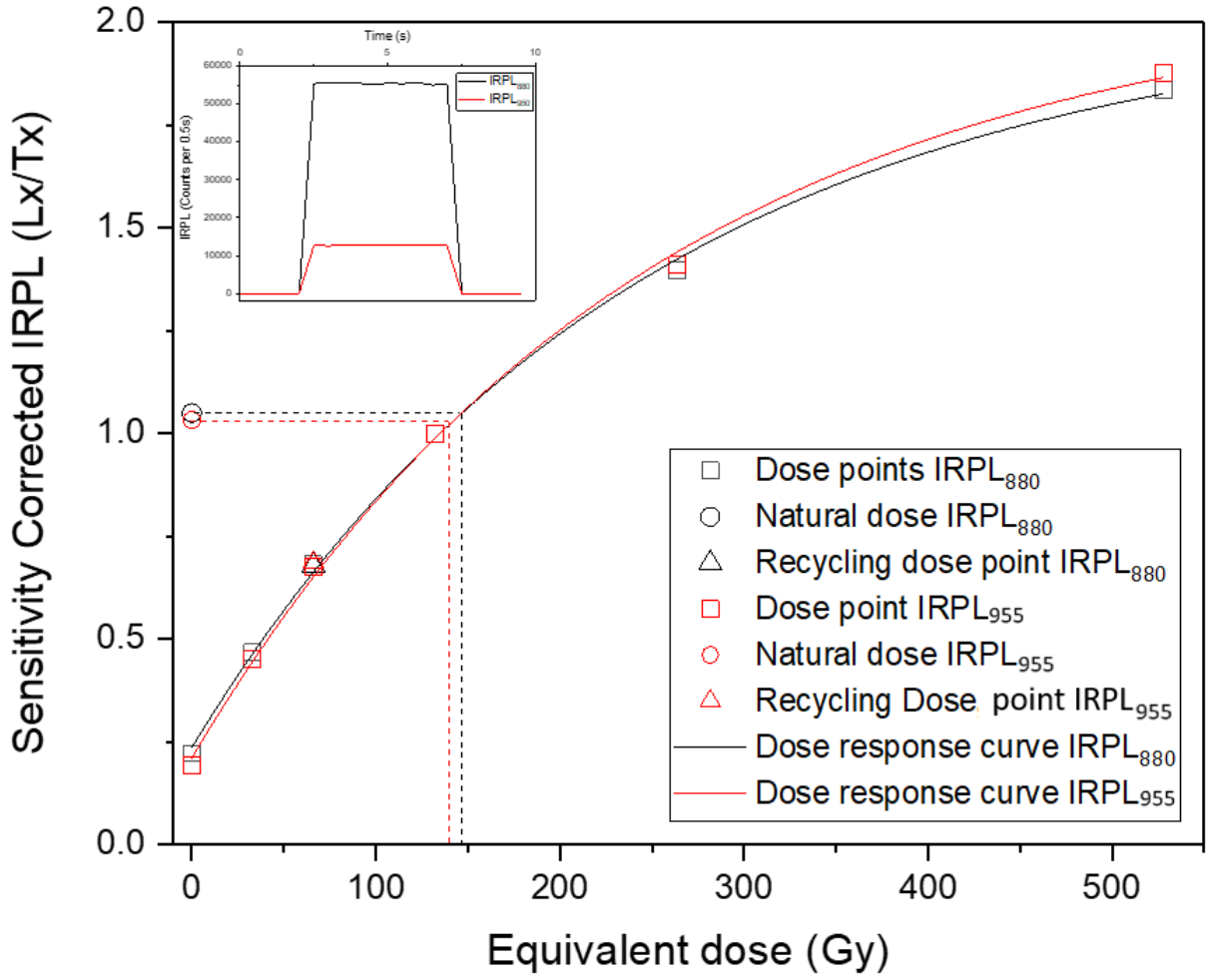

Fig. 5.6: Representative dose response curve of the IRPL signals (after $IRSL_{130}$) for SG_2 (main graph). The insert is the direct IRPL signal used to determine the natural dose Lx/Tx point.

A wide range of D_e results were obtained (Table 5.6) for each sample. Across samples SG_1, SG_2 and SG_3 the $IRPL_{955}$ D_e results underestimate slightly relative to $IRPL_{880}$ results, in contrast sample SG_4 shows the reverse trend. The D_e values of both the $IRPL_{880}$ and $IRPL_{950}$ settings reveal an elevated D_e for the first measurement (before the preheat) and a significantly lower D_e in the measurement after the preheat (Table 5.), likely due to the preheat evacuating the shallowest traps. Thereafter for samples SG_1, SG_2 and SG_4 the IRPL D_e results stabilise with only a minor increase in D_e with each successive IRPL measurement. In contrast sample SG_3 exhibits a marked increase in D_e with each successive IRPL measurement, significantly overestimating the D_e relative to the expected D_e for the latter IRSL measurements (Table 5.6). Additionally, the error range for sample SG_3 was significantly larger than the other samples indicating a larger scatter of D_e results for individual aliquots. For all samples the IRSL D_e results initially underestimate significantly at low temperature and increase with increased temperature. A number of aspects should be addressed when assessing these results. Firstly, the $IRSL_{50}$, $IRSL_{90}$ and $IRSL_{130}$ measurements are expected to suffer from fading and they do significantly underestimate the D_e relative to both IRPL measurements and the reference ages (Table 5.7).

A second aspect to consider is the general rejection criteria of the SAR measurement protocol such as the recycling ratio and recuperation. The recycling ratio is the ratio of two Lx/Tx measurement cycles with the same given dose and is considered successful when the ratio 1±0.1. All IRPL and IRSL measurements gave recycling ratios within 10% of 1 (Fig. 5.7a). The recuperation is the percentage ratio Lx/Tx for the zero-dose step and the Lx/Tx for the natural dose measurement, and should generally is less than 5%. Across all samples the same trend holds that the $IRPL_{955}$ emission measurement results in lower recuperation ratios relative to the $IRPL_{880}$ emission (Fig. 5.7b). Additionally, only the first IRPL result step (before the preheat) strictly falls within or close to the 5% acceptance criteria. The recuperation increases with every subsequent IRPL measurement. Kumar et al. (2021) exhibits results with trends consistent with our results and attributes this recuperation to the intensity of the clean out bleaching step coupled with the subsequent preheat step in the next cycle. This may be a symptom of an ineffective cleanout step at the end of each SAR cycle, Kumar et al. (2021) found that a lower temperature cleanout of 260 °C for 60 s resulted in a higher recuperation relative to a clean out temperature of 290 °C for 100 s. Perhaps a higher clean out temperature could improve the recuperation aspect.

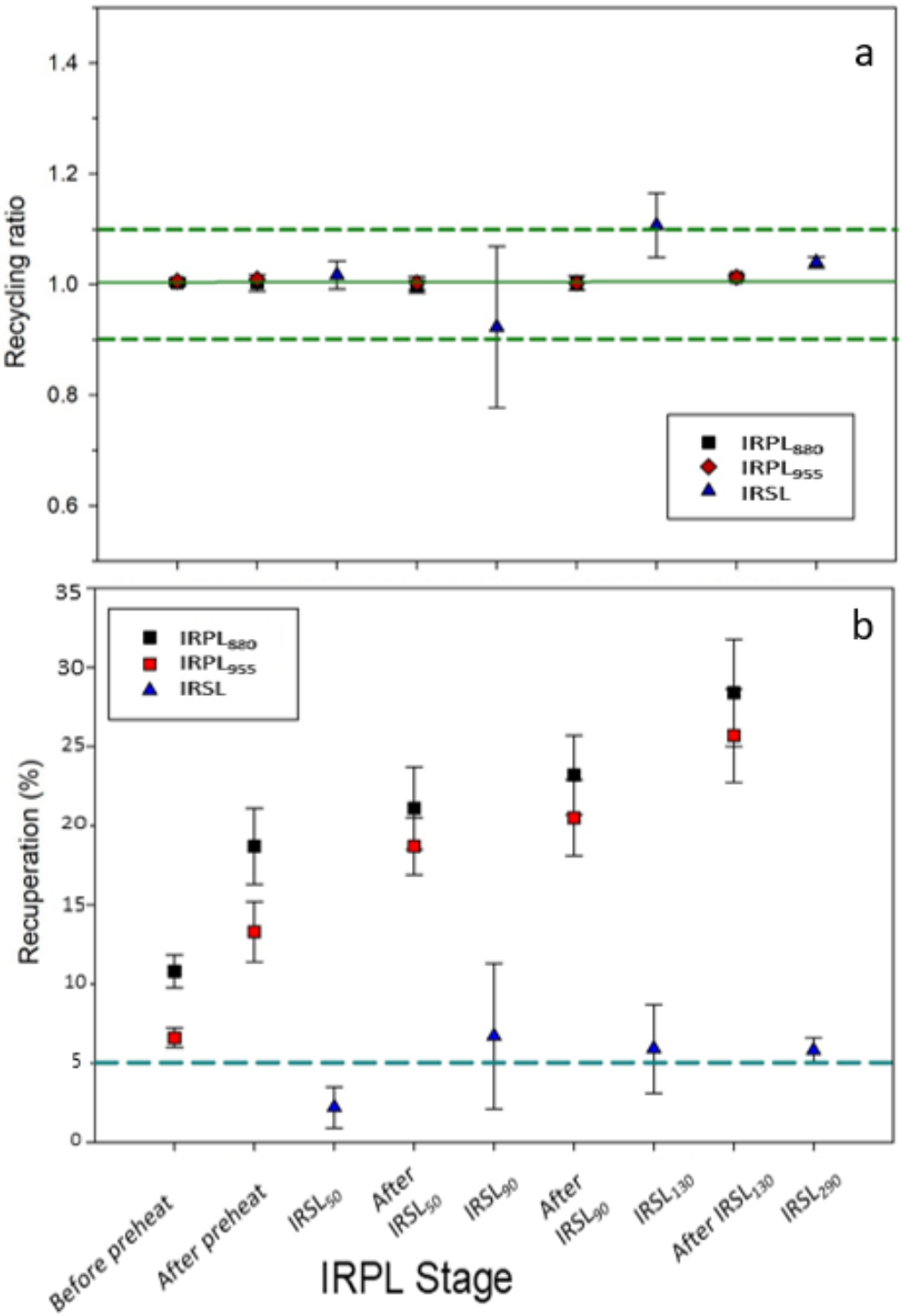

Fig. 5.7: General rejection criteria results of OSL SAR for the IRPL signals of sample SG_2, a) recycling ratio where a ratio of 1±0.1 is successful and b) recuperation which should be less than 5%.

Samples SG_1 and SG_2 both exhibit ages for both signals that are all consistent with the expected ages with minor increases from the second IRPL step trending closer to the exact expected age with increased temperature (Fig. 5.8). Sample SG_3 exhibits ages consistent with the expected ages only for the first three IRSL steps and significantly overestimates for subsequent IRPL steps. Sample SG_4 exhibited age underestimations initially, trending towards the expected age and was consistent with the expected age for the last two IRPL steps.

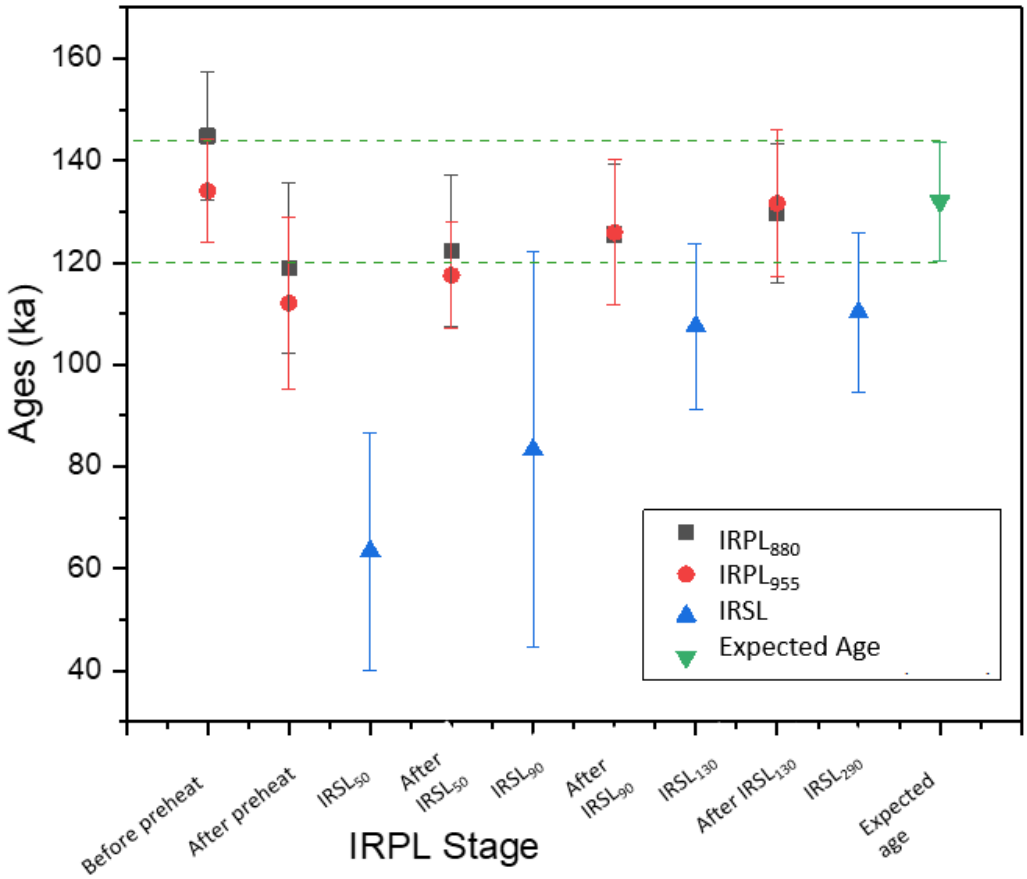

Fig. 5.8: Age results example for the IRPL protocol steps comparing the age results for the $IRPL_{880}$, $IRPL_{955}$ and IRSL signals.

Table 5.6: IRPL D_e values (Gy)

Sample	Before preheat (Gy)		After preheat (Gy)		$IRSL_{50}$ (Gy)	After $IRSL_{50}$ (Gy)		$IRSL_{90}$ (Gy)	After $IRSL_{90}$ (Gy)		$IRSL_{130}$ (Gy)	After $IRSL_{130}$ (Gy)		$IRSL_{290}$ (Gy)
	880nm	955nm	880nm	955nm		880nm	955nm		880nm	955nm		880nm	955nm	
SG_1	267±11	241±8	195±3	182±4	126±8	205±2	205±5	168±45	213±2	206±7	198±32	218±3	214±6	208±9
SG_2	172±15	160±12	142±20	133±20	76±28	146±18	140±12	99±46	149±16	150±17	128±19	154±16	157±17	131±19
SG_3	457±45	412±41	390±88	406±35	336±73	478±28	492±55	540±85	530±71	548±86	539±162	569±78	517±33	607±9
SG_4	302±17	290±13	293±37	272±23	177±23	314±27	322±14	306±50	341±16	346±19	351±35	348±34	366±21	370±11

Table 5.7: IRPL ages (ka)

Sample	Before preheat (ka)		After preheat (ka)		$IRSL_{50}$ (ka)	After $IRSL_{50}$ (ka)		$IRSL_{90}$ (ka)	After $IRSL_{90}$ (ka)		$IRSL_{130}$ (ka)	After $IRSL_{130}$ (ka)		$IRSL_{290}$ (ka)
	880nm	955nm	880nm	955nm		880nm	955nm		880nm	955nm		880nm	955nm	
SG_1	166±7	150±5	121±2	113±3	78±5	127±1	127±3	104±28	132±0,3	128±4	123±20	135±2	132±3	128±6
SG_2	145±12	134±10	119±17	112±17	63±23	122±15	117±10	83±39	125±14	126±14	107±16	130±14	132±14	110±16
SG_3	197±19	177±17	168±38	175±15	144±31	206±12	212±24	233±36	228±30	236±37	232±69	245±34	223±14	261±4
SG_4	192±11	185±8	186±23	173±15	113±15	200±17	205±9	195±32	217±10	220±12	224±22	222±22	233±13	236±7

5.4. Comparison of ages

Both IR-RF signals are largely consistent with the recalculated reference ages of Thiel et al. (2010) within 1σ with two exceptions: 1) sample SG_2 where the RF_{RT} signal overestimates, and 2) sample SG_4 where the RF_{70} result overestimates significantly; however, both overestimating signals are within 2σ (Fig. 5.9a). In the case of the three younger samples the RF_{70} and RF_{RT} signals show good agreement with each other and the RF_{RT} signal ages are slightly older than the RF_{70} signal ages.

The slight overestimation of the RF_{RT} signal relative to the RF_{70} signal in the majority of the samples is likely due to the sight differences in the observed normalized regenerated curve shape for lower doses. The significant overestimation of the age for the RF_{70} signal on sample SG_4 is likely due to the slower bleaching characteristic of RF_{70} relative to RF_{RT} (Frouin et al., 2017). The over estimation observed in SG_4 is consistent with the residual-corrected dose recovery observations and the slightly different curve shapes of the regenerated curves for the latter part of the dose response curve could go some way to accounting for the overestimation relative to RF_{RT}. This may indicate that at larger doses that the RF_{70} protocol will consistently overestimate relative to the RF_{RT} protocol, as the shape of the regenerated curves trend is the same across all four samples; though the extent to which this contributes to the overestimation is unclear and bears further investigation. Few studies comparing IR-RF results with independent age control have been done thus far (Buylaert et al., 2012; Frouin et al., 2007), in an evaluation of the Erfurt and Krbetschek (2003) protocol Buylaert et al. (2012) measured 13 samples ranging from ~20 ka to ~130 ka and found that the protocol over estimated in the younger samples (20-40 ka) and underestimated in the older samples (~130 ka), this inconsistency was attributed to signal instability, sensitivity changes and the difficulty with establishing an appropriate bleaching setting. In contrast Frouin et al. (2017) found that their RF_{70} protocol gave reliable ages within 2σ with the exception of one sample that significantly overestimated, this was attributed to the poor bleaching of the sample in nature.

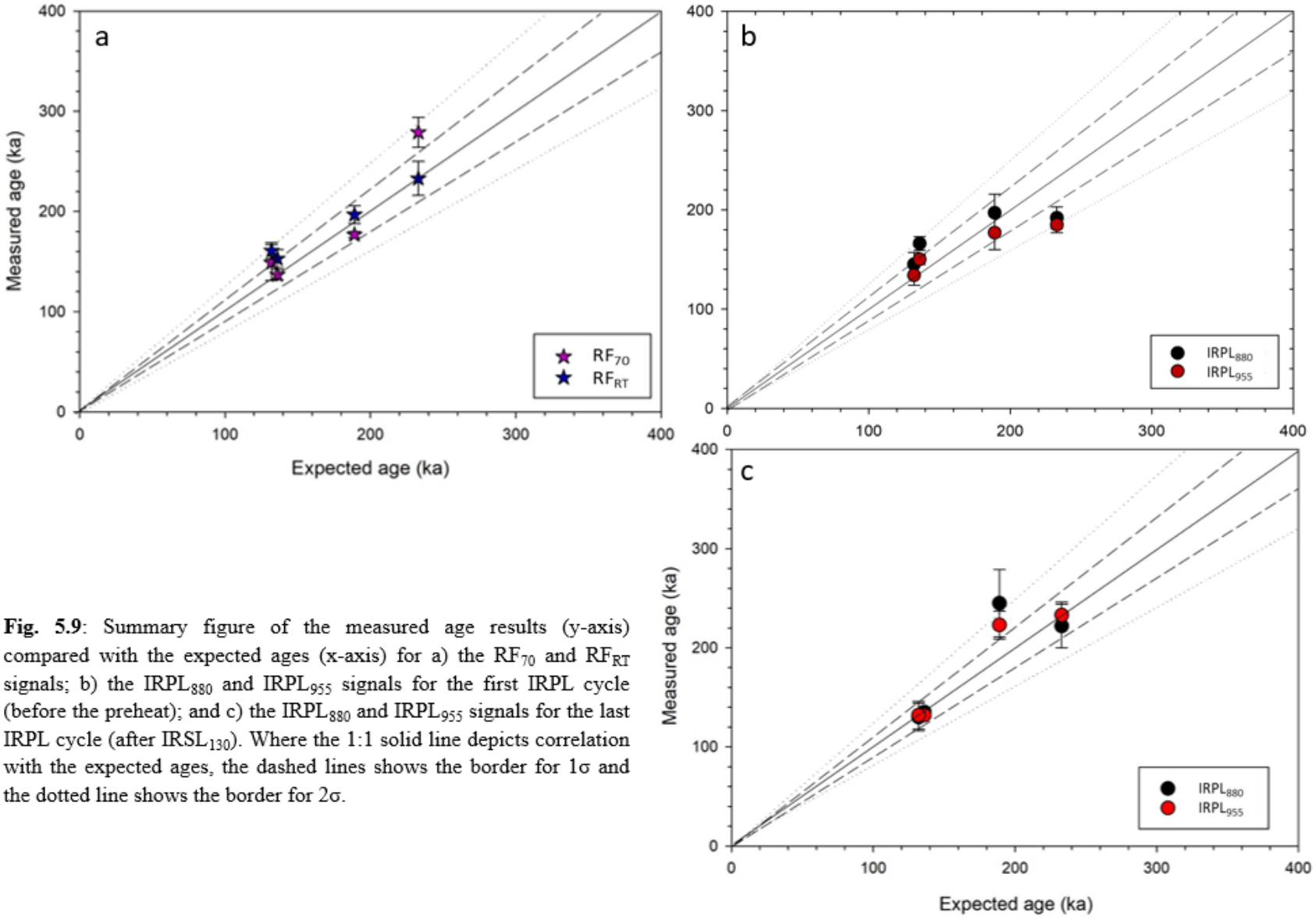

Fig. 5.9: Summary figure of the measured age results (y-axis) compared with the expected ages (x-axis) for a) the RF_{70} and RF_{RT} signals; b) the $IRPL_{880}$ and $IRPL_{955}$ signals for the first IRPL cycle (before the preheat); and c) the $IRPL_{880}$ and $IRPL_{955}$ signals for the last IRPL cycle (after $IRSL_{130}$). Where the 1:1 solid line depicts correlation with the expected ages, the dashed lines shows the border for 1σ and the dotted line shows the border for 2σ.

With regards to the IRPL ages there are a number of aspects to consider. One expects that with each IRSL step the successive IRPL signal would be increasingly stable and represent increasingly stable traps (that are increasingly difficult to reset or bleach). The trend (for all samples) during the IRPL measurement of the ages increasing with each successive IRPL step with the removal of each IRSL signal at increasing temperatures suggests that initially (after the very first IRPL measurement before the preheat) the IRPL signals suffers from minor fading though after each subsequent IRSL step the effect of fading decreases. In the younger samples this effect is minor with all IRPL steps being consistent with the expected ages, while in the older samples this effect is significant. This effect and the fact that the majority of samples exhibit a trend toward the expected ages with successive IRPL steps suggests that the later IRPL steps should be a more successful measure of the correct age. The last IRPL cycle shows good age correlations within 1σ, for samples SG_1, SG_2 and SG_4, and overestimation within 2σ for SG_3. Conversely in the case of sample SG_3 it is the earlier steps in the protocol that are consistent with the expected age, suggesting that there is another factor to consider such as possibly a residual dose present in this sample.

However, when we strictly apply the SAR acceptance criteria we cannot discount the observation that the recuperation percentages are almost entirely over the limit of 5% with only the first IRPL signal being close to acceptable. The ages of the first IRPL cycle are all consistent with the recalculated reference ages of Thiel et al. (2010) within 2σ, the $IRPL_{880}$ signals overestimating slightly for the younger samples and both signals underestimating for sample SG_4 (Fig 5.9b). Both the first and last IRPL cycle ages are in good agreement with the reference ages, and despite the poor recuperation results the last cycle gives the bests age results for samples SG_1, SG_2 and SG_3.

Additionally, the $IRPL_{880}$ signal consistently overestimates relative to the $IRPL_{955}$ signal (except for in the case of SG_4, for the last IRPL cycle) this is consistent with results obtained by Kumar et al. (2021) and suggests that the $IRPL_{955}$ signal is slightly less stable than and therefore bleaches better than the $IRPL_{880}$ emission. Kumar et al. (2021) compares two IRPL protocols on samples with reference ages (100-300 Gy, 20-128 ka), the protocol measured in this study corresponds with protocol A in their study. They found that for both the IRPL signals the most successful measurement in the sequence is the measurement taken directly after the $IRSL_{50}$

measurement, and that the signal after the preheat and the signal before the preheat were similarly successful for $IRPL_{955}$ and $IRPL_{880}$ respectively. While the age results of the measurement after $IRSL_{50}$ are consistent with the expected results within errors for the younger samples, samples SG_1, SG_2 and SG_4 show better correlation with the IRPL measurements taken after $IRSL_{130}$ and sample SG_3 appears to correlate better with the measurements before and after the preheat.

In a comparison of IRPL and IR-RF in Kumar et al., (2020) their study found that the IR-RF measurement data (originally from Buylaert et al., 2012a) underestimates significantly relative to the IRPL data, theorizing that this difference is likely due to sensitivity changes rather than signal instability. This trend was not observed in this study as the younger samples showed consistency of both the IRPL signal ages with both the IR-RF ages within errors and very minor overestimation of the IR-RF signals. For sample SG_3 both the IRPL signal ages overestimate relative to the IR-RF signal ages and for sample SG_4 both IRPL signal ages correlate with RF_{RT} while RF_{70} overestimates. A minor trend is that the $IRPL_{880}$ signal minorly overestimates relative to the $IRPL_{955}$ for all samples except SG_4, so too does the RF_{RT} signal relative to RF_{70}. A study of these signals across a larger sample size of a single large sequence would be beneficial to ascertain whether the $IRPL_{880}$ signal could be linked to the RF_{RT} signal behavior or whether this is sample/ minor chemistry dependent. Kumar et al. (2018) theorised that both signals likely originate in the same defects but that the IRPL stimulation probes specific defects. While the IR-RF signal may have contributions from other defects, e.g. the Fe^{3+}, leading to a more mixed response. Which suggests that minor chemistry could be a significant factor and needs further investigation.

5.5. Conclusion

The main aim of this study was to compare the application of the novel dating methods in coarse grained K-feldspar; IR-RF and IRPL, in an attempt to overcome signal instability of k-feldspar. The reliability of the methods used was assessed by comparing them with chronologically controlled samples provided by quartz OSL and fading corrected feldspar $pIRIR_{225}$ ages (Thiel et al., 2010). On the basis of the results obtained in this study we observed that the younger samples (SG_1 and SG_2) showed good correlation with the expected ages for both IR-RF signals and for both IRPL signals for both the first and last IRPL cycles within 2σ. Sample SG_3 showed good

age correlation within 1σ for both IR-RF signals, the first IRPL cycle showed good age correlation within 1σ and the last IRPL cycle showed correlation within 2σ with $IRPL_{880}$ over estimating marginally beyond 2σ. Sample SG_4 showed age correlation of the RF_{RT} within 1σ and RF_{70} signal overestimated within 2σ, the first IRPL cycle showed good age correlation within 1σ for both signals and the last IRPL cycle showed correlation with both signals underestimating within 2σ.

In conclusion all signals showed reasonably good correlation with the reference ages of Thiel et al. (2010) within 2σ, despite poor recuperation in the case of the IRPL signals and residual doses larger than 10% on the IR-RF signals. The RF_{RT} signal appears to perform marginally better than the RF_{70} signal in these samples, possibly due to resetting differences though the bleaching tests did not reveal significant differences. The $IRPL_{955}$ signal appears to perform marginally better than the $IRPL_{880}$ signal with regards to recuperation. While both the first and last IRPL cycles show good correlation with reference ages, the first IRPL cycle before the preheat was favoured due to the better recuperation results.

It is important to acknowledge that while some interesting points have come out of this study, the sample size is small and it would be of great benefit to compare these signals on a large sequence spanning the full datable age range of K-feldspar to get a truly comprehensive view of the trends and interactions of the different signals as well as a comprehensive chemical analysis of the samples to track any possible correlations with their chemistry.

References

Balescu, S., Lamothe, M., Mercier, N., Huot, S., Balteanu, D., Billard, A. & Hus, J. 2003: Luminescence chronology of Pleistocene loess deposits from Romania: testing methods of age correction for anomalous fading in alkali feldspars. Quaternary Science Reviews 22, 967-973.

Buylaert, J.-P., Jain, M., Murray. A.S., Thomsen, K.J. & Lapp, T. 2012a: IR-RF dating of sand-sized K-feldspar extracts: A test of accuracy. Rad. Meas. 47, 759-765.

Buylaert, J.-P., Jain, M., Murray, A. S., Thomsen, K. J., Thiel, C. & Sohbati, R. 2012b: A robust feldspar luminescence dating method for Middle and Late Pleistocene sediments. Boreas, Vol. 41, pp. 435–451.

Buylaert, J.P., Thiel, C., Murray, A. S., Vandenberghe, D. A. G., Yi, S. & Lu, H. 2011: IRSL and post-IR IRSL residual doses recorded in modern dust samples from the Chinese Loess Plateau. Geochron. 38, 432–440.

Duller., G.A.T., 1996. Recent developments in luminescence dating of quaternary sediments. Prog. In Phys. Geogr. 20 (2), 127-145.

Erfurt, G. & Krbetschek, M.R. 2003: IRSAR-a single-aliquot regenerative-dose dating protocol applied to the infrared radiofluorescence (IR-RF) of coarse-grain K-feldspar. Ancient TL 21, 35-42.

Frouin, M., Huot, S., Kreutzer, S., Lahaye, C., Lamothe, M., Philippe, A., & Mercier, N. 2017: An improved radiofluorescence single-aliquot regenerative dose protocol for K-feldspar. Quat. Geochron. 38, 13-24.

Frouin, M., Huot, S., Mercier, N., Lahaye, C., & Lamothe, M. 2015: The issue of laboratory bleaching in the infrared-radiofluorescence dating method. Rad. Meas. 81, 212-217.

Huntley, D. J. & Lamothe, M. 2001: Ubiquity of anomalous fading in K-feldspars and the measurement and correction for it in optical dating. Canadian Journal of Earth Sciences 38, 1093–1106.

Kars, R.H., Busschers, J. & Wallinga, J. 2012: Validating post IR-IRSL on K-feldspars through comparison with quartz OSL ages. Quat. Geochron. 12, 74-86.

Kars, R. H., Wallinga, J. & Cohen, K. M. 2008: A new approach towards anomalous fading correction for feldspar IRSL dating – tests on samples in field saturation. Rad. Meas. 43, 786–790.

Kumar, R., Kook, M. & Jain, M. 2021: Sediment dating using Infrared Photoluminescence. Quat. Geochron. 62

Kumar, R., Kook, M., Murray, A. S. & Jain, M. 2018: Towards direct measurement of electrons in metastable states in K-feldspar: Do infrared-photoluminescence and radioluminescence probe the same trap? Rad. Meas. 120, 7-13.

Kumar, R., Kook, M., Jain, M. 2022: Does hole instability cause anomalous fading of luminescence in feldspar? Jour of Lum. 252. https://doi.org/10.1016/j.lumin.2022.119403

Lamothe, M., Auclair, M., Hamzaoui, C. & Huot, S. 2003: Towards the prediction of long-term anomalous fading of feldspar IRSL. Rad. Meas. 37, 493-498.

Lapp, T., Kook, M. H., Murray, A. S.; Thomsen, K. J., Buylaert, J. P. & Jain, M. 2015: A new luminescence detection and stimulation head for the Risø TL/OSL reader. Rad. Meas. 81, 178-184.

Li, B., Li, SH. 2011: Luminescence dating of K-feldspar from sediments: A protocol without anomalous fading correction. Quat. Geochron. 6 (5), 464-479. https://doi.org/10.1016/j.quageo.2011.05.001

Li, B., Jacobs, Z., Roberts, R.G. & Li, s. 2014: Review and assessment of the potential of post-IR IRSL dating methods to circumvent the problem of anomalous fading in feldspar luminescence. Geochron. 41(3), 178-201.

Prasad, Amit Kumar, Poolton, Nigel R.J., Kook, Myungho, Jain, Mayank, 2017. Optical dating in a new light: a direct, non-destructive probe of trapped electrons. Scientific Reports.

Rahimzadeh, N., Tsukamoto, S., Thiel, C., Frechen, M., 2023. Progress and pitfalls of the SAR protocol for the quartz violet stimulated luminescence (VSL) signal: A case study from Sardinia. Quat. Geochron. 75. https://doi.org/10.1016/j.quageo.2023.101433

Thiel, C., Buylaert, J. P., Murray, A., Terhorst, B., Hofer, I., Tsukamoto, S. & Frechen, M. 2011: Luminescence dating of the Stratzing loess profile (Austria) – Testing the potential of an elevated temperature post-IR IRSL protocol. Quat. Int. 234, 23–31.

Thiel, C., Coltorti, M., Tsukamoto, S. & Frechen, M. 2010: Geochronology for some key sites along the coast of Sardinia (Italy). Quat. Int. 222, 36–47.

Thomsen, K.J., Murray, A.S. Jain, M., Bøtter-Jensen, l. 2011: Laboratory fading rates of various luminescence signals from feldspar-rich sediment extracts. Rad. Meas. 43, 1474-1486. http://doi.org/10.1016/j.radmeas.2008.06.002

Chapter 6: Conclusions

Interest in the development and efficacy of the infrared radiofluorescence (IR-RF) signal has increased steadily over the last decade, as our understanding of the mechanisms governing feldspar luminescence dating and the importance of the principle trap have evolved over time. In this dissertation I evaluated the applicability of the IR-RF signal for the dating of natural sediments using coarse-grained K-feldspar, polymineral fine-grained, K-feldspar mid-grains and Na-feldspar rich mid-grains from the Luochuan loess-palaeosol sequence and using coarse-grained K-feldspar samples from the coast of Sardinia.

6.1 Research questions

6.1.1 How does the IR-RF signal perform when dating coarse grained sediments in nature? What is the upper dating limit of IR-RF in nature?

In chapter three, the natural limits of IR-RF dating were tested on sediments that make up the well-documented Luochuan loess-palaeosol sequence on the Chinese Loess Plateau. The Luochuan loess-palaeosol sequence spans over 2.5 Ma of continuous deposition, has comprehensive independent age control (Ding et al., 2002; Zhang et al., 2022) and is an ideal natural laboratory for testing new luminescence signals. Six coarse-grained samples with depositional ages ranging from ~25 ka to ~ 900 ka were initially measured using the RF_{70} protocol (modified after Frouin et al., 2017) and a bleaching setting of 1500 s (UV LED, 395–410 nm, 900 mW) between the natural and regenerative measurements. D_e results were determined with the use of the horizontal slide method and initial measurements resulted in the consistent and significant under estimation of all sample ages but the youngest sample which was consistent with the age control. Ten samples were then measured using the RF_{70} protocol but with a significantly longer bleaching duration of 20 000 s between the natural and regenerated measurements. The longer bleaching duration resulted in age results that were consistent with the age control for all samples up to 300 ka, samples older that 300 ka once again underestimate relative to age control.

Two possible explanations for the significant underestimation were investigated: 1) the insufficient bleaching of the IR-RF signal between the natural and regenerated signal, and 2) the sensitivity change between the natural and regenerative measurements. In order to evaluate the bleachability of the natural IR-RF signal bleaching tests were done at different bleaching durations

up to 20 000 s. Results of the bleaching tests showed that the IR-RF signal could be bleached down to less than 2% of the natural D_e, showing that the natural signal was fully bleached and that there was no significant difference in bleachability between the two bleaching durations measured.

In order to account for the potential sensitivity, change the D_e results of the shorter bleach measurements were redetermined by the horizontal and vertical slide method (Murari et al., 2018). This method resulted in the increase of D_e values for all samples, though for most samples the new age results were still underestimating significantly and resulting in an over estimation in the youngest sample age. This suggests that bleaching induced sensitivity change could likely contribute to the underestimation of the shorter bleach measurements, it cannot fully account for the differences observed. Dose recovery tests were conducted using both bleaching duration measurements, and as an initial bleaching step was carried out before adding a known dose, bleaching induced sensitivity was mostly eliminated. The dose recovery tests resulted in dose recovery ratios that were consistent with the age results of both of the respective bleaching duration measurements. The shorter bleaching duration measurement dose recovery ratios significantly underestimate (except the youngest), this confirmed that bleaching induced sensitivity change was not the only contributor to the underestimation.

Natural and laboratory dose response curves (DRC) were constructed with data collected across the datable range of the sequence (fitted with single exponential decay curves) to gain insight into whether either of the sets of measurements (laboratory DRC) could describe the natural aging processes. It was observed that for the shorter bleach measurements the two DRCs diverge in shape at a low dose of ~400 Gy while in contrast for the longer bleach measurements the DRCs overlap, however the average measured regenerated curve diverges form these two DRCs at ~1100 Gy. This suggests that the stretched exponential function, which is normally used to fit the IR-RF regenerative curve which is in essence a laboratory DRC for a single sample, does not reflect the natural dose response (across the whole sequence) as constructed in this study. We attempted to define the upper dating limit for these samples in a similar vein as traditional OSL: where $2D_0$ is ~85 % of the dynamic range. When defined in this way we were able to date beyond $2D_0$, up to $4D_0$ however, natural IR-RF signal of this sample is on the horizontal part of the regenerative curve and individual aliquot data exhibit wide scatter indicating that it is possibly beyond the limit of the datable age range. In conclusion, we exhibited that it is possible to date up to ~300 ka (~1100 Gy)

using the RF_{70} signal (with a long bleaching duration) of K-feldspar in the Luochuan sequence but not the theoretical laboratory-generated dating limit of ~3500 Gy (~1000 ka).

6.1.2 Are polymineral fine-grains a suitable dosimeter with regards to the IR-RF signal in nature, or does the polymineral nature of the material result in different signals and exclude it?

In chapter four, we investigated the potential of the IR-RF signal for dating on polymineral fine grains on six samples (~30 to 480 ka) from the Luochuan loess-palaeosol sequence on the Chinese Loess Plateau. Initial observations revealed that the natural and regenerated IR-RF signals from the polymineral fine-grains were uncharacteristically flat with little or no dynamic range using both the bleaching durations investigated by Buchanan et al. (2022) (1500 s and 20000 s) between the natural and regenerated measurements. These uncharacteristic curve shapes were theorised to be linked to the polymineral nature of the samples, to test the theory X-ray fluorescence (XRF) analyses were undertaken. XRF results revealed that the polymineral fine-grained samples were dominated by quartz and Na-feldspars. K- and Na-feldspar mid-grains were prepared and compared with the polymineral fine-grains. The Na-feldspar mid-grains exhibited similarly flat IR-RF signals for both the natural and regenerated measurements and the K-feldspar mid-grains exhibited the characteristic IR-RF curve shape. The flattened nature of the curves was attributed to the dominance of Na-feldspar and quartz in the polymineral fine-grain samples.

The polymineral fine-grain ages were consistent with age control up to 300 ka and older samples underestimated for both bleaching durations investigated. The Na-feldspar mid-grains were consistent with the reference ages up to 350 ka, and the K-feldspar mid-grains were consistent with the reference ages up to 200 ka (both using the horizontal sliding method). In an attempt to improve the performance of the K-feldspar mid grains, the vertical and horizontal sliding method was used to account for possible sensitivity changes. However, this additional analysis caused an increase in all samples and resulted in age overestimation of the samples younger than 200 ka, and consistency with reference ages for samples between 200 ka and 300 ka and underestimated in samples older than 300 ka. The sample set with the successful dose recovery tests resulted in the poor dating results (K-feldspar mid-grains) and the sample set with the unsuccessful dose recovery tests gave the best dating results (Na-feldspar mid-grains, polymineral fine-grains).

The inverse relationship of dose recovery and age results suggested that in the case of polymineral fine-grains and mid-grains, dose recovery tests were a less useful indicator of whether IR-RF dating of a sample will be successful than in the case of coarse-grained K-feldspar for these samples. The bleaching tests showed that the polymineral fine-grains bleached out earlier than the mid-grains. Additionally, the observations that the different bleaching durations did not alter the age results for the polymineral fine-grains but did alter the mid-grain age results suggest that grain size is a significant factor to consider when determining a suitable bleaching duration.

In conclusion, while the presence of quartz and Na-feldspar in polymineral fine-grains can alter the shape of the regenerated IR-RF curve, this should not exclude the use of polymineral fine-grains in IR-RF dating. Despite the uncharacteristic regenerated curve shapes, polymineral fine-grains are a suitable dosimeter for IR-RF dating up to 300 ka. The IR-RF dating of polymineral fine-grains may be particularly suited to depositional environments that exhibit partial bleaching in coarse-grains as they do not require the long bleaching durations that coarser grains require.

6.1.3 How does the IR-RF signal compare with the recently developed IRPL signal (principal trap) when dating sediments?

In chapter five, two IR-RF (RF_{70} and RF_{RT}) signals were compared with two IRPL ($IRPL_{880}$ and $IRPL_{955}$) signals for dating coarse grained K-feldspar, using a case study from Sardinia. The reliability of these methods was evaluated by comparing the ages derived from the different signals with the recalculated age control of Thiel et al (2011) the ages for which were based on quartz OSL signals for the younger samples and fading corrected $pIRIR_{225}$ signals for the older samples (and minimum OSL ages).

The IR-RF signals were further evaluated for bleachability with bleaching tests that verified that the samples could be fully bleached using the UV LED in the Risø TL/OSL reader for 1800 s. Additionally dose recovery tests were done which evaluated whether a dose could be retrieved using the signals measured as well as residual dose tests that allowed for the correction of the dose recovery ratios. Residual doses were larger than 10 % and the residual corrected dose recovery ratios were all within 10% of 1 except one result which significantly overestimated for the RF_{70} signal on sample SG_4. Observations in the comparison of the IR-RF signals revealed

that the RF_{70} signal was significantly dimmer than the RF_{RT} signal due to the elevated temperature measurement avoiding a significant proportion of the available unstable traps. A comparison of the normalised (due to the different signal intensities) regenerated curves reveals slightly different curve shapes consistent across all samples suggesting that the RF_{70} signal at high doses is likely to overestimate relative to the RF_{RT}.

The two IRPL signals show very similar dose response curve shapes beginning to diverge at high doses. The coupled IRPL-IRSL measurement showed excellent recycling ratios but poor recuperation percentages larger than 5% for all but the first IRPL measurement in most cases and increasing for every subsequent measurement, the $IRPL_{955}$ signal performed marginally better than the $IRPL_{880}$ signal with regards to recuperation. This was theorised to be due to insufficient resetting of the signal coupled with the high temperature preheat. The IRPL ages were at their lowest in the second IRPL step immediately after the preheat, increase with each successive IRPL step and trended toward a plateau that theoretically trends toward the most stable signal and in most cases trend toward the age control of Thiel et al. (2010). However, the first IRPL step (before the preheat) has the best recuperation results. Therefore, we compared these two IRPL step ages to each other.

With regards to the two younger samples SG_1 and SG_2, the IR-RF and both the IRPL signal cycles ages had good correlation with the expected ages largely within 1σ and only a few within 2σ. The older samples performed slightly differently, SG_3 exhibits good age correlation within 1σ for both IR-RF signals, the first IRPL cycle showed good age correlation within 1σ and the last IRPL cycle correlate with the expected age with the $IRPL_{955}$ signal slightly overestimated within 2σ and $IRPL_{880}$ overestimating marginally beyond 2σ. Sample SG_4 exhibited good age correlation of the RF_{RT} within 1σ and RF_{70} signal overestimated within 2σ, the first IRPL cycle showed good age correlation within 1σ for both signals and the last IRPL cycle showed correlation with both signals underestimating within 2σ. For these sample the RF_{RT} signal performed slightly better likely due to poor resetting in SG_4. Additionally, as the first and last IRPL cycles both performed reasonably well, the first cycle $IRPL_{955}$ signal was preferred due to the better recuperation results.

6.2 Outlook

An increasing amount of work is already being done to better constrain the IR-RF signal. Currently the focus appears to be in improving our understanding of the origin of the signal through spectrographic studies of the different IR-RF peaks for different feldspar chemistries. Attempting to observe the types of individual traps that produce stable and useful IR-RF signals and how these can best be utilised would be an important step forward. Additionally, single grain IR-RF could be beneficial in terms of targeting feldspar grains with well constrained chemistry as we have shown in our study that chemistry has a significant impact on the shape of the IR-RF curve.

References

Ding, Z.L., Derbyshire, E., Yang, S.L., Yu, Z.W., Xiong, S.F., Liu, T.S., 2002. Stacked 2.6- Ma grain size record from the Chinese loess based on five sections and correlation with the deep-sea δ18O record. Paleoceanography 17, 5-1-5-21.

Frouin, M., Huot, S., Kreutzer, S., Lahaye, C., Lamothe, M., Philippe, A., Mercier, N., 2017. An improved radiofluorescence single-aliquot regenerative dose protocol for K-feldspars. Quat. Geochronol. 38, 13–24. https://doi.org/10.1016/j.quageo.2016.11.004

Thiel, C., Coltorti, M., Tsukamoto, S. & Frechen, M. 2010: Geochronology for some key sites along the coast of Sardinia (Italy). Quat. Int. 222, 36–47.

Zhang, J., Hao, Q., Li, S.-H., 2022. An absolutely dated record of climate change over the last three glacial–interglacial cycles from Chinese loess deposits. Geol. 50, 1116-112